



**UNIVERSITY OF
KWAZULU-NATAL**

**INYUVESI
YAKWAZULU-NATALI**

**STABILITY OF THE GRID INCORPORATING MULTI
TERMINAL HVDC: CASE STUDY OF A SOUTH AFRICAN
NETWORK**

By

ONI, EMMANUEL OLUWAFEMI

Thesis submitted in fulfilment of the academic requirements for the degree of Doctor of Philosophy
in Electrical Engineering at the School of Engineering, University of KwaZulu-Natal

Supervisor: Dr Andrew G. Swanson

Co – Supervisor Dr Rudiren Pillay Carpanen

JUNE 2021

As the candidate's supervisor, I agree with the submission of this thesis.

Signed: Date.....

Supervisor: Dr Andrew G. Swanson

Signed: Date.....

Co – Supervisor Dr Rudiren Pillay Carpanen

DECLARATION 1 – PLAGIARISM

I, **Oluwafemi E. Oni**, declare that:

1. The research reported in this thesis, except where otherwise indicated, is my original research.
2. This thesis has not been submitted for any degree or examination at any other university.
3. This thesis does not contain other persons' data, pictures, graphs, or other information unless specifically acknowledged as being sourced from other persons.
4. This thesis does not contain other persons' writing, unless specifically acknowledged as being sourced from other researchers. Where other written sources have been quoted, then:
 - a. Their words have been re-written, but the general information attributed to them has been referenced
 - b. Where their exact words have been used, then their writing has been placed in italics and inside quotation marks, and referenced.
5. This thesis does not contain text, graphics or tables copied and pasted from the Internet, unless specifically acknowledged, and the source being detailed in the thesis and in the References sections.
6. A modified section of the Eskom network was used and is well acknowledged for the research project.

Signed:

Date

Oluwafemi E. Oni.

DECLARATION 2 – PUBLICATIONS

This section includes details of publication that form part of the research presented in this thesis. These manuscripts include published, submitted, and in press manuscripts. All publications are written by the student, Oluwafemi Emmanuel Oni, and by the research supervisors, Dr Andrew Swanson and Dr Rudiren Pillay Carpanen.

Publication 1: O. E. Oni, A. G. Swanson, and R. P. Carpanen, "Modelling and Control of Multiterminal LCC HVDC," Presented at the *2018 IEEE PES/IAS PowerAfrica*, Cape Town, 2018, pp. 274-279, doi: 10.1109/PowerAfrica.2018.8520967.

Publication 2: O. E. Oni, A. G. Swanson, and R. P. Carpanen, "Small Signal Stability Analysis of a four Machine System with Strategic Placement of Monopolar LCC-HVDC link," Presented at the *SAUPEC/RobMech/PRASA Conference*, Bloemfontein, South Africa, 2019, pp. 437-443, doi: 10.1109/RoboMech.2019.8704735.

Publication 3: O. E. Oni, A. G. Swanson, and R. P. Carpanen, "Impact of Partial De-blocking of MTDC Link during DC Fault," Presented at the *IEEE PES/IAS PowerAfrica*, Abuja, Nigeria, 2019, pp. 510-514, doi: 10.1109/PowerAfrica.2019.8928915.

Publication 4: O. E. Oni, A. G. Swanson, and R. P. Carpanen, "Generator Dynamic Response During Total and Partial De-blocking of a Bipolar MTDC System," Presented at the *International SAUPEC/RobMech/PRASA Conference*, Cape Town, South Africa, 2020, pp. 1-5, doi: 10.1109/SAUPEC/RobMech/PRASA48453.2020.9041082.

Publication 5: O. E. Oni, A. G. Swanson, and R. P. Carpanen, Impact of LCC–HVDC multiterminal on generator rotor angle stability, *International Journal of Electrical and Computer Engineering*; Feb 2020: Vol. 10 (1), pp. 22-34. DOI:10.11591/ijece.v10i1.pp22-34.

Publication 6: O. E. Oni, A. G. Swanson, and R. P. Carpanen, "Small signal stability analysis of a four-machine system with placement of multi-terminal high voltage direct current link. *Journal of Energy in Southern Africa*, 2020. Vol. 31 (1), pp. 73-87. <https://dx.doi.org/10.17159/2413-3051/2020/v31i1a7430>.

Publication 7: O. E. Oni, A. G. Swanson, and R. P. Carpanen, "LCC Converter Response during Total and Partial De-blocking of a Bipolar MTDC System," Accepted by *International Journal of Engineering Research in Africa*.

Publication 8: O. E. Oni, A. G. Swanson, and R. P. "Implementation of a Multiterminal LCC HVDC with Auxiliary Controller on South Africa's 765kV Corridor," schedule to be Submitted to *IEEE Canadian of Electrical and Computer Engineering*.

Signed: Date:

Oluwafemi E. Oni

ACKNOWLEDGEMENTS

Firstly, I give God the glory for the opportunity to complete this research work. He granted me wisdom, gave me courage, and made me stand among equals. I could not have done this if not for your love—all glory and adoration to HIS name.

I am also using this medium to appreciate my supervisors, Dr Andrew Swanson and Dr Rudiren Pillay Carpanen, for all their contribution and support. I cannot imagine the success of this program without them.

I would also appreciate Eskom Power Plant Engineering institute EPPEI for their financial support throughout this study.

I want to appreciate the effort of all my colleagues for the innumerable input to the successful completion of this research study.

My warm gratitude also goes to my parent, Mr. and Mrs. Oni, my brother, Olusola Mike, and my dear wife, Kehinde Oni.

ABSTRACT

Transmission lines make one of the significant parts of power systems; faults or disturbances along any of the transmission medium often transcend to both the generating ends and the loads' end. Besides, the strength of any particular grid depends solely on the impedance of the tie-lines of that grid. Therefore, in this thesis, the line commutated converter (LCC) multiterminal high voltage direct current (MTDC) system is modelled and improved for the stability of an AC network. The converter control architecture and modelling are emphasized and explained. The effective short circuits ratio (ESCR) of the interconnecting AC lines is first described and analyzed as well. The existing CIGRE control techniques for a point-to-point LCC HVDC system have been enhanced and adapted for this study. The control and the filter parameters have also been calculated to generate a better and efficient result during a steady-state and dynamic analysis of the study.

The work carried out in this study is divided into four sections, with each section focusing on each of the research objectives. In the first section, dynamic modelling and control of LCC MTDC systems were carried out with consideration to the ESCR of the inverter side of the AC substation. The impact of large-disturbance at the inverter is investigated. This analysis has been proposed to study the impact of AC short circuit fault on the three substations. The results from this study, which are shown on a subplot, show that the system experienced a large transient overcurrent and non-severe commutation failures. Also, a voltage dip at the faulted inverter station was recorded; however, the efficacy of the converter controller disallowed the transfer of such voltage dip to the other two converters.

The second section of this study focuses on the application of MTDC system. We have carried out a comparative analysis of MTDC and AC transmission line on a single machine infinite bus (SMIB) network. The main focus of the investigation was on the transient and rotor angle stability of the SMIB network with or without MTDC link. The study also carried out a power-angle curve with the use of equal area criterion.

The third section focuses on the interarea oscillation reduction in a power system. Kundur's two-area four-machine network was adapted to suit the scenarios of this study. Different fault analysis was carried out, and the response of the generator active power, frequencies, and DC-bus voltages are recorded. The results in this study show the better performance of the MTDC implemented in this study over the other well-known method of AC

transmission medium. Also, the integration of the MTDC link is constrained by the variation of the current order of the overall power controller. The result is observed in the damping rate of the interarea oscillation of the network.

The final section of this study carried out dynamic modelling of the South African grid, and detailed dynamic response to different stability studies was carried out. An auxiliary controller for the MTDC system capable of reducing the active power oscillation by generating a new current order is proposed. This secondary control for the MTDC system is based upon dynamic sensitivity analysis of the oscillations, and thereby generate a DC current compensation for the reduction of active power oscillations in the MTDC converters' station. Two network configurations were considered in this section. System disturbance during the first configuration shows a loss of synchronizing effect from both the AVR and PSS, which causes the generator to lose synchronism with subsequent oscillations. A negative damping torque for the rotor angle and negative synchronizing torque for the interarea oscillations was also observed. Meanwhile, the results during the second configuration recorded quick damping of the interarea oscillations with a significant improvement to the voltage profile. Among all of these benefits, the power carrying capacity at a reduced loss and cost stood out. The conclusion from this section is that the implementation of the MTDC link on the South African grid provided a better system performance. Therefore, the adoption of this research into South African transmission network will surely help enhance the stability margin of the grid. The proposed secondary controller also provided potential mitigation of excessive active power dip of the MTDC link during the system disturbance.

TABLE OF CONTENT

DECLARATION 1 – PLAGIARISM	ii
DECLARATION 2 – PUBLICATIONS	iii
ACKNOWLEDGEMENTS	iv
ABSTRACT	v
TABLE OF CONTENT	vii
LIST OF FIGURES	x
LIST OF TABLES	xiii
LIST OF ABBREVIATIONS	xiv
LIST OF SYMBOLS AND UNITS	xvi
CHAPTER 1: INTRODUCTION	17
1.1 Introduction	17
1.2 Aims & Objectives	18
1.3 Hypothesis	19
1.4 Contribution of the study	19
1.5 Layout of the study	20
1.6 References	21
CHAPTER 2: Modelling and Control of Multiterminal LCC HVDC	23
2.1 Introduction	24
2.2 Modelling and Control of Parallel MTDC	26
2.2.1 Current Control	26
2.2.2 Voltage/gamma Control	28
2.2.3 Master Controller	28
2.3 ESCR Analysis	30
2.4 Simulation Result	32
2.4.1 Effect of AC Fault on Converter 1 (Rect)	34
2.4.2 Effect of AC Fault on Converter 2 (Inv-1)	35
2.4.3 Effect of AC fault on converter 3 (Inv-2)	36

2.5	Conclusion	38
2.6	Acknowledgment	39
2.7	References	39
CHAPTER 3: IMPACT OF LCC–HVDC MULTITERMINAL ON GENERATOR ROTOR ANGLE STABILITY		41
3.1	Introduction	42
3.2	ESCR Analysis	45
3.3	Generator Modelling and Control	48
3.4	Rotor Angle Stability	48
3.5	System Model	52
3.6	Simulation Results	53
3.7	Conclusion	60
3.8	Acknowledgements	61
3.9	References	61
3.10	Appendix	65
CHAPTER 4: SMALL SIGNAL STABILITY ANALYSIS OF A FOUR-MACHINE SYSTEM WITH PLACEMENT OF MULTI-TERMINAL HIGH VOLTAGE DIRECT CURRENT LINK		67
4.1	Introduction	68
4.2	Methodology	70
4.3	Background Theory	71
4.4	System Model	74
4.4.1	Synchronous Generator Model	76
4.4.2	Load Model	76
4.4.3	Multiterminal Direct Current Model	77
4.5	Results and Discussion	80
4.5.1	First Scenario	80
4.5.2	Second Scenario	82
4.6	Conclusion	92
4.7	Acknowledgement	92
4.8	References	93

CHAPTER 5: Implementation of a Multiterminal LCC HVDC with Auxiliary Controller on South Africa's 765kV Corridor	100
5.1 Introduction	101
5.2 Challenges and Possibility of SA Grid	103
5.3 Network Modelling	107
5.3.1 MTDC Link with Complementary Controller	107
5.3.2 Transmission Line Data	110
5.3.3 Converter Harmonic filter design	110
5.4 Simulation result	112
5.5 Conclusion	119
5.6 References	120
5.7 Appendix	123
CHAPTER 6: CONCLUSION AND RECOMMENDATION	126
6.1 Conclusions	126
6.1.1 Modelling and Control of the MTDC Network	126
6.1.2 Impact of LCC–HVDC Multiterminal on Generator Rotor Angle Stability	126
6.1.3 Small Signal Stability Analysis of a Four-Machine System with Placement of Multi-Terminal High Voltage Direct Current Link	127
6.1.4 Implementation OF A Multiterminal LCC HVDC with Auxiliary Controller on South Africa's 765kV Corridor	127
6.2 Recommendation	128

LIST OF FIGURES

Figure 2.1: Three-terminal LCC-HVDC system	27
Figure 2.2: Current controller.....	28
Figure 2.3: Voltage controller	29
Figure 2.4: Master controller with current balancer	29
Figure 2.5: AC/DC system interconnection.....	30
Figure 2.6: Active power – DC current characteristics with respect to SCR level	32
Figure 2.7: Maximum Available Power based on Pd-Id characteristics	32
Figure 2.8: DC voltage (kV).....	33
Figure 2.9: DC current (kV)	33
Figure 2.10: Active power (MW).....	34
Figure 2.11: Per-unit RMS voltage.....	34
Figure 2.12: Rectifier AC voltage (kV).....	35
Figure 2.13: Rectifier firing angle (α)	35
Figure 2.14: Inverter-1 AC voltage (kV).....	36
Figure 2.15: Extinction angle for Inverter 1	36
Figure 2.16: Inverter 1 ignition angle	37
Figure 2.17: Inverter 2 Extinction angle (γ)	37
Figure 2.18: Inverter 2 firing angle (α).....	38
Figure 2.19: Inverter 2 ignition angle	38
Figure 3.1: AC/DC system interconnection.....	46
Figure 3.2: Active power – DC current characteristics with respect to SCR level	47
Figure 3.3: IEEE ST4A excitation system with AVR and PSS1A stabiliser.....	48
Figure 3.4: Equivalent SMIB network.....	49
Figure 3.5: Generator Rotor Angle for SMIB system during 70ms fault	51
Figure 3.6: Pe – δ diagram for both stable and unstable system condition.....	51
Figure 3.7: Parallel MTDC system embedded in AC Network model	52
Figure 3.8: Synchronous generator power output.....	54
Figure 3.9: DC power across the three converters.....	55
Figure 3.10: MTDC current.....	55
Figure 3.11: DC voltage for the three converters	56
Figure 3.12: Synchronous generator rotor angle response (deg)	57
Figure 3.13: Synchronous generator exciter field voltage (pu)	57
Figure 3.14: Synchronous generator speed (rad/s)	58
Figure 3.15: Generator Power – angle (Pe- δ) diagram during stable condition.....	59
Figure 3.16: Generator power – angle (Pe- δ) diagram during unstable condition while using 2x500kV AC circuits (MTDC link out of service).....	59
Figure 3.17: Generator output voltage.....	60
Figure 3.18: Synchronising torque	60

Figure 4.1: Simple two machine two-area network, where E , P , H , and δ = generator terminal voltage, active generator power, generator inertia constant and generator rotor angle respectively; R , L , Z , and U = load resistance, load inductance, line impedance, and line voltage respectively; G_{A1} and G_{A2} = generators in areas 1 and 2 respectively.71

Figure 4.2: Kundur’s two-area four-machine system with three-terminal LCC-HVDC link, where $L7_8$, $L7_8b$ = first and second transmission line between bus 7 and 8 respectively; Tap_Rect-1 , Tap_Rect-2 , Tap_Inv = tap changers for rectifier station 1, rectifier station 2, and the inverter station respectively, $SyncGen$ = synchronous generator; $I_{d-Rect-1}$, $I_{d-Rect-2}$, I_{d-Inv} = direct current for rectifier station 1, rectifier station 2, and the inverter station respectively.75

Figure 4.3: Power system stabiliser with automotive voltage regulator, where K_{STAB} = stabilising gain, T_1 = first lead time constant, T_2 = first lag time constant, T_W = washout time constant, K_A = regulator integral gain, T_R = transducer time constant, $\Delta\omega_r$ = change in angular speed, E_{fd} = exciter output voltage, E_{Fmin} , E_{Fmax} = minimum and maximum regulator outputs, V_{ref} = reference voltage regulator, V_s = combined power system stabiliser and possibly discontinuous control output after any limits or switching, and E_t = terminal voltage of transducer and load compensation elements.76

Figure 4.4: Rectifier current controller, where $I_{dcfilt.}$ = filtered current, $V_{dcfilt.}$ = filtered voltage, $*const.$ = constant, $VDCOL$ = voltage-dependent current order limiter, Pi = constant (3.142), PI = proportional and integral controller, I_{ord} = current order, I_{dc} and V_{dc} = direct current voltage and current, α_{order} = firing angle order.78

Figure 4.5: Inverter voltage controller, where $I_{dcfilt.}$ = filtered current, $V_{dcfilt.}$ = filtered voltage, $*const.$ = constant, $VDCOL$ = voltage-dependent current order limiter, Pi = constant (3.142), PI = proportional and integral controller, I_{ord} = current order, I_{dc} and V_{dc} = direct current voltage and current, γ_{order} = firing angle order, CEC = current error, γ_{meas} , γ_o , and γ_{max} = measured, initial, and maximum extinction angles respectively.78

Figure 4.6: Overall current controller for the multiterminal direct current system, where P_1 , P_2 , and P_3 = power setpoint for each converter station, V_{dcRect} = rectifier direct voltage, I_1 , I_2 , and I_3 = calculated current from each converter station, I_{1max} , I_{2max} , and I_{3max} = maximum setpoint for each converter station current, and I_{ord_Rect-1} , I_{ord_Rect-2} , and I_{ord_Inv} = rectifier 1, rectifier 2, and inverter current order respectively.79

Figure 4.7: Synchronous generator active power during the first scenario, where $Gen1$, $Gen2$, $Gen3$, and $Gen4$ = synchronous generators 1 to 4.81

Figure 4.8: Generator speed during the first scenario, where $Gen1$, $Gen2$, $Gen3$, and $Gen4$ = synchronous generators 1 to 4.81

Figure 4.9: Generator field voltage during the first scenario, where $Gen1$, $Gen2$, $Gen3$, and $Gen4$ = synchronous generators 1 to 4.82

Figure 4.10: Synchronous generator active power during the second scenario, where $Gen1$, $Gen2$, $Gen3$, and $Gen4$ = Synchronous generator 1 to 4.83

Figure 4.11: Generator speed during the second scenario, where $Gen1$, $Gen2$, $Gen3$, and $Gen4$ = Synchronous generator 1 to 4.84

Figure 4.12: Generator field voltage during the second scenario, where <i>Gen1</i> , <i>Gen2</i> , <i>Gen3</i> , and <i>Gen4</i> = synchronous generators 1 to 4.....	85
Figure 4.13: Converter power, where <i>Rect-1</i> , <i>Rect-2</i> , and <i>Invtr</i> = rectifier 1, rectifier 2, and inverter station respectively.....	85
Figure 4.14: Converter current, where <i>Rect-1</i> , <i>Rect-2</i> , and <i>Invtr</i> = rectifier 1, rectifier 2, and inverter station respectively.....	86
Figure 4.15: Converter voltage, where <i>Rect-1</i> , <i>Rect-2</i> , and <i>Invtr</i> = rectifier 1, rectifier 2, and inverter station respectively.....	87
Figure 4.16: Inverter (alternating current) voltage.....	87
Figure 4.17: Mode shift for rectifier 2 station, where <i>Rect-2Iorder</i> = rectifier 2 current order, <i>VDCOL</i> = voltage dependent current order limiter.....	88
Figure 4.18: Mode shift for the inverter extinction angle.....	88
Figure 4.19: Converter firing angle, where <i>Rect-1</i> , <i>Rect-2</i> , and <i>Invtr</i> = rectifier 1, rectifier 2, and inverter station respectively.....	89
Figure 4.20: Bus voltage during the first scenario of high voltage alternating current lines.....	90
Figure 4.21: Bus voltage during the second scenario of the multi-terminal direct current link.....	90
Figure 4.22: Inter-area power transfer during both operating scenarios, where AC and DC are alternating current and direct current respectively.....	91
Figure 4.23: Damping rate for different converter power value across Rectifier 2 station, where AC and DC = alternating and direct current.....	92
Figure 5.1: South African provincial load demand [25].....	105
Figure 5.2: Extract of the South Africa grid.....	108
Figure 5.3: Three-terminal LCC HVDC topology.....	108
Figure 5.4: Current and voltage controller.....	109
Figure 5.5: Overall power controller.....	110
Figure 5.6: Auxilliary controller.....	110
Figure 5.7: Tower geometry for the overhead lines (a) 400kV geometry, and (b) 765kV geometry.....	111
Figure 5.8: (a) C-type filter, (b) high pass filter, and (d) capacitor bank.....	111
Figure 5.9: Active power for the synchronous generator (a) without the MTDC link, (b) with MTDC link, (c) Comparative plot of the active power of three generators in each grid.....	114
Figure 5.10: Rotor angle for the synchronous generator (a) without the MTDC link, (b) with MTDC link.....	115
Figure 5.11: Angular Speed for the synchronous generator (a) without the MTDC link, (b) with MTDC link.....	116
Figure 5.12: Bus voltage profile (a) without the MTDC link, (b) with MTDC link.....	117
Figure 5.13: MTDC power (where <i>RP1</i> is rectifier 1 Power, and <i>AR1</i> is Rectifier 1 Power with Auxiliary control).....	118
Figure 5.14: Firing angle in (deg).....	118
Figure 5.15: Interarea Power transfer across the Northern and north-east border.....	119

LIST OF TABLES

Table 2.1: MTDC RATING	27
Table 2.2: SCR Indicator For AC/DC Networks Strength	31
Table 3.1: SCR value and the AC/DC networks strength.....	47
Table 3.2: MTDC Converter Parameters	65
Table 3.3: Generator and Transmission line Parameters	66
Table 5.1: Impact of Load Demand During the Winter Season.....	106
Table 5.2: Load Progression in the Central Grid	106
Table 5.3: Synchronous generator	123
Table 5.4: AC Transmission Line Data	123
Table 5.5: Multiterminal High Voltage Direct Current Data.....	123
Table 5.6: Auxiliary Controller	124
Table 5.7: MTDC Transmission line (T-model) data	124
Table 5.8: Filter Design	124

LIST OF ABBREVIATIONS

AC	Alternating Current
AC4A	IEEE Alternator Supplied Rectifier Excitation System #4
AVR	Automatic Voltage Regulator
CC	Constant Current
CCC	Capacitor Commutated Converter
CCT	Critical Clearing Time
CEA	Constant Extinction Angle
CIA	Constant Ignition Angle
CIT	Critical Isolating Time
DC	Direct Current
EMT	Electromagnetic transient simulation
ESCR	Effective Short Circuit Ratio
FACTS	Flexible AC Transmission System
HIL	Hardware in the Loop
HVAC	High Voltage Alternating Current
HVDC	High Voltage Direct Current
IEEE	Institute of Electrical and Electronics Engineers
IGBTs	Insulated Gate Bipolar Transistors
Inv	Inverter
I_{ord}	Current Order
IPPs	Independent Power Producers
LCC	Line Commutated Converter
MAP	Maximum Available Power
MPC	Maximum Power Curve
Ms	milliseconds
NBTA	New Build Transmission Article
OEL	Over Excitation Limiter
OLTC/ULTC	On-Load Tap Changers/Under-Load Tap changers
OPGW	Optical Ground Wire
P.F.	Power Factor
PMUs	Phasor Measurement Units
PSS1A	Single Input Power System Stabiliser
PSSs	Power System Stabilisers
PWM	Pulse Width Modulation
Rect	Rectifier

Rms	Root Mean Square
RMS	Real-Time Simulation
ROW	Right of Way
RLC	Resistor, Inductor, and Capacitor circuits
SCL	Short Circuit Level
SGCC	State Grid Corporation of China
SMIB	Single Machine Infinite Bus
SSC	Short Circuit Capacity
STATCOM	Static Synchronous Compensator
SVC	Static Var Compensator
TAFM	Two Area Four Machine
TCSC	Thyristor Controlled Series Compensator
TDP	Transmission Development Plan
TFSC	Three-Phase Short Circuit Fault
TUF	Transformer Utilisation Factor
UEL	Under-Excitation Limiter
UHVDC	Ultra-High Voltage Direct Current
VC	Voltage control
VDCOL	Voltage-Dependent Current Order Limiter
VI	Voltage - Current
VSC	Voltage Source Converter
WAMs	Wide-Area Monitoring
XLPE	Cross-Linked Polyethylene Insulation

LIST OF SYMBOLS AND UNITS

α	converter firing angle (alpha)
β	converter ignition angle (beta)
π	pi (3.143)
Ω	Ohms
γ	converter extinction angle
μ	overlap angle
GW/MW	gig watt (10^9)/ megawatt (10^6)
kV	kilovolt (10^3)
km	kilometre
ms	milliseconds (10^{-3})
kA	kilo-ampere
p.u	per unit
δ	Rotor Angle

CHAPTER 1: INTRODUCTION

1.1 INTRODUCTION

In recent years, electricity demand has significantly increased, especially in many parts of Africa's urban area. These areas are mostly situated several kilometres from the generation, thus requiring long transmission lines to be used in transmitting the electric power to the load. In this situation, safe, stable, and economical transmission is the utmost priority of power utilities [1]. Stability is of critical concern in all African countries as almost all these countries experience either under-voltage transmission, load shedding, or total/partial system collapse on their main electric grid on a frequent basis. The power systems are continually subject to disturbances and faults. The power utilities are always constrained to operate close to the stability limit of their network, thereby reducing the allowance needed for the power system to recover from any system disturbances. Another challenge faced by power utilities is the different variation in consumer loads. As these load changes, the synchronised generator speed of the entire grid changes continuously in response to the continuous change in the load demand. Therefore, the power system operators will always plan for the foreseeable future to meet possible problems associated with load increase, transmission planning, and stability margin. The need for this evaluation is to maintain uninterrupted power supply from the generating end to the consumer end and to avoid a blackout, or systems collapse originated from loss of generation or an overload of the transmission system caused by congestion. These disturbances increase the loading of other lines, and in the end, leads to a voltage collapses due to the high impedance in the weakened transmission line [2-8].

High Voltage Direct Current (HVDC) technology has been widely used for its inherent benefits in long-distance transmission application. HVDC systems were first commercially used in 1954 for the interconnection of Gotland and Sweden. Moreover, since, it has been widely embraced by different power manufacturers and different power utilities. The technology has since undergone various developments and is mainly favoured for its control capabilities as well as providing efficient and stable transmission. Bulk power transmission over long distances at a reduced right of way (ROW), asynchronous systems, long submarine transmission, and renewable energy integration are another edge over AC systems [9].

The two dominant methods used in converting AC to DC are the line commutated converter (LCC) and the voltage source converter (VSC). The success of these two technologies became possible with the development of power electronics devices [10, 11]. Before the development of power electronic technology, the transverter, electrolytic and the atmospheric converter, were all part of the several attempts made for AC/DC conversion. These entire attempts failed due to technical reasons and safety

measures inherent in using them [12]. However, continuous progress in the power electronics technologies to fabricate highly efficient semiconductor devices for HVDC converter topology makes the HVDC system a better means for long-distance bulk power transmission [13]. These advancements in the converter technology also usher in the era of multiterminal HVDC (MTDC). The potentials of this technology have significantly increased, especially in the integration of renewable energy such as wind farm and solar PV. The topology can utilise either thyristor-based converters or IGBT based converters or both to become a hybrid system [14, 15]. MTDC systems utilise a multiple converter configuration that is commonly referred to as ‘DC Grids’. The power flow into, or out of, each converter can be dynamically changed without any reconfiguration of the DC grid. One of the major challenges of the MTDC grid is the complexity of the control architecture, the higher the number of converters, the higher the control measures needed to maintain how the power is channelled [16].

Series of stability issues may occur in an AC/DC network due to the interaction of MTDC system on AC network, most especially when connected to weak AC networks. The critical questions that this thesis seek to answer are:

- In the event of fault or disturbance, how will the converter controller of the MTDC system be modelled to mitigate the complete loss of the master control station?
- How can the system stability level be improved, considering the network Effective Short Circuits Ratio (ESCR) during normal operation and AC/DC fault conditions?
- What is the impact of the MTDC system on the generator rotor angle, busbar voltage angle during a loss of load or tripping of the generator? This analysis includes investigating the damping out of oscillations during the power swings angle.
- Which of the control architecture for MTDC systems on the South Africa network will bring about high network performance?

1.2 AIMS & OBJECTIVES

This study investigates the operation performance of the LCC MTDC system in the reduction of small-signal and transient stability.

The objectives were:

- To develop a detailed model of multiterminal LCC HVDC system with consideration to the short circuit ratio problem and with consideration to the control architectures.

- To investigate the dynamic transient stability analysis of a single machine infinite bus network during the implementation of the MTDC network.
- To investigate the equal-area criterion of SMIB network with MTDC network.
- To examine the impact of the MTDC system on the interarea power transfer of a two-area four-machine network.
- To investigate the effect of integrating MTDC systems on South Africa's 765kV AC network, taking into consideration the generator stability and performance.

1.3 HYPOTHESIS

Below are the hypotheses which this thesis seeks to prove.

- Transient overcurrent caused by short circuits fault could be reduced with the implementation of a robust controller in a MTDC network.
- The voltage-dependent current order limiter could be upgraded to reduce the impact of DC overcurrent during a fault, which is higher in MTDC system than in a bipolar system due to the contributed impact of each converter station.
- An increase in the current order level of MTDC network above a certain point could result in an unstable operation of the converter network due to the saturation level of the converter rating.
- Additional controller implemented on each converter station should reduce and damp the interarea oscillation caused by a system fault.
- The design of an enhanced controller on MTDC system implemented on a modified SA grid could give an improved performance with reduced transmission loss due to a robust controller design and additional current order support.

1.4 CONTRIBUTION OF THE STUDY

This research work was carried out to investigate the LCC MTDC interaction on the AC network, especially inside a grid network with high impedance. One of the main contributions of this thesis is the integration of the LCC MTDC network on the South African (SA) grid, comprising of the Northern grid to the Western grid, and it was interlinked mainly by 765kV and 400kV transmission line. This transmission corridor has the longest transmission network connecting the most crucial location. Therefore, interruptions due to systems faults and disturbances are so expensive. Besides, the analysis

of this corridor utilizing a multiterminal LCC HVDC system has never been reported in the literature. Therefore, the thesis seeks to contribute further by evaluating the performance of the South African grid when the 600kV MTDC line was used in the replacement of the 765kV lines. This analysis was done to make a detailed comparison of both AC and DC systems, especially the enhancements of fault clearing time and the reduction of interarea oscillations. Other contributions of this study are:

- Design of LCC MTDC overall power controller.
- Transient stability analysis of AC/DC utilizing equal area criterion.
- The variation of the MTDC current order and the impact on the active power of the DC link.
- The development of auxiliary power controller for the MTDC link.

1.5 LAYOUT OF THE STUDY

Chapter 1: The aims and objectives of the study are discussed. The section also introduces the background of the research and the vital contribution, and the organization of the thesis.

Chapter 2: Paper No. 1, a conference paper on the modelling and control of the MTDC network, was described. This chapter addressed the first objective of this study on the methodology in the modelling of the LCC MTDC system. The control architecture was first introduced in this study, and the performance of the final design model was examined.

Chapter 3: This chapter addressed objective No. 2. It describes the performance evaluation of the modelled MTDC system inside a single machine infinite bus (SMIB) network. In this study, the transient stability analysis of the SMIB network was investigated using the equal-area criterion. The final design compared two scenarios using the power angle curve.

Chapter 4: This chapter is structured according to paper No. 4. The efficiency of the proposed method has been verified over two IEEE benchmarks, where results confirmed the applicability of the solutions.

Chapter 5: A modified South African utility network was introduced in this chapter. It was based on paper No. 8. The various scenarios and test cases have been considered. The study focuses on LCC MTDC systems for stability enhancement, taking into consideration the ESCR strength of the South Africa grid. It also discusses the control co-ordination of the modelled system. The generator rotor angle, automatic voltage regulator, as well as the voltage profile of the network was considered to ascertain their compliance with the South Africa grid code.

Chapter 6: In this chapter, the conclusions of the study and some recommendations for future work have been presented.

1.6 REFERENCES

1. S. Kulshrestha, S. Yadav, and A. Gupta, "An Index For Dissection of Voltage Stability and Reactive Power Remuneration of Distribution Network Based on Synthesis Load Model," in *International Conference On Recent Trends In Engineering Science And Management* New Delhi, India, 15 March 2015.
2. A. Larson, "Power Shortages Challenge Eskom, Force Load Shedding in South Africa," ed: TRADEFAIR GROUP 11000 RICHMOND, STE 500, HOUSTON, TX 77042 USA, 2015.
3. A. Colmenar-Santos, C. de Palacio, L. A. Enríquez-García, and Á. López-Rey, "A Methodology for Assessing Islanding of Microgrids: Between Utility Dependence and Off-Grid Systems," *Energies*, vol. 8, no. 5, pp. 4436-4454, 2015.
4. Y. J. Cheema, T. Amair, M. I. Qadir, and M. M. Raza, "Impact of Load Shedding on Socio-Economic Life of the People," *International Journal of Research*, vol. 2, no. 8, pp. 385-387, 2015.
5. R. Faranda, A. Pievatolo, and E. Tironi, "Load shedding: a new proposal," *Power Systems, IEEE Transactions on*, vol. 22, no. 4, pp. 2086-2093, 2007.
6. A. Sebitosi, "Energy efficiency, security of supply and the environment in South Africa: Moving beyond the strategy documents," *Energy*, vol. 33, no. 11, pp. 1591-1596, 2008.
7. Z. Bo, O. Shaojie, Z. Jianhua, S. Hui, W. Geng, and Z. Ming, "An analysis of previous blackouts in the world: Lessons for China' s power industry," *Renewable and Sustainable Energy Reviews*, vol. 42, pp. 1151-1163, 2015.
8. S. J. Mwale and I. E. Davidson, "Security analysis of electric power supply in SADC region," in *AFRICON, 2013*, 2013: IEEE, pp. 1-6.
9. M. H. Okba, M. H. Saied, M. Z. Mostafa, and T. M. Abdel-Moneim, "High voltage direct current transmission - A review, part I," in *EnergYTECH, 2012 IEEE*, 29-31 May 2012 2012, pp. 1-7, doi: 10.1109/EnergyTech.2012.6304650. [Online]. Available: <http://ieeexplore.ieee.org/ielx5/6294016/6304622/06304650.pdf?tp=&arnumber=6304650&isnumber=6304622>
10. M. P. Bahrman, "HVDC transmission overview," in *Transmission and Distribution Conference and Exposition, 2008. T&D. IEEE/PES*, 21-24 April 2008 2008, pp. 1-7, doi: 10.1109/TDC.2008.4517304.

11. H. K. Müller, S. S. Torbaghan, M. Gibescu, M. M. Roggenkamp, and M. A. M. M. van der Meijden, "The need for a common standard for voltage levels of HVDC VSC technology," *Energy Policy*, vol. 63, no. 0, pp. 244-251, 12// 2013, doi: <http://dx.doi.org/10.1016/j.enpol.2013.08.078>.
12. L. de Andrade and T. P. de Leao, "A brief history of direct current in electrical power systems," in *HISTory of ELectro-technology CONference (HISTELCON), 2012 Third IEEE*, 5-7 Sept. 2012 2012, pp. 1-6, doi: 10.1109/HISTELCON.2012.6487566.
13. N. Flourentzou, V. G. Agelidis, and G. D. Demetriades, "VSC-Based HVDC Power Transmission Systems: An Overview," *Power Electronics, IEEE Transactions on*, vol. 24, no. 3, pp. 592-602, 2009, doi: 10.1109/TPEL.2008.2008441.
14. W. Lin, J. Wen, J. Liang, S. Cheng, M. Yao, and N. Li, "A three-terminal HVDC system to bundle wind farms with conventional power plants," *IEEE Transactions on Power Systems*, vol. 28, no. 3, pp. 2292-2300, 2013.
15. L. M. Castro and E. Acha, "A Unified Modeling Approach of Multi-Terminal VSC-HVDC Links for Dynamic Simulations of Large-Scale Power Systems," *IEEE Transactions on Power Systems*, vol. 31, no. 6, pp. 5051-5060, 2016.
16. C. Barker and R. Whitehouse, "Autonomous converter control in a multi-terminal HVDC system," in *9th IET International Conference On AC and DC Power Transmission ACDC*, 2010: IET, pp. 1-5.

CHAPTER 2: MODELLING AND CONTROL OF MULTITERMINAL LCC HVDC

PAPER ONE

This chapter addresses objective one and is presented in manuscript format published in the proceedings of the 2018 IEEE PES/IAS PowerAfrica conference, Cape Town, South Africa. 2018, pp. 274-279.

Modelling and Control of Multiterminal LCC HVDC

Abstract—Recent advances in the development and availability of multiple manufacturers for power electronics industries have made multiterminal-High Voltage Direct Current (HVDC) links possible and feasible. The multiterminal HVDC (MTDC) configuration is commonly referred to as ‘HVDC Grids.’ The power flow into or out of each converter can be dynamically changed without any reconfiguration of the HVDC grid. This configuration can pose a threat to the stability of the system if channelled ineffectively. Another factor that also determines the stability margin of the conventional thyristor HVDC converter is the Effective Short Circuit Ratio (ESCR) of the AC grid. This paper investigates the fault current contribution of each converter of three-terminal systems with respect to the interconnected AC grid. Line Commutated Converter technology was used to model a three-terminal HVDC network on PSCAD. The dynamic modelling and fault contribution to the MTDC network with consideration to AC grid strength was also considered. The results show that disturbances on the AC side of the inverter would cause the system to experience large transient overcurrent and non-severe commutation failures.

Keywords—Short Circuit Ratio (SCR), commutation failure, multiterminal network, HVDC system, transient stability.

2.1 INTRODUCTION

The reduction in the cost of power electronics devices and operational benefits of HVDC systems, and the almost constant cost of DC terminal equipment have paved the way for the increase in the number of multiterminal HVDC (MTDC) systems [1]. Examples of the MTDC are the Sardinia-Corsica-Italy connection, the Quebec-New England connection, and the recently commissioned India North-East Agra interconnection. Apart from interconnecting multiple urban regions with a minimum usage of transmission right of way (ROW), it also aids in the transmission of bulk power with the capability of reinforcing such networks. This has prompted much interest in extending existing HVDC links into MTDC systems and plans in constructing a new MTDC system as seen in 8 GW of North East Agra that comprises of four terminals in three converter stations [2].

In MTDC systems, the converter substations can be configured as either parallel or series-connected. In parallel or constant voltage systems, a substation, either rectifier with firing angle $\alpha \approx 0$ or

inverter with extinction angle $\gamma=\gamma_0$, is assigned the task of controlling and defining the voltage level of the entire network while all other substations are current-controlled. Such a system requires reversing switches for power reversal capability. Series or constant current systems operate close to a two-terminal HVDC concept with some unique characteristics of one converter operating at current control while the other substations control their voltage [3]. This gives the series configuration an edge of controlling the direction of power flow using the source voltage sign since all substation has common current. However, it has low efficiency at partial load and full current [4], [5]. Most realised, planned, or constructed MTDC systems are generally parallel types with current margin control and current reference balancer [6].

References [5], [7]-10] have undertaken studies on two terminals systems utilising either Voltage Source converters (VSC) or Line Commutated Converters (LCC) technologies. VSC provides AC networks with robustness and full controllability of AC power but requires specially configured DC breakers to isolate the converter during a DC line fault. Unlike VSC HVDC, research studies have shown that the LCC HVDC system is immune to DC line fault with the use of conventional DC line protection equipment.

Research work has been carried out on the dynamic modelling and control response of MTDC systems, but little has been done in considering AC network strength using short circuit capacity (Ssc) [2], [4], [5], [11]. In power system analysis, the system strength is normally measured by the ratio of SSC to installed capacity to give the Short Circuit Ratio (SCR) of the network. Effective Short Circuit Ratio (ESCR) is used to indicate system strength when considering a multi-infeed HVDC system [12], [13]. Reactive power generators such as synchronous condensers, harmonic filters, and shunt capacitors are a few of the network elements that affect ESCR. A synchronous condenser increases the ESCR value while capacitor banks and filters reduce its value [13], [14]. A system that is prone to commutation failure requires proper consideration in the control setup during fault conditions by understanding the low SCR value during the system analysis and modelling stage.

One master station controlling the DC voltage on the link and all other converters operating in current control is one of the best methods proposed in the literature [4], [5], [15]. A fault in the voltage controlling station can eventually lead to a total collapse of the MTDC link. This paper has made an improvement by incorporating a voltage controller into two of the converter's stations, preferably the inverters.

The objective of this paper is to present a simple approach to modelling a three-terminal LCC converter system when considering different grid strengths of the AC network using short circuits ratio

(SCR) evaluation.

2.2 MODELLING AND CONTROL OF PARALLEL MTDC

The MTDC network used was of parallel three-terminal thyristor converter configuration shown in Figure 2.1. Converter ratings and line specifications are shown in Table 2.1. The basic MTDC controller models resembled that of the conventional point-to-point system discussed in [8], [9], [16]. A modification was made to the I_{ord} , and PI controller setpoint to obtain the desired performance of the V-I characteristics of the converters. The rectifier was equipped with a current controller while the inverters were operated in voltage control mode. A central master controller was used for power sharing and current balancing between all the converters. The converter stations were similar to that of the CIGRE benchmark model, with little adjustment made to the rectifier station to account for the power transfer to both inverters

2.2.1 Current Control

The rectifier controls DC current by varying the firing angle α or by controlling AC commutation voltage using the on-load tap changers (OLTC). The DC current order (I_{ord}) is an input to the rectifier, which then compares (I_{ord}) with the filtered measure current (I_{dcfilt}) to generate the current error (I_{err}). This error current (I_{err}) is used as an input to a PI controller for amplification and regulation, which in turn determines the firing angle order (α_order) for the rectifier. This controller, shown in Figure 2.2, also uses Voltage-Dependent Current Order Limiter (VDCOL). This helps to readjust the current order value during a disturbance in the AC network, to initiate a fast and controlled restart after AC or DC fault clearance, and to avoid stress on the thyristor valve during continual commutation failure and prevent its reoccurrence.

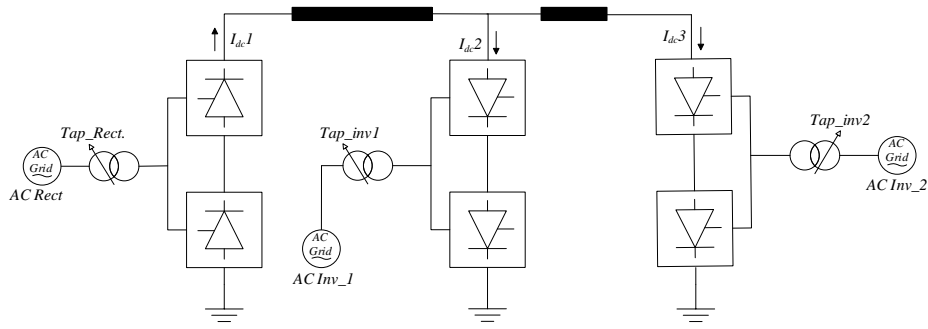


Figure 2.1: Three-terminal LCC-HVDC system

Table 2.1: MTDC RATING

Converter data			
	Rect.	Inv-1	Inv-2
Rating (MW)	2000	1000	1000
DC current (kA)	2	1	1
SCR	2.5	3	2.5
AC voltage (kV)	450	450	500
γ_0 (inverter)		15	15
Transformer per 6 pulse thyristor			
Rating (MVA)	1200	700	600
Voltage (kV)	500/250	500/250	500/250
Leakage reactance (pu)	0.18	0.18	0.18
PI Controller			
Proportional Gain	1.0989	1.5363	1.5363
Integral time constant (s)	0.01092	0.01524	0.01524
VDCOL			
Threshold input	0.4-1.0	0.4-0.9	0.4-0.9
Threshold output	0.55-1.5	0.55-1.0	0.55-1.0
Transmission line (T-model)			
	Line 1	Line 2	
R(Ω)	1.5	2.5	
Reactor (H)	0.5968	0.5968	
DC filter (μF)	26	26	

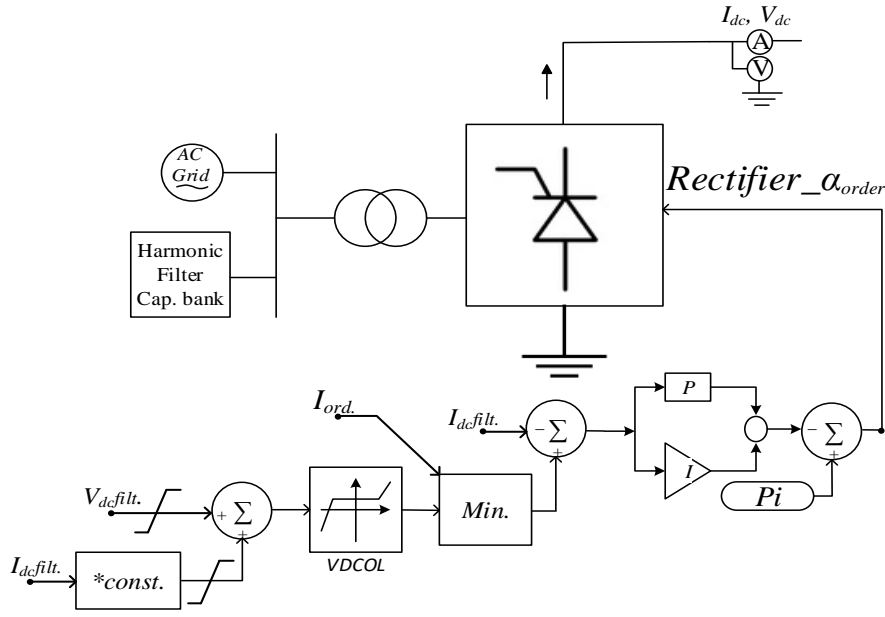


Figure 2.2: Current controller

2.2.2 Voltage/gamma Control

The voltage or constant extinction angle (CEA) control generates the firing angle for the inverter. As shown in Figure 2.3, pre-set extinction angle (γ_0) is compared with the measured (γ_{meas}) to give a desired value which is kept as minimum as possible to minimise the cost incurred from high reactive power demand and high converter losses. An increase in commutation failure could arise when γ_0 becomes too small. Therefore, the value is to be maintained in the range of 15° to 18° .

The two inverters are both equipped with voltage controllers (VC). During normal operation, one of the inverters controls the voltage while the other inverter is in current control (CC) mode. However, during a severe fault condition at the inverter in CC mode, the significant drop of voltage will switch this inverter into VC mode while the inverter that was initially set to operate in VC mode will switch to CC mode. This helps to withstand fault in case one of the inverters loses its voltage controllability.

2.2.3 Master Controller

The master controller, as shown in Figure 2.4, uses measured DC voltage at each converter with a pre-set power order to generate the current order for each of the converter systems. This controller helps to balance the power and current order of the entire converter by ensuring that DC current summation equals zero ($\sum I_{dc}=0$). This has to be maintained according to each converter's current saturation value (I_{min} - I_{max}). It compensates for DC line losses by using the weighting factor (kq) while

(kp) weighting factor is used for power order compensation. Sharing of excess power order value to avoid overloading any of the substations is done using the weighting factor to fulfill $\sum K_q=1$.

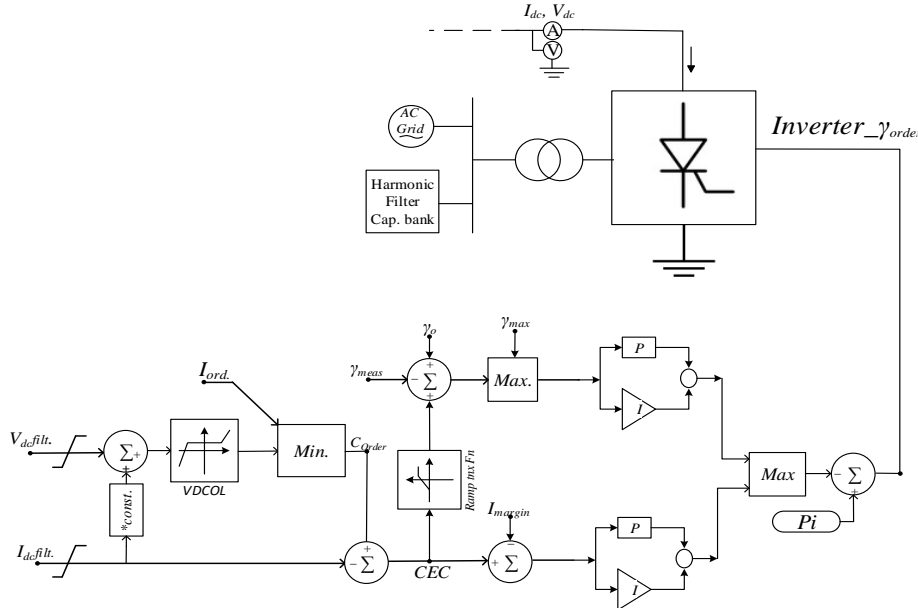


Figure 2.3: Voltage controller

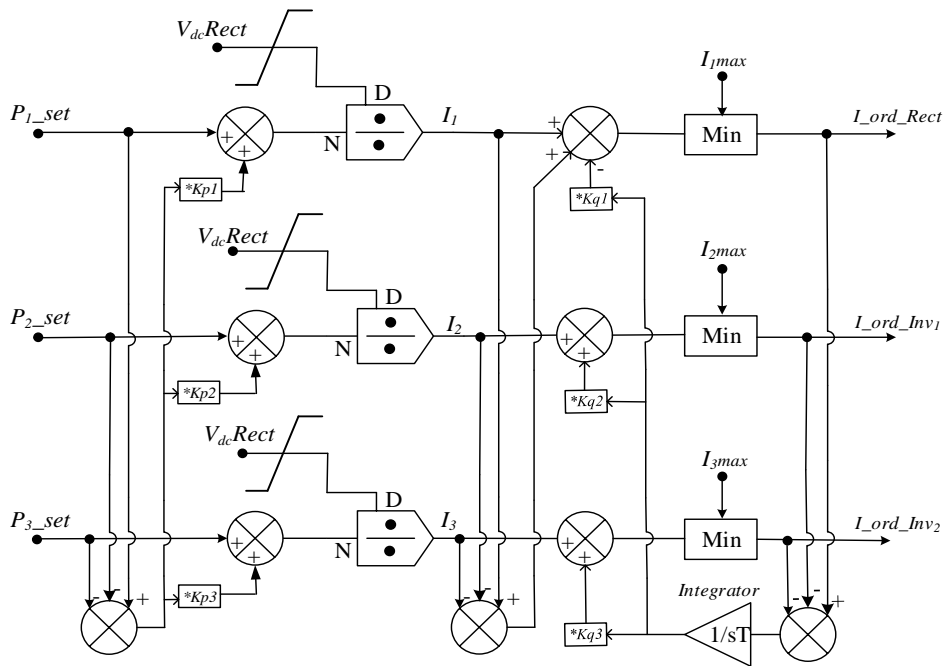


Figure 2.4: Master controller with current balancer

The parallel MTDC system has a fixed voltage polarity. The direction of power flow for each substation depends solely on the current polarity. In order to avoid a change in the voltage polarity, the sum of the inverter reference current is slightly lower than the rectifier reference current. This controller performs the task of assigning this imbalance into one substation with an effective reference current balancer. This, in turn, defines the entire system voltage level [5].

2.3 ESCR ANALYSIS

ESCR analysis is used in the AC/DC system interaction to determine the strength of the AC network SCR to the DC power rating (P_{dc}) of a converter. A weak AC system can be termed as one that has high short circuit impedance with low mechanical inertia.

Equation (2.1) – (2.2) from Figure 2.5 use Thevenin equivalent impedance to calculate the short circuit level of an AC system. This, when divided with rated DC power, gives the short circuit ratio of AC/DC system.

When the reactive power generator and harmonic filters connected to the AC side of the HVDC links are considered, the ESCR of the entire AC/DC line governed by (2.3) is obtained. The harmonic filters behave like shunt capacitors at a fundamental frequency, thereby reducing the grid strength by injecting too much reactive power into the AC network during a disturbance. This tends to increase the Thevenin equivalent impedance at the fundamental frequency of the AC system.

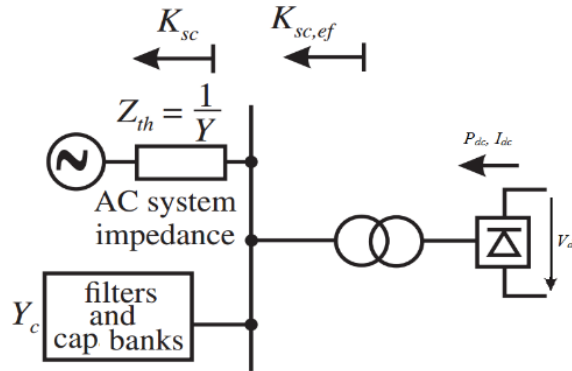


Figure 2.5: AC/DC system interconnection

$$SCL = \frac{V_{ac}^2}{Z_{Th}} \quad (2.1)$$

$$SCR = \frac{SCL(MVA)}{P_{dc} (MW)} = \frac{V_{ac}^2}{P_{dc} Z_{Th}} \quad (2.2)$$

$$ESCR = \frac{SCL - (Q_f + Q_a)}{P_{dc}} = \frac{V_{ac}^2}{P_{dc} Z_{Th}} \quad (2.3)$$

Where Q_f (in MVAR) is the reactive power contribution from the harmonic filters at a fundamental frequency, and Q_a (in MVAR) is the reactive power of any additional shunt capacitors connected to the converter station.

Using the active power (MW) rating of HVDC link, a power utility can estimate the SCR value of their networks at the initial stage of planning. The worst case of SCR has to be used in implementing the AC/DC network converters. AC system strength in relative to DC power transmitted is indicated in Table 2.2 [17].

Table 2.2: SCR Indicator For AC/DC Networks Strength

SCR value	Effect on AC/DC network
$SCR > 3$	Strong grid with little or no fault occurrence
$2 < SCR < 3$	Intermediate grid strength require voltage control ability like functional OLTC or static VAR compensator
$SCR < 2$	A weak network that requires a strong VAR generator, like synchronous condenser or STATCOM

Most MTDC schemes that are currently in service are designed to operate normally at a point lower than the MAP, say at point (i_n), due to their constant extinction angle (γ), though can be varied between 15° to 18° .

HVDC operation is better understood using the quasi-steady-state curve. The converter valve rating is used in limiting the current rating of the converter. At constant voltage, by varying DC current (i_d) in Figure 2.6, the steady-state characteristics are calculated using this quasi curve. Any change in the DC current will bring about a corresponding change in the active power of the converter valve.

Unless changes are made to the system condition, increasing extinction angle (γ) can bring about an increase in active power. However, it will be below the maximum power curve and not above. Thus, for a given system impedance, system voltage, or any other network data in Figure 2.7, there will be a unique Pd–Id characteristic which will represent the maximum power curve [17], [18].

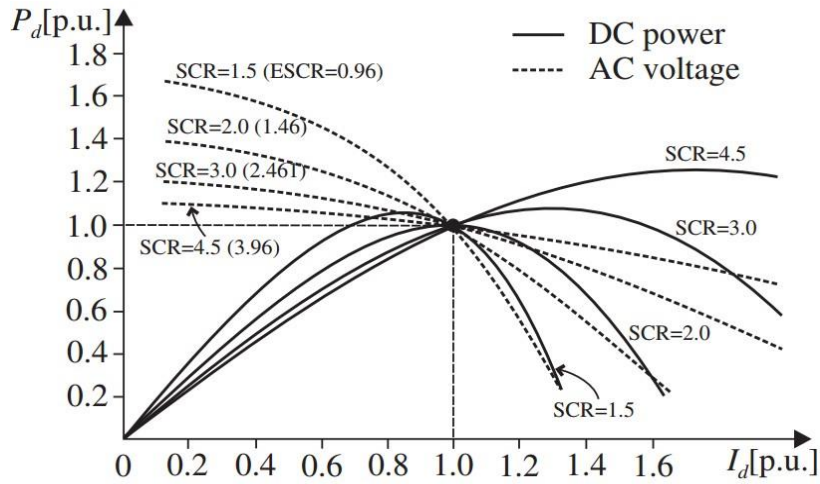


Figure 2.6: Active power – DC current characteristic with respect to SCR level

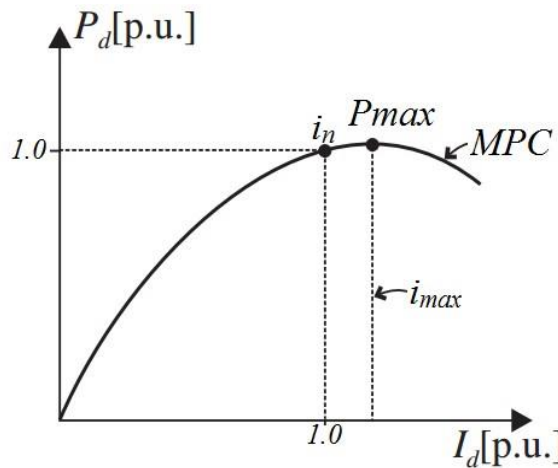


Figure 2.7: Maximum Available Power based on Pd-Id characteristics

2.4 SIMULATION RESULT

In order to test the MTDC network under transient conditions, a three-phase short circuit to ground fault was applied on the AC side of *Inv-1*, (the inverter with the highest rating, yet with a low SCR of 2.5) for 100 ms. The simulation results show the DC voltage, current, and mode switch of the MTDC converter systems during the fault condition. The simulation results were plotted using MATLAB.

DC voltage for the three converters (*Rect.*, *Inv1*, *Inv2*) is presented in Figure 2.8; the fault was applied at 1 s of simulation time, DC voltage for the three converter dips down to -350 kV, a situation which caused a change in the direction of power flow as seen in the active power plot of Figure 2.10. Being a parallel MTDC configuration, on constant DC voltage operation, only a change in the direction of current flow can permanently lead to a change in the direction of power flow. The system was able

to regain its healthy steady-state condition after the fault had been cleared, with less impact of commutation failure on the AC side. Figure 2.9 shows the DC current for the three MTDC converter that has been used, although less than each converter rated current (I_{max}). This was done to avoid overloading the converters above the maximum power curve. The rectifier is capable of handling 4 kA current while Inverter 1 and Inverter 2 can handle 2.2 kA and 1.8 kA respectively. A few oscillations can be observed on active power flow in Figure 2.10; this is a result of the VDCOL trying to readjust the system condition to allow minimum current to pass through each converter during fault time. These oscillations were quickly damped out with the help of smoothening reactors and filters on the DC side of the converter. The current order ($I_{dc}/2$) has been used to control the power transfer.

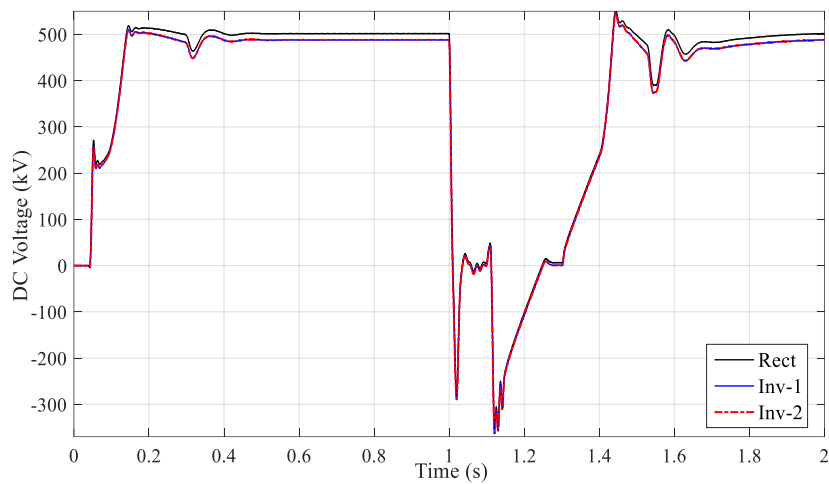


Figure 2.8: DC voltage (kV)

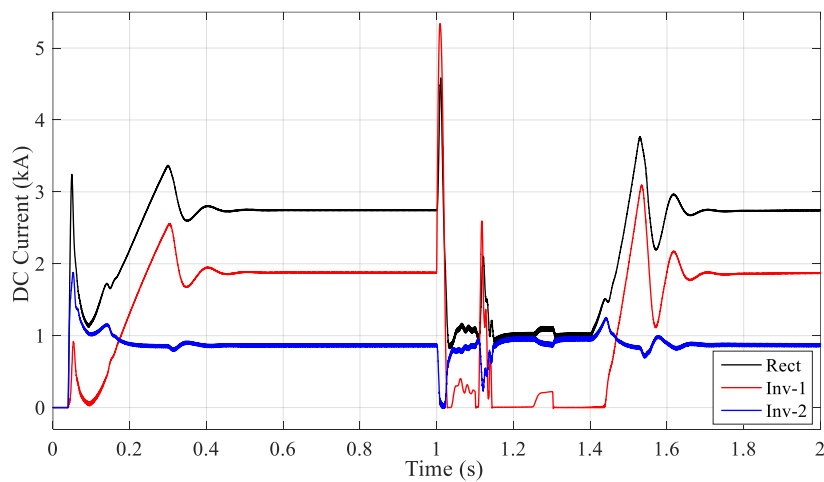


Figure 2.9: DC current (kA)

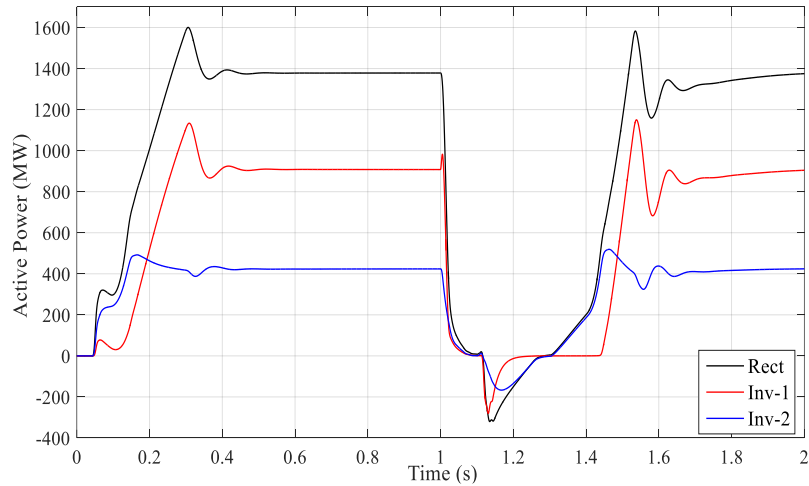


Figure 2.10: Active power (MW)

Per-unit value of the RMS voltage of this network is shown in Figure 2.11. The results show that when the fault is applied at the AC terminal of INV-1, the terminal voltage of INV-1 dipped to 0.03pu. The terminal voltages of RECT and INV-2 substation were slightly affected as the former experience a small increase while the latter decrease (though within an acceptable range) in RMS voltage during fault period. The results thus show the ability of this MTDC system control to withstand the effect of fault in transferring into the AC side of the healthy system.

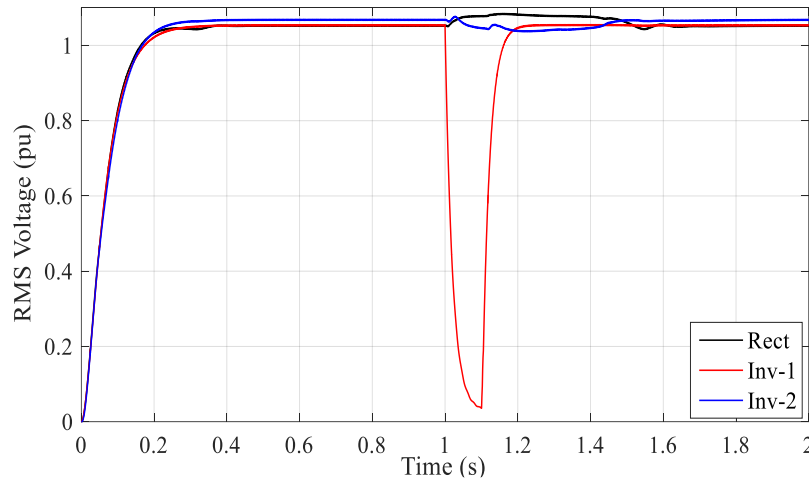


Figure 2.11: Per-unit RMS voltage

2.4.1 Effect of AC Fault on Converter 1 (Rect)

Three-phase voltage for the rectifier station can be seen in Figure 2.12. In the RMS voltage, a slight increase can be seen when the fault is applied. The system maintained a stable steady-state value after the fault. Rectifier firing angle ($\alpha \approx 15.17^\circ$) is represented in Figure 2.13, showing a slight increase

during the fault period.

2.4.2 Effect of AC Fault on Converter 2 (Inv-1)

The three-phase voltage for inverter 1 can be seen in Figure 2.14, showing that the voltage collapsed during a fault, but after the fault has been cleared, the three-phase voltage was restored to its original value. This change in the three-phase voltage following the fault has been achieved with the help of the VC mode of the Inverter 1. The extinction angle, showing the switching mode at 1 sec simulation time, can be seen in Figure 2.15.

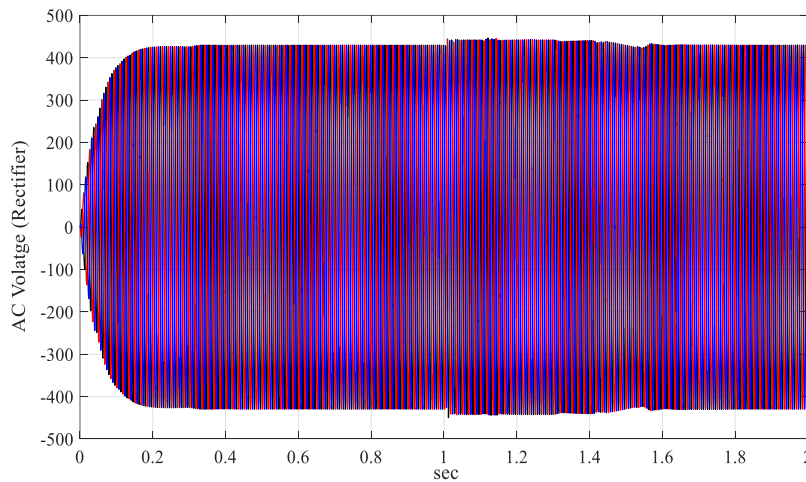


Figure 2.12: Rectifier AC voltage (kV)

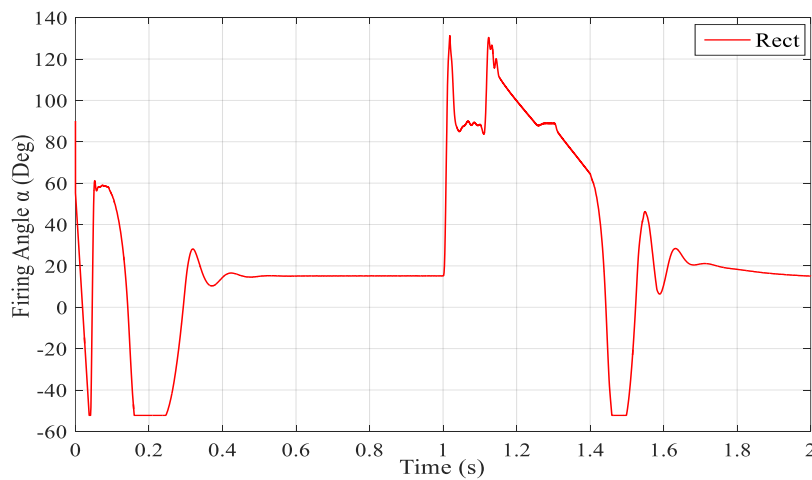


Figure 2.13: Rectifier firing angle (α)

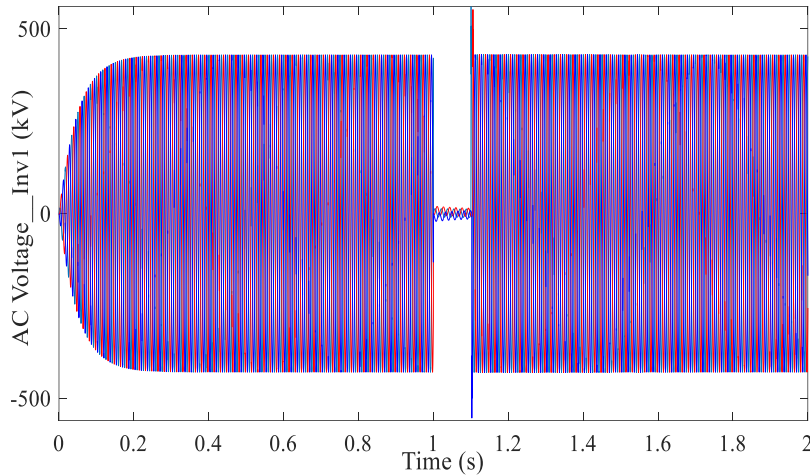


Figure 2.14: Inverter-1 AC voltage (kV)

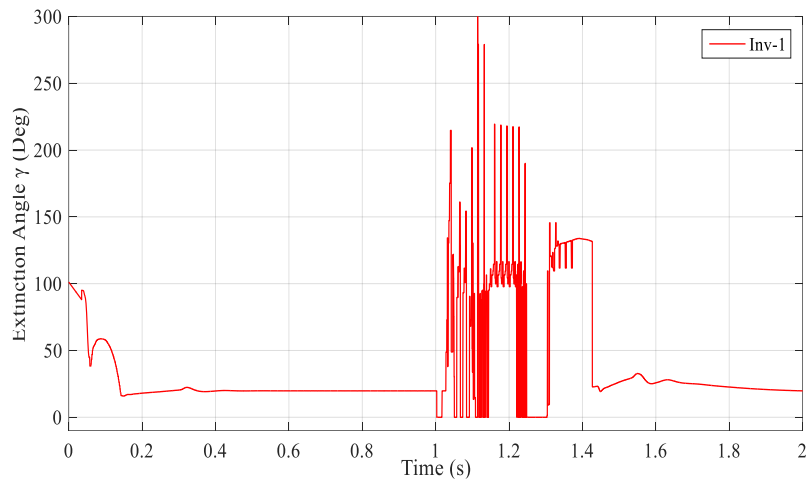


Figure 2.15: Extinction angle for Inverter 1

The ignition angle generated in Figure 2.16 can be obtained either from the voltage control (VC) or current control (CC) mode of the inverter controller. The controller is modelled to select the highest value coming from these two and then subtracted from π , which was fed as the firing angle for the inverter. This value, as seen in Figure 2.16, is kept at a minimum to reduce reactive power consumption by this inverter and also to fasten system recovery from fault.

2.4.3 Effect of AC fault on converter 3 (Inv-2)

Figures 2.17 and 2.18 show the extinction angle and the firing angle for inverter 2 experiences a few oscillations during the fault. However, the control system was able to return both angles to steady-state condition after the fault has been cleared.

Due to the low impact of fault, the results have shown that inverter 2 has remained in current control mode, as shown in Figure 2.19. However, if a three-phase fault to the ground is applied to one of the AC terminals, this would have caused the voltage to drop, and the controller would have switched to VC mode.

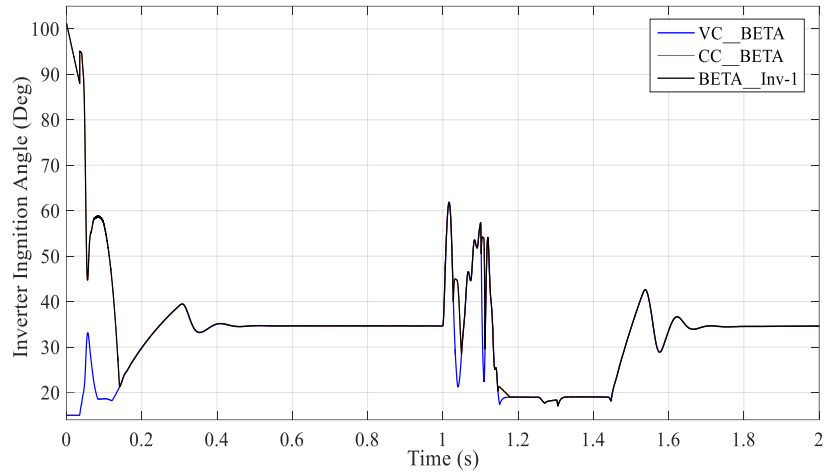


Figure 2.16: Inverter 1 ignition angle

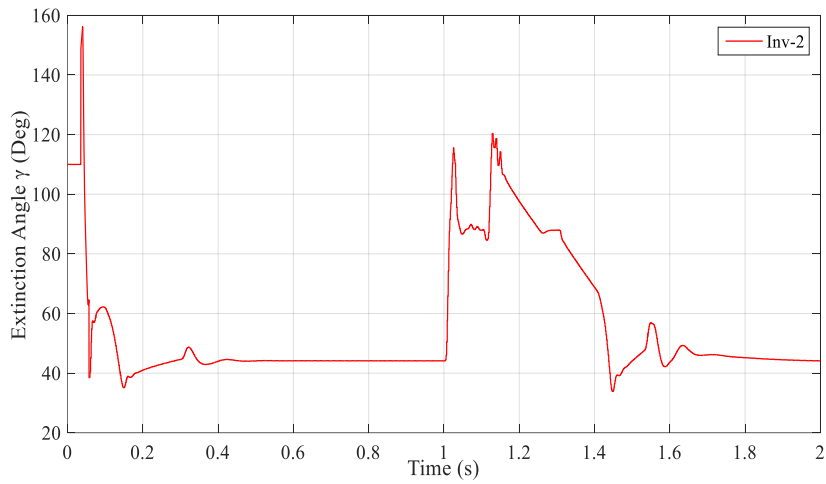


Figure 2.17: Inverter 2 Extinction angle (γ)

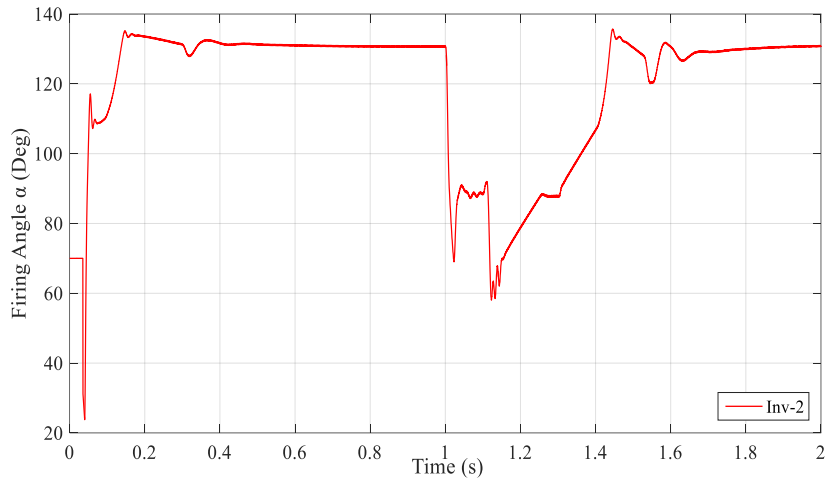


Figure 2.18: Inverter 2 firing angle (α)

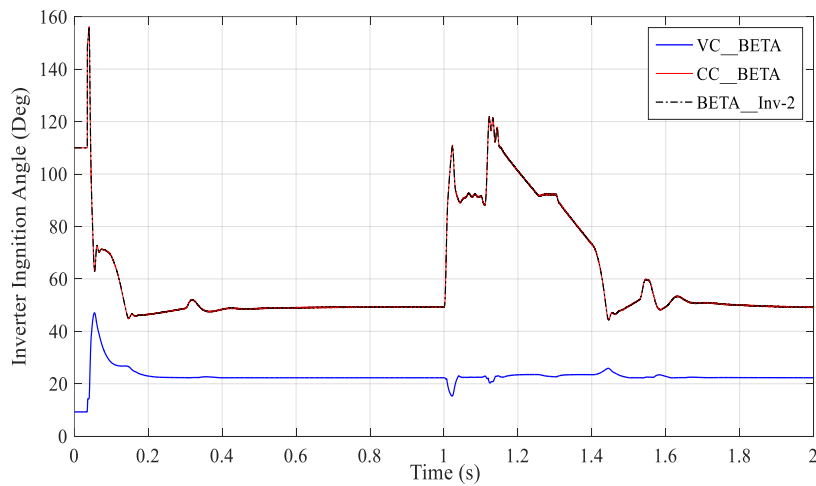


Figure 2.19: Inverter 2 ignition angle

2.5 CONCLUSION

This paper has presented the modelling of a MTDC system on PSCAD. In order to validate this MTDC model under transient conditions, a fault was applied on the AC side of Inv-1. The results have shown that when a disturbance is applied on the AC side of Inv-1, the MTDC system experiences large transient overcurrent and non-severe commutation failures. This has caused the DC voltage at the faulted inverter station 1 to experience voltage dip, and the DC current diverted to inverter 2. The large overcurrent observed in this research study was due to the fault contribution from all the converters in the MTDC system, which was lower than in the two-terminal configurations. Such types of fault require more clearing time in order to prevent the system from subsequent commutation failure due to adverse transient mode shift of the inverter controller.

As applicable to two-terminal HVDC links, the same DC line protection can be used to detect DC line fault and clear it. The MTDC system's robustness from fault conditions requires careful design and control as it requires smooth and quick recovery, and the converter valves must not be blocked for faster recovery unless such recovery causes a cascading effect on the connected AC system.

AC system fault levels need to be incorporated into the system planning and design of the MTDC network. With proper planning, advances in semiconductor devices, and reduce the cost of HVDC networks, LCC MTDC can be used for bulk power transmission and multiple points of connection.

2.6 ACKNOWLEDGMENT

The authors wish to thank the Eskom Power Plant Engineering Institute Specialization Centre for HVDC and FACTS for their support.

2.7 REFERENCES

1. N. Balu, P. Krishnayya, D. Chapman, F. Alvarado, R. Lasseter, and J. Reeve, "Multiterminal HVDC Control Models for Evaluating Power Transfer Capability in Combined AC-DC Systems," in CIGRE International Conference on Large High Voltage Electric Systems, Paris, 1986.
2. P. Krishnayya, S. Lefebvre, V. Sood, and N. Balu, "Simulator study of multiterminal HVDC system with small parallel tap and weak AC systems," IEEE transactions on power apparatus and systems, pp. 3125-3132, 1984.
3. X. Yang, C. Yuan, D. Yao, C. Yang, and C. Yue, "Dynamic performance of series multiterminal HVDC during AC faults at inverter stations," in Power Electronics and Applications (EPE'14-ECCE Europe), 2014 16th European Conference on, pp. 1-9, 2014.
4. J. Reeve, "Multiterminal HVDC power systems," IEEE Transactions on Power Apparatus and Systems, pp. 729-737, 1980.
5. J. P. Bowles, G. Liss, C. J. B. Martin, and E. RUMPF, "Control in HVDC Systems; The state of the art. Part II: Multiterminal Systems," in Cigre International Conference on Large High Voltage Electric Systems, Paris, 1980.
6. R. Joetten, T. Wess, and D. Woodford, "On the Control of a Multiterminal HVDC System having also Weak Inverter Stations," Cigre Working Group 02 of study committee 14, ELECTRA 171, 1997.

7. M. Hadjikypris and V. Terzija, "Transient fault studies in a multiterminal VSC-HVDC grid utilising protection means through DC circuit breakers," in IEEE PowerTech (POWERTECH), pp. 1-6, 2013.
8. V. Sood, V. Khatri, and H. Jin, "EMTP Modelling of CIGRE Benchmark Based HVDC Transmission System Operating with Weak AC systems," in Proceedings of the International Conference on Power Electronics, Drives and Energy Systems for Industrial Growth, pp. 426-432, 1996.
9. M. Faruque, Y. Zhang, and V. Dinavahi, "Detailed modeling of CIGRE HVDC benchmark system using PSCAD/EMTDC and PSB/SIMULINK," IEEE transactions on power delivery, vol. 21, pp. 378-387, 2006.
10. ElMehdi, A. Momen, and B. K. Johnson, "Dynamic reactive compensation requirements at the rectifier end of an LCC HVDC link connected to a weak AC system," in North American Power Symposium (NAPS), pp. 1-6, 2014.
11. R. L. Vasquez-Arnez, J. A. Jardini, and M. T. Bassini, "Dynamic Performance of Line Commutated Converter-Based Multiterminal HVDC Systems," Przegląd Elektrotechniczny, vol. 91, pp. 247-253, 2015.
12. G. Chunyi, Z. Yi, A. Gole, and Z. Chengyong, "Analysis of dual-infeed HVDC with LCC-HVDC and VSC-HVDC," in IEEE Power and Energy Society General Meeting (PES), pp. 1-6, 2013.
13. L. Yan and C. Zhe, "A Flexible Power Control Method of VSC-HVDC Link for the Enhancement of Effective Short-Circuit Ratio in a Hybrid Multi-Infeed HVDC System," IEEE Transactions on Power Systems, vol. 28, pp. 1568-1581, 2013.
14. Z. Liu, Ultra-High Voltage AC/DC Grids: Academic Press, 2014.
15. L. Bergstrom, L.-E. Juhlin, G. Liss, and S. Svensson, "Simulator study of multiterminal HVDC system performance," IEEE Transactions on Power Apparatus and Systems, pp. 2057-2066, 1978.
16. O. E. Oni, K. N. I. Mbangula, and I. E. Davidson, "A Review of LCC-HVDC and VSC-HVDC Technologies and Applications," in Proceedings of the 16th IEEE international Conference on Environment and Electrical Engineering, Florence, Italy, 2016.
17. M. Eremia, C.-C. Liu, and A.-A. Edris, Advanced Solutions in Power Systems: HVDC, FACTS, and Artificial Intelligence vol. 52: John Wiley & Sons, 2016.
18. Gavrilovic, P. Krishnayya, and C. Peixoto, "Interaction between DC and AC Systems," in CIGRE Symposium on AC/DC interactions Boston, 1987.

CHAPTER 3: IMPACT OF LCC–HVDC MULTITERMINAL ON GENERATOR ROTOR ANGLE STABILITY

PAPER FIVE

This chapter addresses objective two and is presented in a manuscript format. It has been published in the International Journal of Electrical and Computer Engineering; Feb 2020: Vol. 10 (1), pp. 22-34. DOI:10.11591/ijece.v10i1.pp22-34.

Impact of LCC–HVDC multiterminal on generator rotor angle stability

Abstract: Multiterminal High Voltage Direct Current (HVDC) transmission utilising Line Commutated Converter (LCC-HVDC) technology is on the increase in interconnecting a remote generating station to any urban centre via long-distance DC lines. This Multiterminal-HVDC (MTDC) system offers reduced right-of-way benefits, reduction in transmission losses, as well as robust power controllability with enhanced stability margin. However, utilising the MTDC system in an AC network bring about a new area of associated fault analysis as well as the effect on the entire AC system during a transient fault condition. This paper analyses the fault current contribution of an MTDC system during transient fault to the rotor angle of a synchronous generator. The results show a high rotor angle swing during a transient fault and the effectiveness of fast power system stabiliser connected to the generator automatic voltage regulator in damping the system oscillations. The MTDC link improved the system performance by providing an alternative path of power transfer and quick system recovery during transient fault, thus increasing the rate at which the system oscillations were damped out. The results show a significant improvement compared to when power was being transmitted via AC lines.

Keyword: Short circuit Ratio, Transient stability, MTDC system, Thyristor converters, Voltage-Dependent Current Order Limiter (VDCOL)

3.1 INTRODUCTION

An increase in demand for electricity has brought Southern African power utilities into planning to expand their transmission corridor utilising Multiterminal High Voltage Direct Current (HVDC) Transmission. This Multiterminal–HVDC (MTDC) is not only key in the integration of renewable energy such as wind farms and solar parks, but also the deployment of distributed generators into the grid. It is also important for large-scale interregional power transmission [1]. This will help bring about a smart, eco-friendly, and decentralised power system. Being a region with relatively weak interconnections and high susceptibility to a transient fault, the proper analysis needs to be made to give power system planners and engineers seeking to utilise this MTDC system more understanding of the impact on

generator rotor angle stability. Major setbacks of excessive usage of HVDC systems are the concern associated with the reliability and interaction with AC networks, in which the generator is a major recipient [2, 3]. During a system fault, the generator loses a large amount of power, and this impacts the entire interconnected system as well as other connected synchronous machines.

MTDC system can adopt either thyristor converter technology (LCC-HVDC) or the Insulated Bipolar Junction (IGBTs) Voltage Source Converter (VSC-HVDC) technology [4, 5]. While VSC provides AC networks with robustness and full controllability of AC active and reactive power, but the capacity of the available solid-state devices with turn-off capability is limited and still requires specially configured Direct Current (DC) breakers to isolate the converter during a DC line fault [6]. Unlike VSC HVDC, research studies have shown that the LCC HVDC system is less susceptible to DC line fault with the use of conventional DC line protection and rugged controller [7-9]. This converter technology has the capabilities of withstanding high power and voltage ratings for bulk power transmission. Although with obstacles such as; reactive power consumption and cases of commutation failure during a fault, however, this technology still has the largest footprint with many point-to-point installations and three MTDC links around the globe. An example is the 1920 MW, ± 533 kV Cahora Bassa point to point interconnection linking Mozambique and South Africa; while that of MTDC are the 8 GW North-East Agra system (four terminals in three converter stations), 300 MW, 200 kV Sardinia-Corsica-Italy system, and the 2,000 MW, ± 450 kV Hydro Québec–New England system [10-13].

Research on LCC HVDC shows that the stability level depends predominantly on the Effective Short Circuit Ratio (ESCR) of the AC grid [14-16]. The first impact is seen in the frequent occurrence of commutation failure at the inverter station during any system disturbances leading to power oscillations of the synchronous generator, which can further lead to total system collapse due to the inability of the converter station to recover from the disturbances. Power systems are often subjected to different degrees and severities of faults as a result of occurrences such as; adverse weather conditions leading to loss of transmission line, flashover discharge, or sudden loss of load, etc. There is a need for power system planners to carry out a selected set of contingencies analysis on the system for proper design and smooth-running operation of the system. The entire system is said to be transiently stable when it has the ability to maintain synchronism when subjected to a transient disturbance

[17, 18].

The long-established method of addressing transient stability has been by using an Automatic Voltage Regulator (AVR), which helps in controlling the electromagnetic torque of the synchronous generator. The excitation system with Power System Stabilizers is also added to offer a quick response in adjusting the field current supplied during fault to match the generator capability [19, 20]. Different FACTS devices such as Static Synchronous Compensator (STATCOM), Static Var Compensator (SVC), Thyristor Controlled Series Compensator (TCSC), capacitor banks, etc. were discussed in [21, 22] as other means of enhancing power system stability. Kenné et al. in [23] proposed an adaptive nonlinear excitation control for fast response and damping out of oscillations during a transient disturbance on the synchronous generator. Also, Oni and Mbangula in [2, 8, 24] observed that a point-to-point HVDC scheme gives an enhanced critical clearing time when integrated into an AC network, which in turn improves the generator rotor angle as well as the entire voltage profile. A report on MTDC state of the art control strategy and converter architecture was given in [25]. Jiang and Ekstrom in [26] gave an analysis of LCC MTDC systems in reducing the impact of a ground fault on sub-transmission and distribution networks. They focused on the converter response of the MTDC link neglecting the synchronous generator response of the AC network. Vasquez-Arnez et al. in [27] cover both the converter response as well as the synchronous generator response in their analysis of dynamic modelling of LCC–MTDC system in an AC network but failed to consider the AC network strength using Short Circuit Capacity (SSC) with regards to the entire network stability margin, and its effect on the interconnected synchronous machine.

In order to enhance the transient stability margin of an AC network, this paper gives the performance evaluation of a three-terminal HVDC model implemented on a Single Machine Infinite Bus (SMIB) network, and results were obtained through simulations analysis on PSCAD. Two case studies were considered; the first scenario involved using MTDC system in parallel with AC line to interconnect the infinite bus with the synchronous generator, while the second scenario involved replacing the MTDC link with another AC line to make a double AC transmission circuit linking the synchronous generator with the infinite bus. The results of which were analysed to determine which system helped in alleviating the effect of the three-phase short circuit fault on the synchronous generator. An improvement of incorporating a voltage controller into two of the converter stations, preferably the

inverters, was also implemented. The Short Circuit Ratio (SCR) of the AC network and the control setup of the DC converters to avoid reoccurring commutation failure during the modelling of the MTDC link were all taken into consideration. The fault current contribution of each converter with respect to the interconnected AC synchronous generator has been analysed. The power swing equation using equal area criterion was used in analysing the maximum power transfer and the fault clearing angle to allow the generator damper and protection circuit to work effectively in stabilising the entire system.

The organisation of the paper follows section 2 analysing the short circuit ratio and short circuits level of the AC networks, while section 3 gives the generator AVR modelling and control. Section 4 gives the rotor angle stability analysis of the synchronous machine using equal area criterion. The system model and system parameters are presented in section 5, while section 6 gives the results and discussion. Section 7 finally presents the conclusion and contributions.

3.2 ESCR ANALYSIS

The ESCR analysis is used in the AC/DC system interaction to determine the strength of the AC network. The ratio of SC to the DC power rating (P_{dc}) of a converter gives the SCR of an AC/DC interconnection. A weak AC system can be termed as a system with high short circuit impedance and low mechanical inertia.

Equations (3.1) – (3.2) from Figure 3.1 use the Thevenin equivalent impedance to calculate the short circuit level SCL of an AC system. When the SCL of the system is divided with rated DC power, the short circuit ratio of AC/DC system is obtained [28].

When the reactive power generator and harmonic filters connected to the AC side of the HVDC links are considered, the ESCR of the entire AC/DC line governed by (3.3) is obtained. The harmonic filters behave like shunt capacitors at the fundamental frequency, thereby reducing the grid strength by injecting too much reactive power into the AC network during a disturbance [29]. This tends to increase the Thevenin equivalent impedance at the fundamental frequency of the AC system.

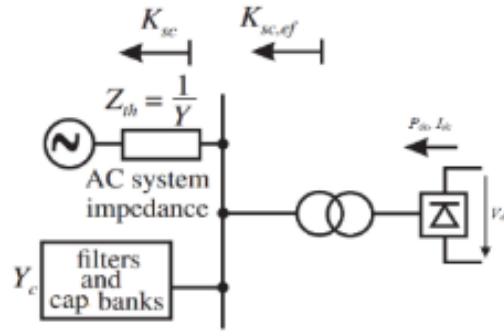


Figure 3.1: AC/DC system interconnection

$$SCL = \frac{V_{ac}^2}{Z_{Th}} \quad (3.1)$$

$$SCR = \frac{SCL(MW)}{P_{dc}} = \frac{V_{ac}^2}{P_{dc}Z_{Th}} \quad (3.2)$$

$$ESCR = \frac{SCL - (Q_f + Q_a)}{P_{dc}} \quad (3.3)$$

Where Q_f (in MVAR) is the reactive power contribution from the harmonic filters at the fundamental frequency, and Q_a (in MVAR) is the reactive power of any additional shunt capacitors connected to the converter station.

Using the active power (MW) rating of the HVDC link, a power utility can estimate the SCR value of the networks at the initial stage of planning. The worst case of SCR has to be used in implementing the AC/DC network. AC system strength in relative to DC power transmitted is indicated in Table 4.1 [28].

Table 3.1: SCR value and the AC/DC networks strength

SCR value	Effect on AC/DC network
$SCR > 3$	These values of SCR signify a grid with low impedance. The rate of occurrence of commutation failure is very low.
$2 < SCR < 3$	Intermediate grid strength, require voltage control ability like functional OLTC or static VAR compensator for the improvement of this type of grid.
$SCR < 2$	Weak grid that requires a strong VAR generator, like synchronous condenser or STATCOM

Most MTDC schemes that are currently in service are designed to operate normally at a point lower than I_{max} (maximum rated current of the converters), say at point ($i_n=1.0p.u.$), due to their constant extinction angle γ (the margin of commutation) that can be varied between 15° to 18° . Unless changes are made to the system condition, an increasing extinction angle (γ) can bring about an increase in active power. However, the increase must be below the maximum power curve and not above. Thus, for a given system impedance, system voltage, or any other network data in Figure 3.2, a definite value of SCR will bring about a unique P_d - I_d characteristic that will represent the maximum power curve.

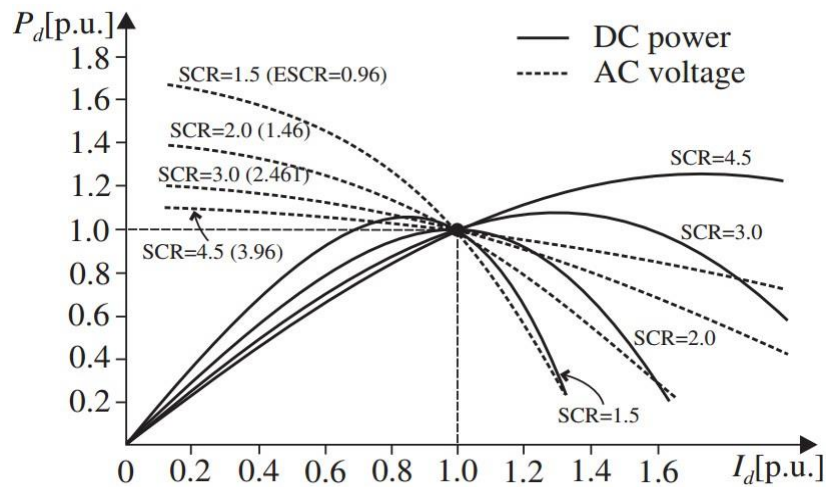


Figure 3.2: Active power – DC current characteristics with respect to SCR level

3.3 GENERATOR MODELLING AND CONTROL

Synchronous generator control model consists of the excitation system, Power System Stabilizer (PSS), and the generator itself. Generating plants are equipped with an Automatic Voltage Regulator (AVR) in order to maintain generator stator voltage. The excitation system used in this model is the bus-fed thyristor type that includes a PSS and an AVR [30]. It is also equipped with an Under-Excitation Limiter (UEL) and Over Excitation Limiter (OEL). The UEL prevents loss of synchronism when the excitation voltage falls below the reference level, and the OEL helps to prevent the generator from overheating during long-term excitation overcurrent [22, 31, 32].

Figure 3.3 shows the PSS connected to the exciter. The shaft speed from the generator is fed into the PSS, which is in turn used in damping out oscillations during power system disturbance.

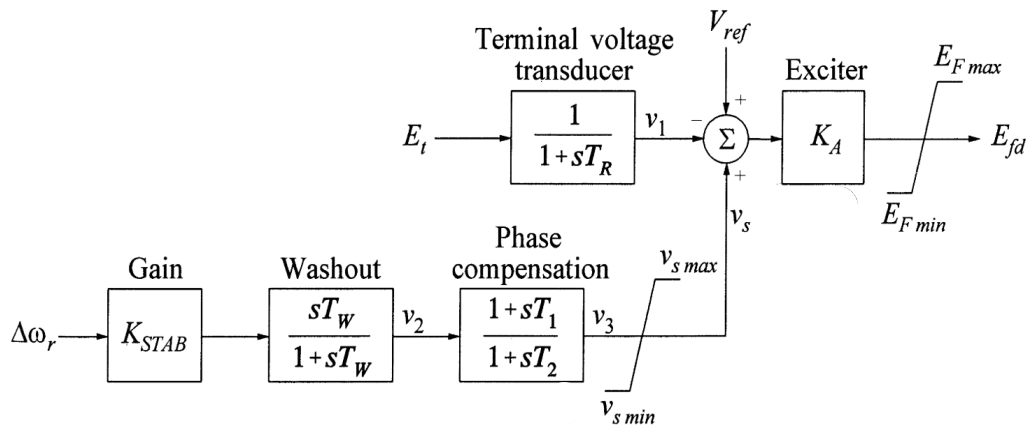


Figure 3.3: IEEE ST4A excitation system with AVR and PSS1A stabiliser

3.4 ROTOR ANGLE STABILITY

The Single Machine Infinite Bus (SMIB) system in Figure 3.4 [30] consists of a synchronous generator with a constant field voltage, linked to an infinite bus with constant frequency and voltage magnitude via two transmission lines. The equivalent system equation is given in (3.4, 3.5), where P_e is the terminal Power, X_l is the total line reactance. P_e equals

P_{max} at $\delta=90^\circ$, corresponding to maximum power transfer during steady state. Following a three-phase to ground fault on any of the transmission lines, the power transmitted by that particular faulted line drops to zero, and hence P_m will be higher than P_e , leading to an increased rotor angle (δ). The swing equation in consideration to the inertia constant H and the change in angular speed ω_o is given in equation (3.6). Integrating (3.7) gives equation (3.8), thus for a stable operation, the deviation of rotor angle δ must be bounded, i.e., the speed deviation must become zero to give the criterion for stability in equation 3.9 [30].

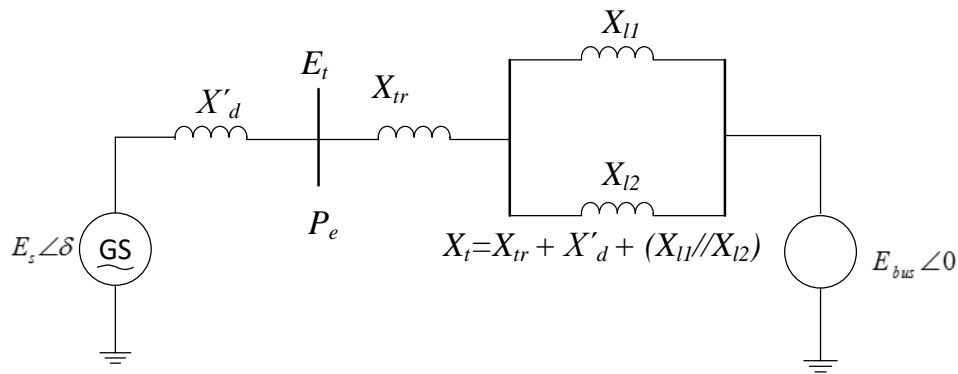


Figure 3.4: Equivalent SMIB network

$$P_e = \frac{E_G E_B}{X_t} = P_{max} \sin \delta \quad (3.4)$$

$$P_{max} = \frac{E_G E_B}{X_t} \quad (3.5)$$

$$P_m - P_{max} \sin \delta = \frac{2H}{\omega_o} \frac{d^2 \delta}{dt^2} \quad (3.6)$$

$$(P_m - P_e) \frac{\omega_o}{2H} = \frac{d^2 \delta}{dt^2} \quad (3.7)$$

$$\left[\frac{d\delta}{dt} \right]^2 = \int \frac{\omega_o (P_m - P_e)}{H} d\delta \quad (3.8)$$

$$\int_{\delta_o}^{\delta_m} \frac{\omega_o}{H} (P_m - P_e) d\delta = 0 \quad (3.9)$$

$$\int_{\delta_o}^{\delta_m} \frac{\omega_o}{H} (P_m - P_e) d\delta = 0 \quad (3.10)$$

$$\int_{\delta_o}^{\delta_1} (P_m - P_e) d\delta - \int_{\delta_1}^{\delta_m} (P_e - P_m) d\delta \leq 0 \quad (3.11)$$

$$A_1 - A_2 \leq 0 \quad (3.12)$$

Consider a three-phase short circuit fault of zero fault reactance being applied at line L2 of the SMIB network shown in Figure 3.4, and the fault is cleared by isolating the faulted line with a circuit breaker. Using the equal area criterion, a power – angle (P_e - δ) diagram used in understanding the basics relationship between the generator accelerating power and its rotor angle according to equation (10), the network conditions before (2 lines in operation), during (three-phase fault on line L2), and post-fault (line L2 out of service) was evaluated. These results will give the stability limit of the system by weighing the maximum rotor angle of the system. From Figure 3.5, during a stable operating state, the system is bounded by area A1 (abco), a fault on the system will shift the steady-state condition from point ‘a’ to point ‘b’, causing the rotor to accelerate until operating point c is reached because $P_m > P_e$, the operating point will thus shift to point b after the fault has been cleared at δ_{c1} , causing a decelerating rotor angle. The kinetic energy gained by the rotor from area A1 is then dissipated to area A2 (odef), thus shifting further the operating point from ‘d’ to ‘e’, such that δ has reached its maximum value δ_m , and if area A1 is equal to area A2, the rotor begins to decelerate, and the operating point follows the path of e to d according to P_e - δ diagram. The amplitude of the oscillations reduces with the help of a damper circuit; otherwise, it continues to oscillate with a constant amplitude [33].

However, with a prolonged fault clearing time, the clearing angle will reach δ_{c2} , the rotor angle operating point will reach point ‘e’ leading to an unexpended kinetic energy which results in a continuous increase of the rotor speed and angle ($P_e < P_m$ beyond ‘e’). This will cause the pre-fault area A1 ($abc'o'$) to be greater than post-fault area A2 ($o'd'e'$) (11), this

eventually leads to loss of synchronism [34, 35].

A simulation result of the SMIB network during the three-phase fault at circuit 2 for 0.07s is shown in Figure 3.6. This system recorded slow damping of rotor angle oscillations when the generator uses a constant field supply. AVR without PSS generator control mode witnessed a second swing instability. At the same time, the AVR with PSS generator control setup gives a positive fast damping result.

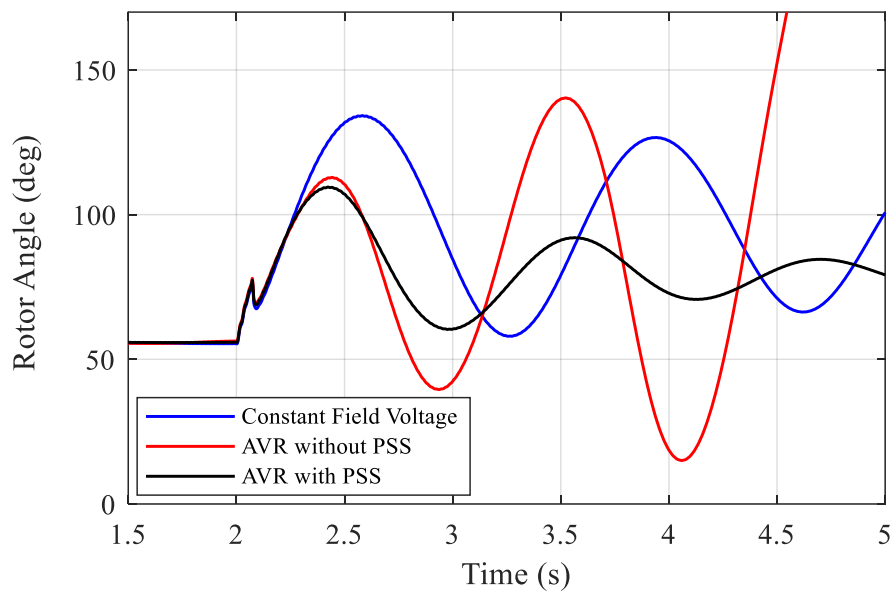


Figure 3.5: Generator Rotor Angle for SMIB system during 70ms fault

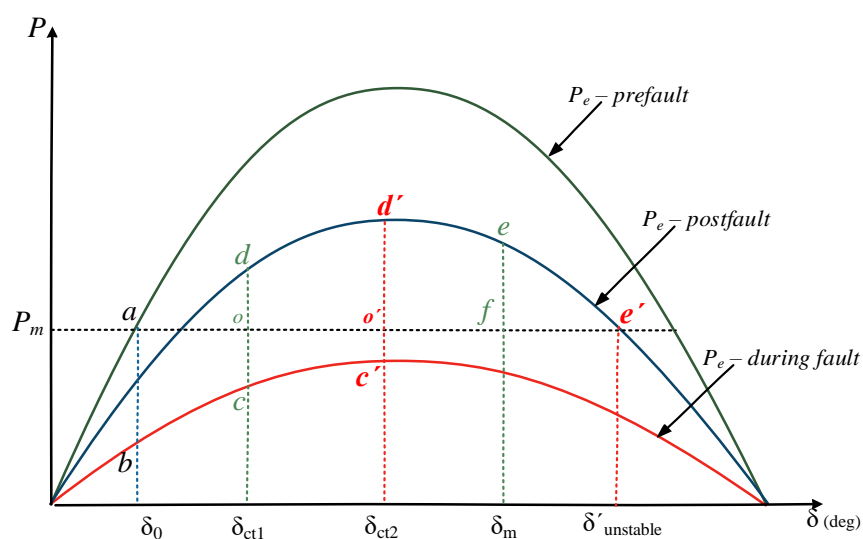


Figure 3.6: $P_e - \delta$ diagram for both stable and unstable system condition

3.5 SYSTEM MODEL

The Single Machine Infinite Bus (SMIB) system considered in the research work has the parameters of the SMIB system used in [30]. The transmission system has been extended to include a parallel three-terminal thyristor converter configuration with a parallel AC line, as shown in Figure 3.7. In order to evaluate the performance of this MTDC system on the generator transient stability, a 24 kV, 2220 MVA synchronous generator was modelled with alternator supplied exciter with $E_{f_{max}}$ and $E_{f_{min}}$ independent of the terminal voltage. The exciter was IEEE type AC4A exciter with IEEE PSS1A stabilizer for damping out oscillations during the system disturbance. Each converter's controller parameters, rated and actual power transfer, and DC line specifications are shown in Table 4.2, while the generator ratings and AC lines specifications are shown in the Appendix section (Table 4.3). The MTDC controller models used resemble that of the conventional point-to-point system, which has been discussed in [12, 25, 36] with modification made to the PI and the VDCOL control parameters to obtain the desired V-I characteristics of the converter. The rectifier converter is on current control mode, while the inverters are capable of switching between voltage control mode or current control mode based on system condition. The *INV_1* substation with extinction angle $\gamma=\gamma_o$ controls and defines the voltage level of the entire network while all other substations are in current-controlled mode. A central master controller was used for power-sharing and the current balancer between all the converters, and the rectifier station rated moderately to cater for the power transfer to both inverters.

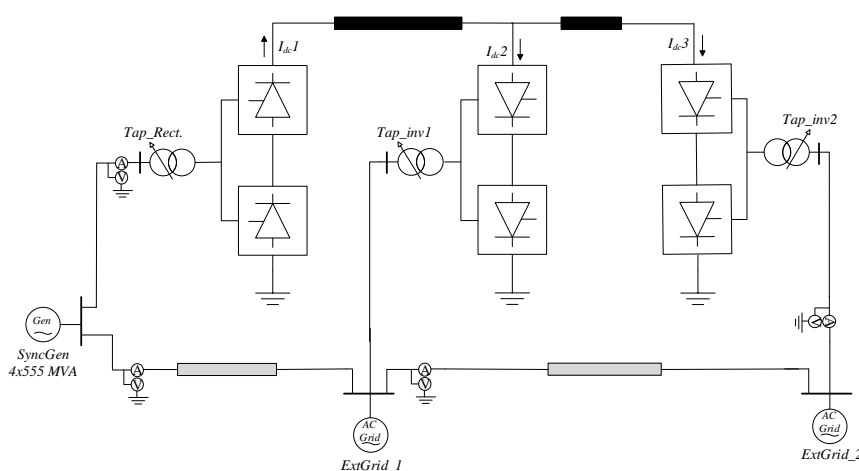


Figure 3.7: Parallel MTDC system embedded in AC Network model

3.6 SIMULATION RESULTS

To investigate the impact of MTDC system on power system rotor angle stability, a solid three-phase short circuits fault was applied at the *RECT*, *INV_1*, and *INV_2* substations one after the other, and the critical clearing time T_c was recorded. The generator power output, rotor angle, generator speed, exciter field voltage, and the synchronizing torque are the primary observation of this study. These parameters, including $P_e-\delta$ diagram, were depicted on a subplot to illustrate system performance before, during, and after the fault period. DC power, voltage, and current were also illustrated on a plot to analyse the converter current contribution during and after the fault condition of the system.

After applying fault at simulation time $t=2s$, it was found out that *INV_1* linking synchronous generator with *INV_2* has the least critical clearing time $T_c=0.081s$, while the generator bus and the *INV_2* bus has a clearing time of 0.11 s and 0.18 s respectively. Solution time steps of $50\mu s$ and channel plot step of $500\mu s$ were used in computing the results.

Figure 3.8 shows the active and reactive power output from the synchronous generator. From this plot, a disturbance on the weakest *INV_1* bus resulted in a large drop in the active power generated from 1750MW to 280MW, which result in the increase of the reactive power supplied to the system. The oscillations generated were quickly damped out with the help of the MTDC VDCOL controller, which acts as a fault minimizer. This shows that the system is transiently stable.

The DC power, current, and voltage are shown in figures 3.9 to 3.11. From Figure 3.9, the fault caused the VDCOL controller to reduce the current order to allow minimum power flow across the converter. As also seen in Figures 3.10 and 3.11, the current shoot above 5kA while the voltage dips down to -200kV; however, with VDCOL set point, the MTDC system only recorded a high current inflow due to the current contribution from the three converters but recorded no commutation failure at the two inverters.

Rotor angle dynamics can be seen in Figure 3.12 following a three-phase short circuits fault on the *INV_1* bus. A change of operating point was observed, causing the generator rotor angle δ to accelerate until it reached its maximum $\delta_{max}=175^\circ$, the point above which the systems become unstable. This can be in the second scenario where double AC transmission lines were used in replacement of the MTDC system. The generator, having yielded its excitation control and without supplementary controller support from the MTDC

link, caused the synchronous machine to lose its stability at the first swing. The generator excitation voltage in Figure 3.13 also follows the same condition of a stable operating state during MTDC link interconnection. It, however, became unstable during the second scenario of double AC circuit replacement. This caused the synchronous machine to have yielded all its controlling capability leading to the field voltage swings between its V_{Fmin} and V_{Fmax} value of -6.4 and 7.0pu respectively. This was not so when the MTDC link was in operation, as the system maintained its stability with positive damping of oscillations.

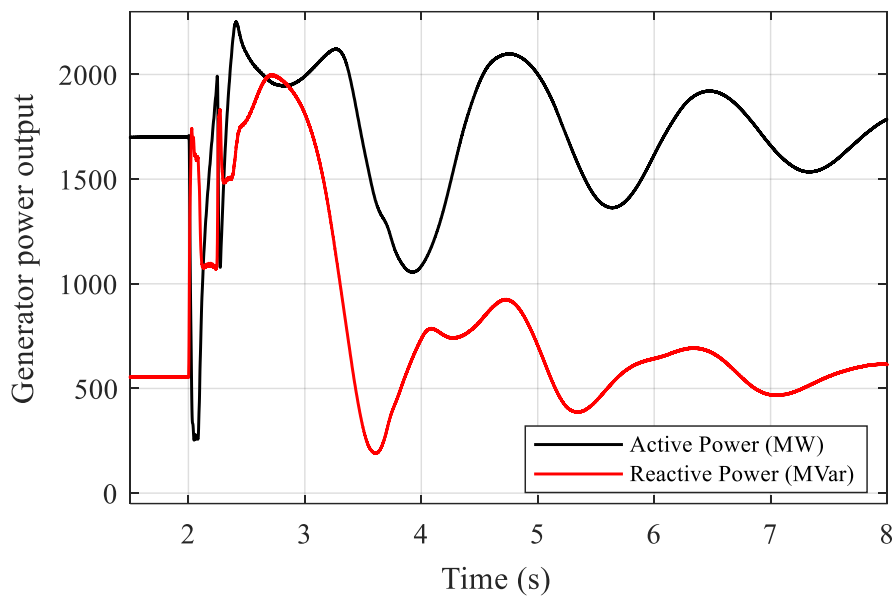


Figure 3.8: Synchronous generator power output

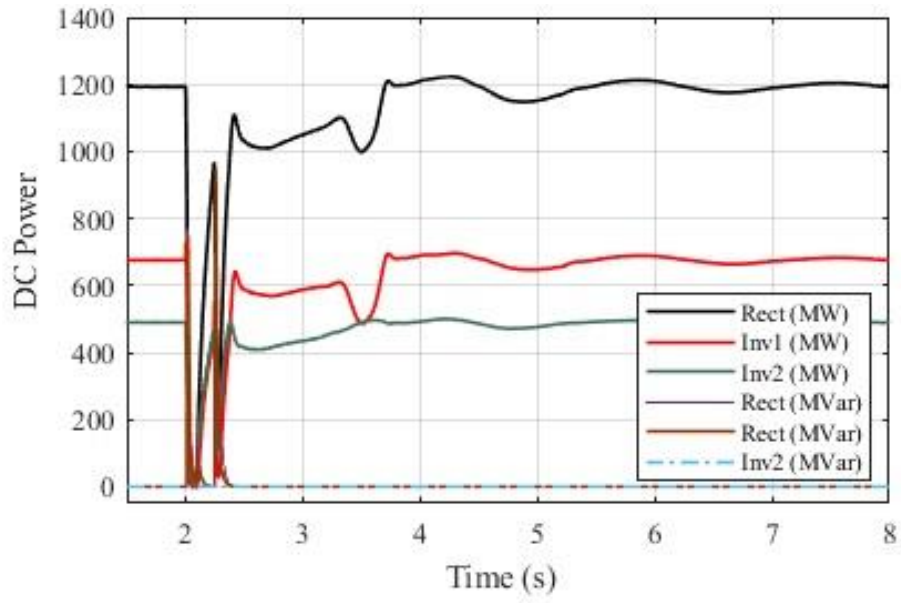


Figure 3.9: DC power across the three converters

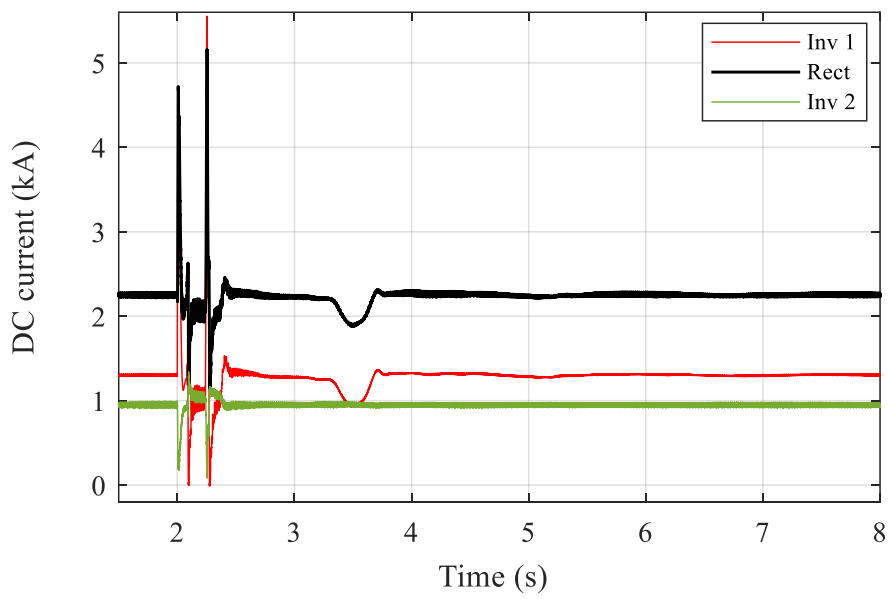


Figure 3.10: MTDC current

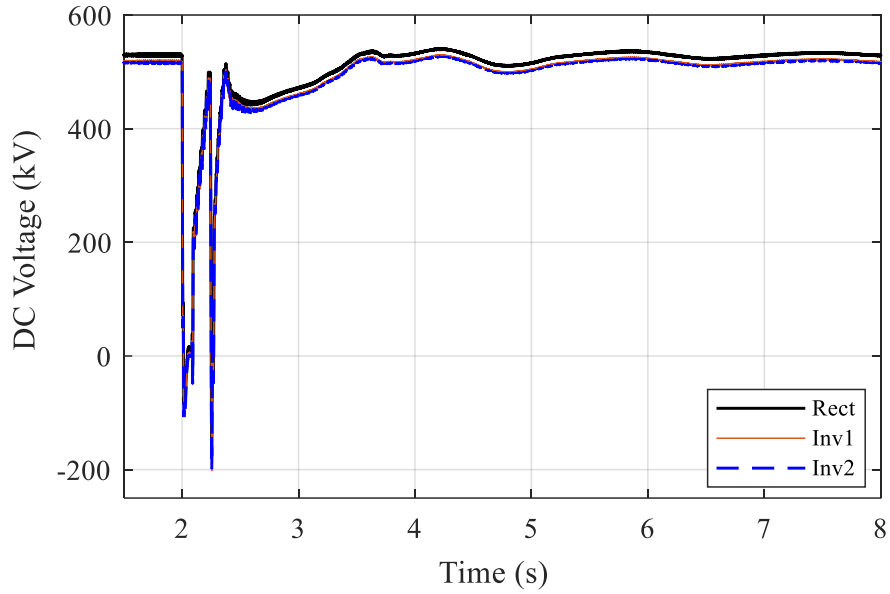


Figure 3.11: DC voltage for the three converters

The rotor angular speed in Figure 3.14 during MTDC link interconnection recorded an increase in frequency up to 380.8rad/s, and after that dipping down to 373.5 rad/s. These swings were quickly damped out from the second and subsequent oscillations of the rotor angle. The same generator angular speed experience the same disturbance with the second scenario of double AC transmission lines. This caused the generator speed to increase to 382.8rad/s which further led to unexpanded kinetic energy, which results in a continuous increase of the rotor speed and angle ($P_e < P_m$) and thus to loss of synchronism due to lack of decelerating torque to reduce the rotor speed.

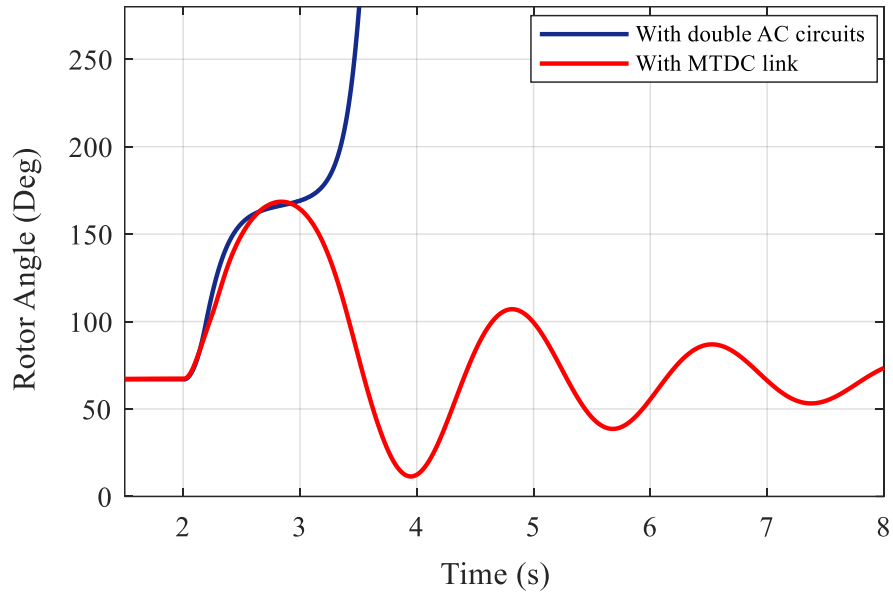


Figure 3.12: Synchronous generator rotor angle response (deg)

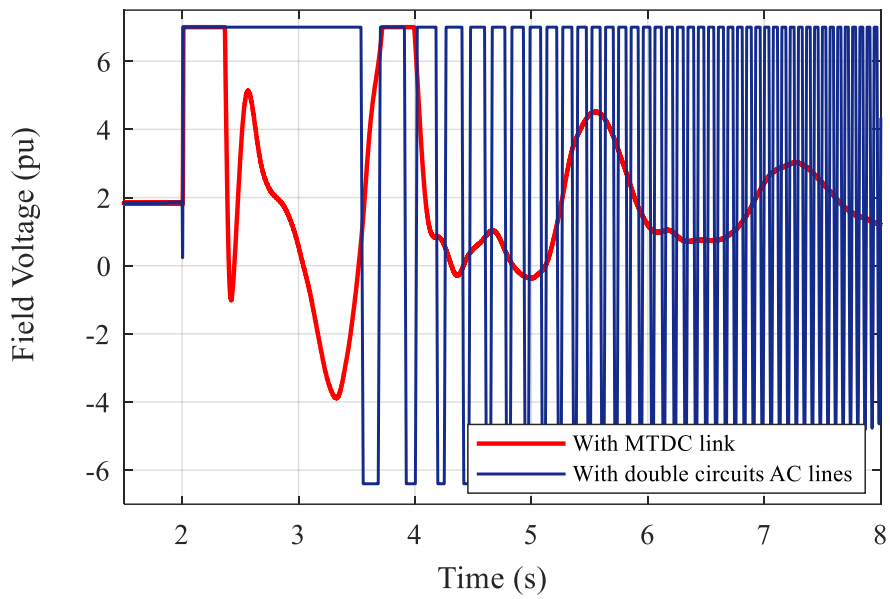


Figure 3.13: Synchronous generator exciter field voltage (pu)

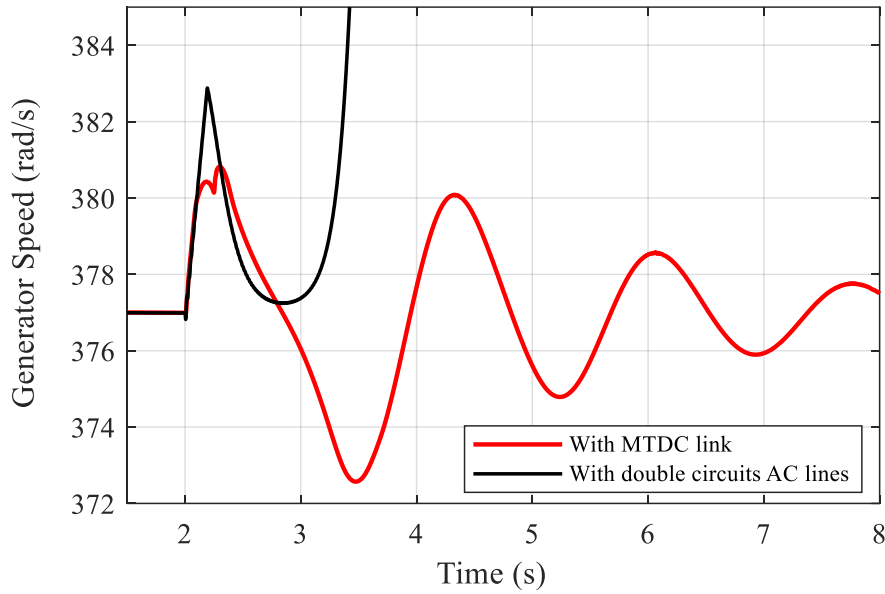


Figure 3.14: Synchronous generator speed (rad/s)

Figures 3.15 and 3.16 show the $P_e - \delta$ diagram for two case studies of MTDC system and double AC transmission lines respectively. From Figure 3.15, following a fault at $t=2s$, the active power was observed to dip to 280MW at $\delta=70^\circ$. When the fault was cleared at $t=2.081s$, a sharp increase of active power was observed, reaching a maximum value $P_{emax}=2300MW$, and $\delta_{max}=175^\circ$. This plot also shows bounded post-fault oscillations, with the system returning to its pre-fault steady-state condition. This shows that the pre-fault and post-fault bounded areas A_1 and A_2 respectively are of equal or less accelerating power (*i.e.* $A_1 - A_2 \leq 0$). Figure 3.16 shows the second scenario of 500kV double circuits AC transmission lines used, instead of the MTDC link, in interconnecting the infinite buses to the synchronous generator. This plot shows a continuous increase of the rotor angle above $\delta_{max}=175^\circ$ at first swing with the continuous oscillation of the active power (P_{ac}) between $\pm 2000MW$. This oscillation tends to reduce in amplitude but at an exceedingly large rotor angle degree. This results from the loss of synchronizing effect from both the AVR and PSS causes the generator to lose synchronism with subsequent oscillations and the additional impedance. This resulted in a more weakened grid strength leading to the cascading of the entire SMIB network.

Figure 3.17 shows the generator output voltage compared to its reference value. The generator used was set to a constant reference value of 1.01pu. It can be observed that following the fault, the machine output voltage deviates from its reference value but is

eventually settling to a steady-state value. The synchronizing torque is shown in Figure 3.18. It can be observed that following the fault, the synchronizing torque experiences a dip, but it then increases after the fault has been cleared, and the electrical torque is eventually settling to a normalized reference value.

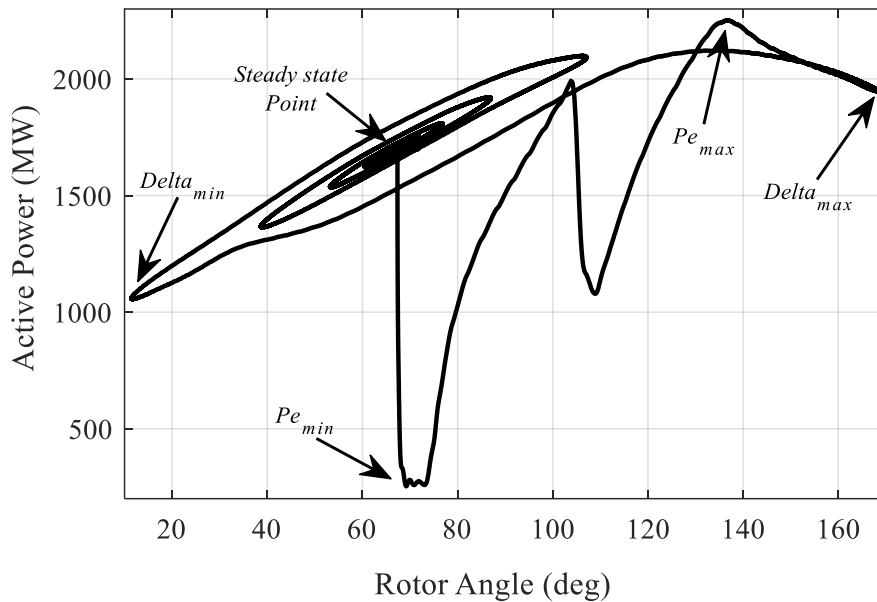


Figure 3.15: Generator Power – angle (P_e - δ) diagram during stable condition,

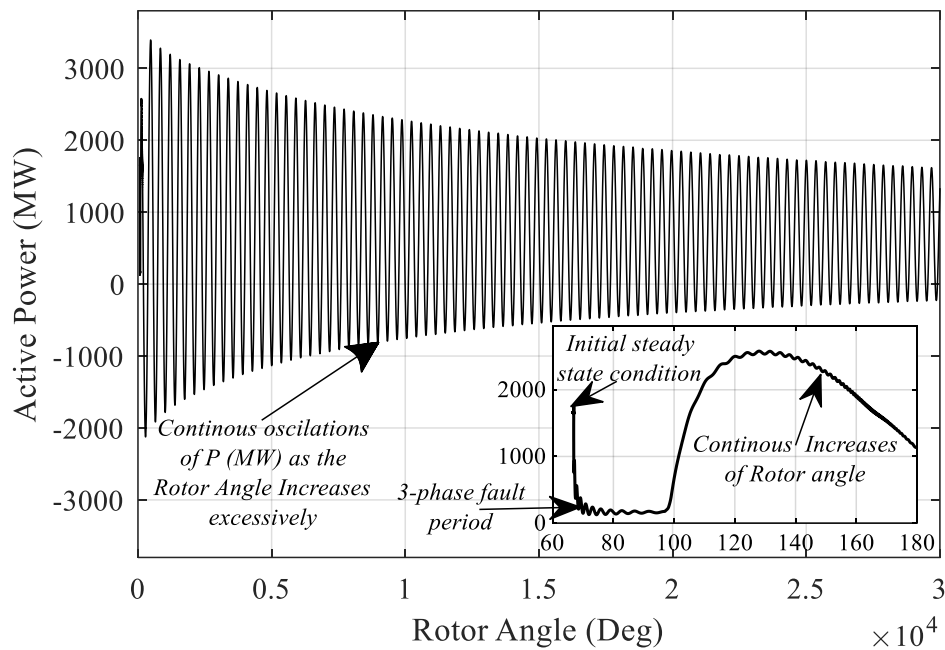


Figure 3.16: Generator power – angle (P_e - δ) diagram during unstable condition while using 2x500kV AC circuits (MTDC link out of service)

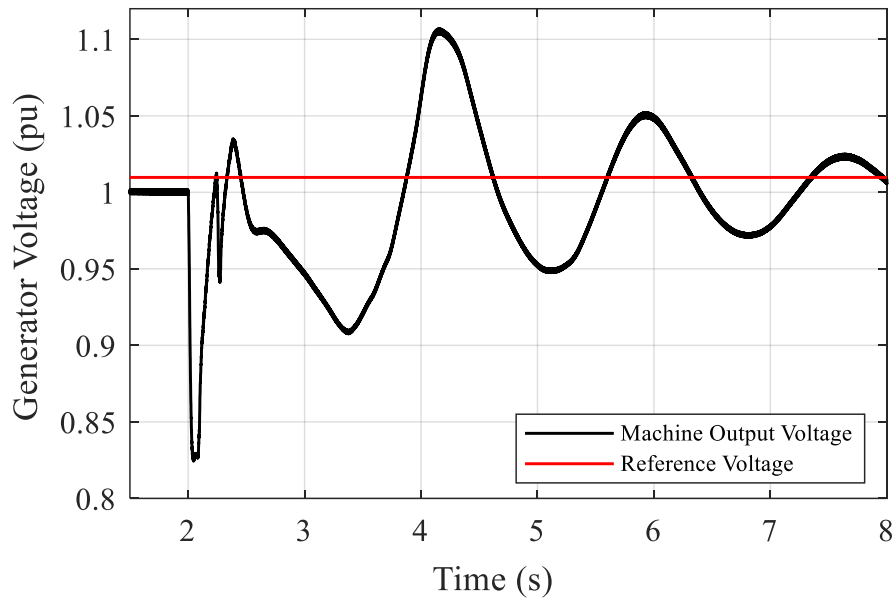


Figure 3.17: Generator output voltage

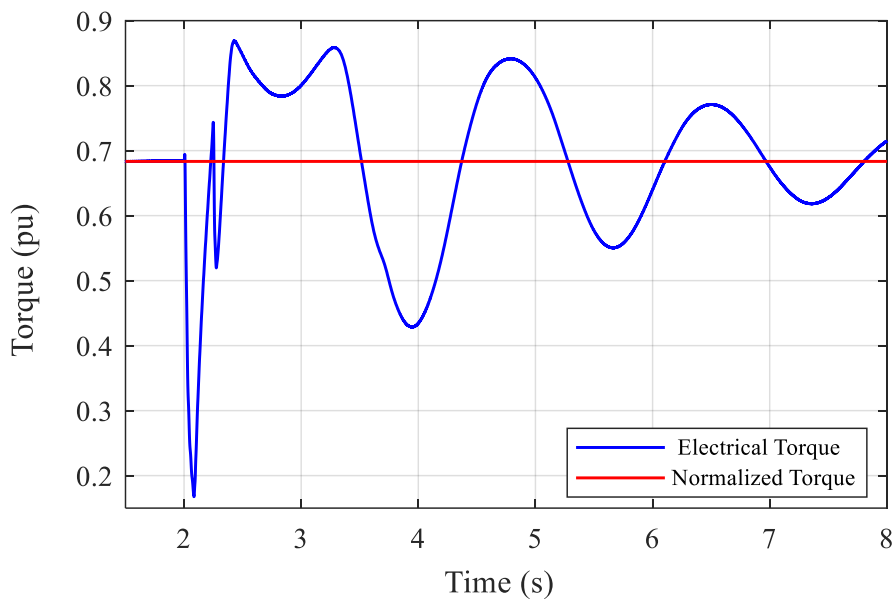


Figure 3.18: Synchronising torque

3.7 CONCLUSION

The performance evaluation of a three-terminal HVDC model on rotor angle stability of a weak SMIB transmission network has been investigated in this paper. In order to investigate the impact of this MTDC link on the transient stability of the study system, two case studies have been considered in this paper. A case study where the MTDC link was replaced with 500 kV double circuits AC line was initially investigated. In this particular case

study, the results showed a continuous power oscillation at increasing rotor angle degree during the three-phase short circuits fault at the *INV-1* station (linking the synchronous generator and the infinite bus). Subsequently, the second case study involved the placement of a three-terminal HVDC model in parallel with a single AC line into the SMIB network, and the same three-phase short circuits fault was applied at the AC side of *INV_1* substation with the transmission system having the same operating points of power transfer in each line as in the previous study. The results have shown that this disturbance caused a transient increase in the DC current and a non-severe commutation failure at the converters station. Being a meshed network, with *INV_1* substation linking both the synchronous generator bus and the *INV_2* substations, this fault led to an increase in generator rotor angle reaching $\delta=175^\circ$, and with the help DC converter controller and fast response of the PSS, the system oscillations were quickly damped out. Thus, the results in this paper show that MTDC system incorporated into a weak AC network helped in improving the system operating condition and also allows quick recovery of the system after an AC fault. Thus, utilizing MTDC lines compared to AC lines of the same ratings will not only increase power carrying capacity but will help in the reduction and quick damping of oscillations amplitude and serves as AC reactive power support. The results in this paper thus give system planners more knowledge of the LCC-MTDC system in a weak AC grid and its fault current contribution into such AC grid and the interconnecting synchronous generator. The power system stability margin can further be enhanced with the proper utilisation of faster fault detection and isolation controllers.

3.8 ACKNOWLEDGEMENTS

The author wishes to thank the Eskom Power Plant Engineering Institute Specialization Centre for HVDC and FACTS and Eskom TESP for their support.

3.9 REFERENCES

1. G. Stein and T. M. Letcher, "Integration of PV Generated Electricity into National Grids," in A Comprehensive Guide to Solar Energy Systems, ed: Elsevier, 2018, pp. 321-332.

2. K. Mbangula, O. Oni, and I. Davidson, "The Impact of HVDC Schemes on Network Transient Rotor Angle Stability," in 24th Southern African Universities Power Engineering Conference, South Africa January, 2016.
3. S. Akkari, "Control of a multi-terminal HVDC (MTDC) system and study of the interactions between the MTDC and the AC grids," Université Paris-Saclay, 2016.
4. O. E. Oni, I. E. Davidson, and K. N. Mbangula, "A review of LCC-HVDC and VSC-HVDC technologies and applications," in 2016 IEEE 16th International Conference on Environment and Electrical Engineering (EEEIC), 2016, pp. 1-7.
5. E. Kontos, R. T. Pinto, S. Rodrigues, and P. Bauer, "Impact of HVDC transmission system topology on multiterminal DC network faults," IEEE Transactions on Power Delivery, vol. 30, pp. 844-852, 2015.
6. L. Tang and B.-T. Ooi, "Protection of VSC-multi-terminal HVDC against DC faults," in 2002 IEEE 33rd Annual IEEE Power Electronics Specialists Conference. Proceedings (Cat. No. 02CH37289), 2002, pp. 719-724.
7. D. T. Oyedokun, K. A. Folly, and S. P. Chowdhury, "Effect of converter DC fault on the transient stability of a Multi-Machine Power System with HVDC transmission lines," in AFRICON, 2009. AFRICON '09., 2009, pp. 1-6.
8. O. E. Oni, I. E. Davidson, and K. N. Mbangula, "Dynamic voltage stability studies using a modified IEEE 30-bus system," in 2016 IEEE 16th International Conference on Environment and Electrical Engineering (EEEIC), 2016, pp. 1-6.
9. O. E. Oni, I. E. Davidson, and K. N. Mbangula, "Voltage stability improvement of a multi-machine system using HVDC," in 2016 Clemson University Power Systems Conference (PSC), 2016, pp. 1-8.
10. P. Rodriguez and K. Rouzbehi, "Multi-terminal DC grids: challenges and prospects," Journal of Modern Power Systems and Clean Energy, vol. 5, pp. 515-523, 2017.
11. M. Hu, C. Fu, J. Wang, H. Rao, and H. Liu, "Real time digital simulation of the parallel multi-terminal HVDC transmission system," in 2012 IEEE International Conference on Power System Technology (POWERCON), 2012, pp. 1-5.

12. M. Hegi, M. Bahrman, G. Scott, and G. Liss, "Control of the Quebec-New England Multiterminal HVDC System," in Cigre International Council on Large Electric systems, 1988, pp. 14-04.
13. V. C. Collet Billon, J. P. Taisne, V. Arcidiacono, and F. Mazzoldi, "The Corsican tapping: from design to commissioning tests of the third terminal of the Sardinia-Corsica-Italy HVDC," *IEEE Transactions on Power Delivery* vol. 4, pp. 794-799, 1989.
14. R. S. Thallam, "Review of the design and performance features of HVDC systems connected to low short circuit ratio AC systems," *IEEE Transactions on Power Delivery*, vol. 7, pp. 2065-2073, 1992.
15. Y. Liu and Z. Chen, "Short Circuit Ratio analysis of multi-infeed HVDC system with a VSC-HVDC link," in *IECON 2011 - 37th Annual Conference of the IEEE Industrial Electronics Society*, 2011, pp. 949-954.
16. H. Xiao, Y. Li, J. Zhu, and X. Duan. (2016, Efficient approach to quantify commutation failure immunity levels in multi-infeed HVDC systems. *IET Generation, Transmission & Distribution* 10(4), 1032-1038. Available: <https://digital-library.theiet.org/content/journals/10.1049/iet-gtd.2015.0800>
17. L. Yan and C. Zhe, "Transient voltage stability analysis and improvement of a network with different HVDC systems," in *Power and Energy Society General Meeting, 2011 IEEE*, 2011, pp. 1-8.
18. J. Renedo, A. Garcí'a-Cerrada, and L. Rouco, "Active Power Control Strategies for Transient Stability Enhancement of AC/DC Grids With VSC-HVDC Multi-Terminal Systems," *IEEE Transactions on Power Systems*, vol. 31, pp. 4595-4604, 2016.
19. C. D. Vournas, P. W. Sauer, and M. A. Pai, "Relationships between voltage and angle stability of power systems," *International Journal of Electrical Power & Energy Systems*, vol. 18, pp. 493-500, 1996/11/01/ 1996.
20. J. Song, "Power System Stability: Modelling, Analysis and Control [Bookshelf]," *IEEE Control Systems Magazine*, vol. 37, pp. 99-100, 2017.
21. S. R. Salkuti, "Transient Stability Enhancement using Thyristor Controlled Series Compensator," *International Journal of Electrical and Computer Engineering (IJECE)*, vol. 9, pp. 884~893, 2019.

22. L. Cong, Y. Wang, and D. Hill, "Transient stability and voltage regulation enhancement via coordinated control of generator excitation and SVC," *International Journal of Electrical Power & Energy Systems*, vol. 27, pp. 121-130, 2005.
23. G. Kenné, R. Goma, H. Nkwawo, F. Lamnabhi-Lagarrigue, A. Arzandé, and J. C. Vannier, "An improved direct feedback linearization technique for transient stability enhancement and voltage regulation of power generators," *International Journal of Electrical Power & Energy Systems*, vol. 32, pp. 809-816, 2010/09/01/ 2010.
24. K. Mbangula, I. Davidson, and R. Tiako, "Improving power system stability of South Africa's HVAC network using strategic placement of HVDC links," *CIGRE Science & Engineering Journal (CSE)*, vol. 5, pp. 71-78, 2016.
25. R. Jotten, J. P. Bowles, G. Liss, C. J. B. Martin, and E. Rumpf, "Control in HVDC Systems: The state of the art. Part II : Multiterminal Systems," in *Cigre International Conference on Large High Voltage Electric Systems*, Paris, 1980.
26. J. Hongbo and A. Ekstrom, "Multiterminal HVDC systems in urban areas of large cities," *IEEE Transactions on Power Delivery*, vol. 13, pp. 1278-1284, 1998.
27. R. L. Vasquez-Arnez, J. A. Jardini, and M. T. Bassini, "Dynamic Performance of Line Commutated Converter-Based Multiterminal HVDC Systems," *Przeegląd Elektrotechniczny*, vol. 91, pp. 247-253, 2015.
28. M. Eremia, C.-C. Liu, and A.-A. Edris, *Advanced solutions in power systems: HVDC, FACTS, and Artificial Intelligence vol. 52*: John Wiley & Sons, 2016.
29. J. Tu, Y. Pan, J. Zhang, B. Zeng, J. Jia, and J. Yi, "Transient reactive power characteristics of HVDC during commutation failure and impact of HVDC control parameters," *The Journal of Engineering*, vol. 2017, pp. 1134-1139, 2017.
30. P. Kundur, N. J. Balu, and M. G. Lauby, *Power System Stability and Control vol. 7*. New York: McGraw-Hill, 1994.
31. C. J. Mozina, M. Reichard, Z. Bukhala, S. Conrad, T. Crawley, J. Gardell, et al., "Coordination of generator protection with generator excitation control and generator capability," in *54th Annual Conference on Record of Pulp and Paper Industry Technical Conference*, 2008, pp. 62-76.

32. A. Murdoch, G. Boukarim, B. Gott, M. D'antonio, and R. Lawson, "Generator over excitation capability and excitation system limiters," in IEEE Power Engineering Society Winter Meeting, 2001, pp. 215-220.
33. M. Pavella, D. Ernst, and D. Ruiz-Vega, Transient stability of power systems : a unified approach to assessment and control: Springer US, 2019.
34. L. L. Grigsby, Power System Stability and Control, Third Edition: Taylor & Francis, 2012.
35. Y. Dong and H. R. Pota. (1993, Transient stability margin prediction using equal-area criterion. IEE Proceedings C (Generation, Transmission and Distribution) 140(2), 96-104. Available: <http://digital-library.theiet.org/content/journals/10.1049/ip-c.1993.0014>
36. M. Szechtman, T. Wess, and C. Thio, "A benchmark model for HVDC system studies," in International Conference on AC and DC Power Transmission, 1991, pp. 374-378.

3.10 Appendix

Table 3.2: MTDC Converter Parameters

	Rect.	Inv-1	Inv-2
Rated/Actual power (MW)	2000/1200	1000/700	1000/500
Rated/Actual DC current (kA)	4.0/2.4	2.0/1.4	2.0/1.0
SCR	2.5	3	2.5
AC voltage (kV)	450	450	500
γ_0 (inverter)		15	15
Transformer per 6 pulse thyristor			
Rating (MVA)	1200	700	600
Voltage (kV)	500/250	500/250	500/250
Leakage reactance (pu)	0.18	0.18	0.18
PI Controller			
Proportional Gain	1.0989	1.5363	1.5363
Integral time constant (s)	0.01092	0.01524	0.01524
VDCOL			
Threshold input	0.4-1.0	0.4-0.9	0.4-0.9
Threshold output	0.55-1.5	0.55-1.0	0.55-1.0
DC Transmission line (T-model)			
	Line 1	Line 2	
R(Ω)	1.5	2.5	
Reactor (H)	0.5968	0.5968	
DC filter (μF)	15	26	

Table 3.3: Generator and Transmission line Parameters

Synchronous machine data			
Generator Data		AVR and PSS	
Ra (pu)	0.003 pu	Input signal	Speed
Xp (pu)	0.130 pu	T_R	0.015 sec
Xd (pu)	1.81 pu	Vimax	10 pu
Xd' (pu)	0.3 pu	Vimin	-10 pu
Xd'' (pu)	0.23 pu	K_A	200 pu
T_{d_0}'	8.0 sec	Efmax	7.0 pu
T_{d_0}''	0.0294 (s)	Efmin	-6.4 pu
Xq	1.76 pu	K_{STAB}	9.5
Xq'	0.65 pu	T_W	1.41 sec
Xq_0''	0.25 pu	T_1	0.154 sec
T_{q_0}'	1.0 (s)	T_2	0.033 sec
T_{q_0}''	0.07 (s)	V_{stmax}	0.2
H	3.5 (s)	V_{stmin}	-0.2
AC Transmission line (500kV base)			
		Line 1	Line 2
R (pu/m)		0.012	0.012
X (pu/m)		0.12	0.12
B (pu/m)		2.0	2.0

**CHAPTER 4: SMALL SIGNAL STABILITY ANALYSIS OF A
FOUR-MACHINE SYSTEM WITH PLACEMENT
OF MULTI-TERMINAL HIGH VOLTAGE DIRECT
CURRENT LINK**

PAPER SIX

This chapter addresses objective three and is presented in manuscript format. It has been published in the Journal of Energy in Southern Africa. 2020. Vol. 31 (1), pp. 73-87. <https://dx.doi.org/10.17159/2413-3051/2020/v31i1a7430>.

Small signal stability analysis of a four-machine system with placement of multi-terminal high voltage direct current link

Abstract: Inter-area oscillation caused by weak interconnected lines or low generator inertia is a critical problem facing power systems. This study investigated the performance analysis of a multi-terminal high voltage direct current (MTDC) on the damping of inter-area oscillations of a modified two-area four-machine network. Two case studies were considered, utilising scenario 1: a double alternating current (AC) circuit in linking Bus_10 and Bus_11; and scenario 2: a three-terminal line commutated converter high voltage direct current system in linking Bus_6 and Bus_11 into Bus_9. It was found that scenario 2 utilising MTDC link with a robust controller provided quick support in minimising the network oscillations following a fault on the system. The MTDC converter controllers' setup offered sufficient support for the inertia of the AC system, thus providing efficient damping of the inter-area oscillation of the system.

Keywords: multiterminal direct current, MTDC link, inter-area oscillation, generator inertia, thyristors converter, high voltage direct current, converter controller

4.1 INTRODUCTION

The high increment in the installed capacity of synchronous machines over the recent decade has compounded the inter-area oscillation stability problem [1-3]. Inter-area oscillations usually occur when a group of generators on one area swing against another group of generators on the other side, caused mainly by weakly interconnected tie-lines between the group of generators [4]. A radially connected system that gets upgraded to form a complex and more advanced system with a very long transmission distance, resulting in lower generator inertias, has an increased inter-area oscillation problem [5]. A market-driven economy with high transmission system loading further shifts the power grid to its stability limits. This is done to increase profits as well as to meet consumer demands, but it further adds to the complicating problem of small-signal stability [6, 7]. Power utilities are becoming aware of the crucial impact of small-signal stability performance of large interconnected

power systems, as it contributes to the problems they frequently experience [6, 8]. Siemens stated that most power systems had been faced with inadequately damped low-frequency range of 0.2-0.8 Hz inter-area oscillations because of increasing transmission network growth and unplanned grid expansion [9].

Damping of inter-area oscillations requires extra energy in the form of load or frequency cut of filters to be subtracted from a perturbed system for a quick reduction of the system oscillation amplitude. Based on the operating state of the system, the energy required to damp any particular system adequately depends on the correct phase shift settings relative to the instant systems' condition. Because incorrect phase angles can excite the power system further from the steady-state operating point, it was found that, with a damping ratio of -5%, a system would be able to adequately damp almost 32% of its initial oscillation amplitude in three oscillation periods. Each power system has a different operating point, and therefore requires a different acceptable level of damping energy to reduce the whole system oscillations amplitudes during a fault. The smallest adequate level of damping is not known, as it depends on the system that considers its operating point, but a damping ratio that is negative causes the mode to become unstable [10-12].

Some researchers have addressed small signal stability problems relating to the generator frequency response of the power grid during a system disturbance or the normal operating condition [5, 13-19]. Elizondo *et al.* [13] provided a comprehensive research survey on the inter-area oscillation damping control using high voltage direct current (HVDC) or MTDC system. The approach covered a range of converter control, with active direct current (DC) power modulation in proportion to the change in the frequency of the two areas involve being an example. Li *et al.* [14] made use of a robust controller for flexible alternating current (AC) transmission system devices to provide better compensation to the AC system. Elizondo *et al.* [13] also emphasised the importance of data-capturing of an extensive power system using phasor measurement units (PMUs) and wide-area monitoring systems to HVDC system monitoring and control. A mathematical approach of a single-machine infinite bus system and the power system stability was introduced by Kundur [15] and further analysis made by Oni *et al.* [17], with the emphasis limited to a point-to-point HVDC. Azad *et al.* [16] used supplementary predictive control in a line-commutated converter (LCC) HVDC link to enhance the small-signal stability of the same Kundur [15] network. Idowu [18] implemented an algorithm that maximally generates a damping and

inertia coefficient for a virtual synchronous machine to participate efficiently in the inertia response of frequency control. Eftekharijad *et al.* [19] found that high penetration of photovoltaic (PV) systems has a detrimental impact on the small-signal stability of the power system because of reduced system inertia. Therefore, Wandhare and Agarwal [20] proposed a new control scheme that enables a centralised PV-grid system to damp the low-frequency power swings on the local area network as an ancillary activity. The impact of system disturbance such as generator losses or load shedding on the system frequency was discussed in Zou (2018) [21], where the power system frequency regulation with consideration to the load-damping characteristic was analysed. Saghafi [22] presented a small integrated series compensator in damping power oscillations in standalone micro-grids. Little attention was given to the small-signal analysis of two-area four-machine (TAFM) networks when interconnected with an LCC-MTDC link. The literature is mostly based on a point-to-point HVDC link as an inter-area power transfer link rather than on a comprehensive comparative analysis on MTDC operation during AC disturbance [15, 17, 23].

The present study, therefore, contributed to the performance and reduction analysis of inter-area oscillations of the modified Kundur TAFM networks by comparing the damping rate of the network oscillations when interconnected with an MTDC link, unlike the use of a double AC line. The study also evaluated the impact of modulating MTDC power flow on the AC network inter-area oscillation damping. A swing equation of incoherent two-area machines was firstly presented and analysed. Two operational scenarios were considered, and a dynamic simulation study was carried out on the system during a small-signal perturbation on two of the selected network elements to determine the damping amplitude of the generator oscillations when the MTDC model was connected on the network.

4.2 METHODOLOGY

A scenario was considered, covering a three-phase short circuit fault (TFSC) on the transmission line (L7_8) linking Bus_7 and Bus_8 with a fault clearing time $t_c=0.13s$, as well as a $1.0s$ disturbance on the generator (Gen_4). Both faults occurred at 2.0s simulation time, i.e., a situation where both disturbances occurred simultaneously in two different areas of the study system. These cases of system disturbances were chosen to give the worst-case scenario of power system operation, which also stipulates a situation where the synchronous generator

is delivering half its rated power following a TFSC fault. The same fault impedance and duration were also applied to the studied system when interconnected with the MTDC link (during the second scenario). This was to determine the performance of the MTDC transmission schemes on the small-signal stability of an electric power system. During this study, the following two scenarios were analysed:

Scenario 1: This involved using double transmission lines to link Bus_10 and Bus_11, with each line rated at 350 MVA.

Scenario 2: The MTDC (two rectifiers and one inverter) system was used as a replacement for the AC transmission line (i.e., single AC circuit with DC line). For the AC lines, L7-8 (linking Bus_7 to Bus_8) and line L8-9 (linking Bus_8 to Bus_9), a 300 MW rated rectifier (Rect-1) delivering 200 MW power was connected at Bus_6. Also, a 1000 MW rated rectifier (Rect-2) station was connected at Bus_11 to deliver 700 MW power in replacement of the transmission line L10-11b (linking Bus_10 and Bus_11).

4.3 BACKGROUND THEORY

The inertia swings of the synchronous machine are first analysed to give the damping coefficient required to suppress the power system oscillation maximally, thereby providing sufficient torque in controlling the system frequency. Figure 4.1 shows a simple schematic two-area network comprising two incoherent machines with generator inertias of H_1 and H_2 , while δ_1 and δ_2 represent the respective Area-1 (A1) and Area-2 (A2) rotor angle oscillating at two different frequency and amplitude.

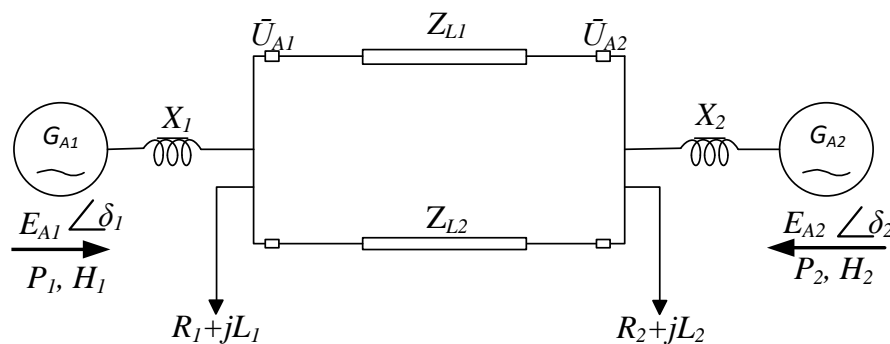


Figure 4.1: Simple two machine two-area network, where E , P , H , and δ = generator terminal voltage, active generator power, generator inertia constant and generator rotor

angle respectively; R , L , Z , and U = load resistance, load inductance, line impedance, and line voltage respectively; G_{A1} and G_{A2} = generators in areas 1 and 2 respectively.

Equations 4.1 and 4.2 give the swing for each of the machines. When they are subtracted from each other, they give Equations 4.3 and 4.4 when divided by the coefficients of inertia just before the second derivative. Simplifying Equation 4.4 gives Equation 4.5. Avoiding the complexity of the swing equations for many coherent machines during stability analysis of a large system requires the combination of all the swing equations to decrease the number of swing equations [21]. Adding the rotating inertia H for each generator unit gives the overall system equivalent rotating inertia.

$$\frac{2}{\omega} H_1 \frac{\partial^2 \delta_1}{\partial t^2} = P_{m1} - P_{e1} \quad (4.1)$$

$$\frac{2}{\omega} H_2 \frac{\partial^2 \delta_2}{\partial t^2} = P_{m2} - P_{e2} \quad (4.2)$$

$$\frac{2}{\omega} \left(\frac{\partial^2 (\delta_1 - \delta_2)}{\partial t^2} \right) = \left(\frac{P_{m1} - P_{e1}}{H_1} - \frac{P_{m2} - P_{e2}}{H_2} \right) \quad (4.3)$$

$$\frac{2}{\omega} \left(\frac{H_1 H_2}{H_1 + H_2} \right) \left(\frac{\partial^2 (\delta_1 - \delta_2)}{\partial t^2} \right) = \left(\frac{H_2 P_{m1} - H_1 P_{m2}}{H_1 + H_2} - \frac{H_2 P_{e1} - H_1 P_{e2}}{H_1 + H_2} \right) \quad (4.4)$$

$$\frac{2}{\omega} H_{12} \frac{\partial^2 \delta_{12}}{\partial t^2} = P_{m12} - P_{e12} \quad (4.5)$$

where H is the generator inertia, δ is the rotor angle for the generator, P_m is the mechanical power, and P_e is the electrical power. The subscripts 1 and 2 stand for areas 1 and 2 respectively.

The respective equivalent inertia constant H_{12} and the change in rotor angle δ_{12} between the two generators are further defined and given by Equations 4.6 and 4.7.

$$H_{12} = \frac{H_1 H_2}{H_1 + H_2} \quad (4.6)$$

$$\delta_{12} = \delta_1 - \delta_2 \quad (4.7)$$

The P_{m12} and P_{e12} given by Equations 4.8 and 4.9 are, respectively, the mechanical and electrical power between the two generators.

$$P_{m12} = \frac{P_{m1}H_2 - P_{m2}H_1}{H_1 + H_2} \quad (4.8)$$

$$P_{e12} = \frac{P_{e1}H_2 - P_{e2}H_1}{H_1 + H_2} \quad (4.9)$$

After solving the second-order differential of Equation 4.5, the equivalent swing behaviour of the synchronous machine with the damping constant K_D is given by Equation 4.10. Equation 4.11 gives the undamped natural frequency (ω_n) in the system, while Equation 4.12 represents the damping coefficient ζ needed to suppress the oscillation amplitude entirely.

The overall system oscillation frequency and the inertia constant are inversely proportional, implying that a system with high inertia constant is immune to a fault and vice versa. This shows that the system inertia constant is directly affected by the output generated power. Therefore, for a more stable operating point of a power system, it requires inertia constant >3.5 pu.

$$\frac{2}{\omega} H_{12} \frac{\partial^2 \delta_{12}}{\partial t^2} + K_D \frac{\partial \delta_{12}}{\partial t} + P_{max} \cos(\delta_o) \delta_{12} = 0 \quad (4.10)$$

$$\omega_n = \sqrt{\frac{\omega P_{max} \cos \delta_0}{2H_{12}}} \quad (4.11)$$

$$\zeta = 1/2 K_D \sqrt{\frac{\omega}{2H_{12} \cos \delta_o P_{max}}} \quad (4.12)$$

where ω_n is the undamped natural frequency, ζ is the damping coefficient, K_D is the damping constant, P_{max} is the maximum active power generated, ω is the angular speed, and δ is the generator rotor angle.

4.4 SYSTEM MODEL

The system considered in this study is a modified version of Kundur's TAFM network, as shown in Figure 4.2. The transmission line interconnecting Bus_10 to Bus_11 was modified from 25 km to an 80 km, leading to high impedance on the AC transmission line. The double transmission circuits were then used to allow more power transfer, and the inter-area oscillations of the entire generator during a system disturbance were then analysed using a time-domain simulation. The dynamic simulation was carried out, and the generators' power output, oscillation speed, field voltage, and inter-area power transfer were analysed.

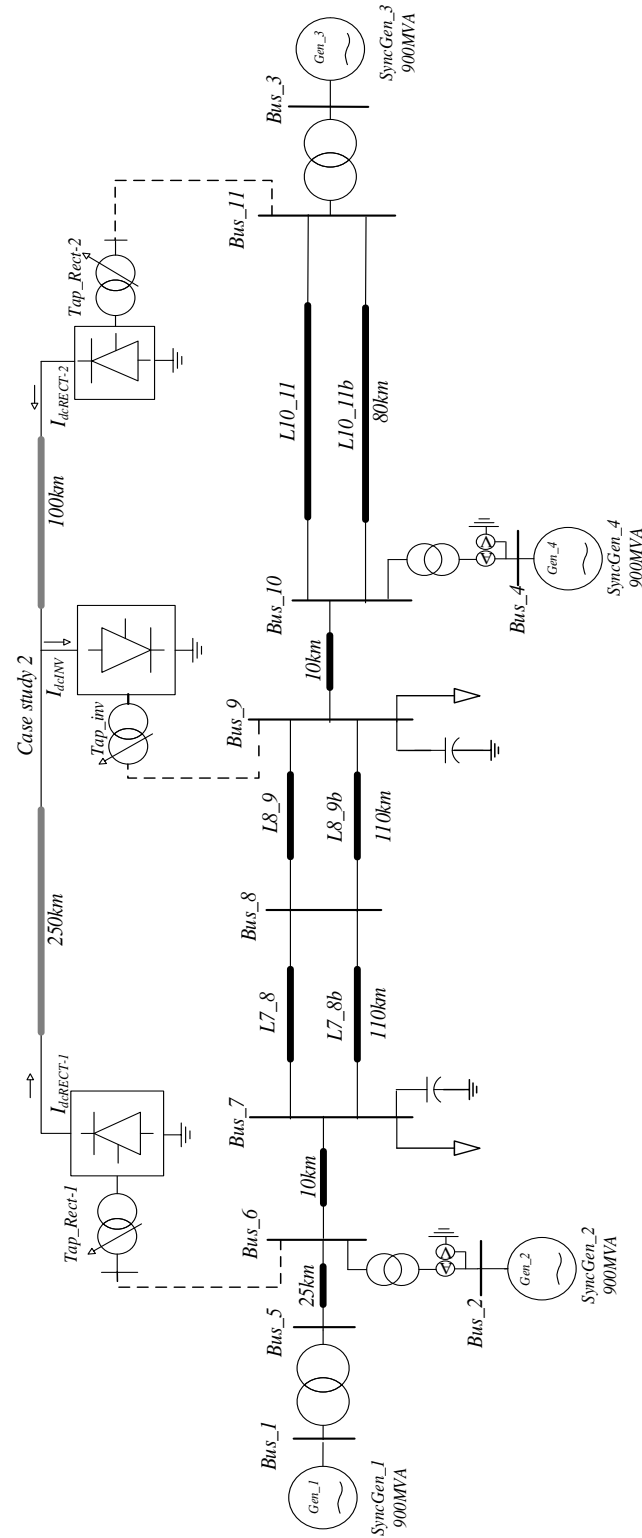


Figure 4.2: Kundur's two-area four-machine system with three-terminal LCC-HVDC link, where $L7_8$, $L7_8b$ = first and second transmission line between bus 7 and 8 respectively; Tap_Rect-1 , Tap_Rect-2 , Tap_Inv = tap changers for rectifier station 1, rectifier station 2, and the inverter station respectively, $SyncGen$ = synchronous generator; $I_{d-Rect-1}$, $I_{d-Rect-2}$, I_{d-Inv} = direct current for rectifier station 1, rectifier station 2, and the inverter station respectively.

4.4.1 Synchronous Generator Model

The synchronous machines used were modelled on power system computer-aided design (PSCAD) software using the Institute of Electrical and Electronics Engineers controller model for the automatic voltage regulator (AVR) as well as the power system stabiliser (PSS), as shown in Figure 4.3. All generators were rated for a realistic inertial time constant and were connected via a 20/230 kV 900 MVA transformer. The governor control of these machines was assumed constant during the investigation period to get a holistic effect of the PSS, AVR and the DC controller impacts in minimising the fault on the entire network. Modelling details of these machine controllers are fully explained in Kundur et al. [15].

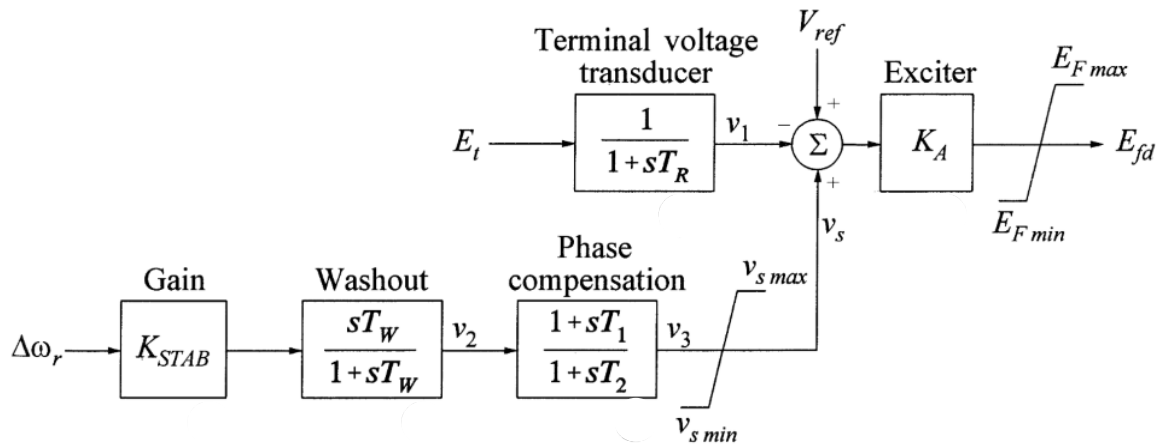


Figure 4.3: Power system stabiliser with an automatic voltage regulator, where K_{STAB} = stabilising gain, T_1 = first lead time constant, T_2 = first lag time constant, T_W = washout time constant, K_A = regulator integral gain, T_R = transducer time constant, $\Delta\omega_r$ = change in angular speed, E_{fd} = exciter output voltage, E_{Fmin} , E_{Fmax} = minimum and maximum regulator outputs, V_{ref} = reference voltage regulator, V_s = combined power system stabiliser and possibly discontinuous control output after any limits or switching, and E_t = terminal voltage of transducer and load compensation elements.

4.4.2 Load Model

The loads were modelled to have constant current and constant impedance characteristics for its active and reactive power components respectively. Equation 4.13 gives the load flow and dynamic calculation of the loads.

$$P + jQ = \left\{ P_0 \left(\frac{U}{U_0} \right)^{kp} (1 + k_{Pf} \cdot dF) \right\} + \left\{ Q_0 \left(\frac{U}{U_0} \right)^{kp} (1 + k_{Qf} \cdot dF) \right\} \quad (4.13)$$

where Q is the equivalent reactive power, P is the real power, P_o is the rated real power/phase, Q_o is the rated reactive power (+inductive) per phase, U is the load root mean square (RMS) voltage, and U_o is the rated line-to-earth RMS voltage; dP/dV and dP/dF are the voltage index and frequency index for real power respectively, while dQ/dV and dQ/dF are the voltage index and frequency index for the reactive power respectively.

4.4.3 Multiterminal Direct Current Model

The multiterminal direct current (MTDC) network used is a three-terminal (two rectifiers and one inverter station), as shown in Figure 4.2, with supplementary parameters given in the Appendix section. Equations 4.14 and 4.15 give the model voltage of the three-terminal system.

$$V_{dR} = \frac{3\sqrt{2}\alpha_R V_{tR} \cos \gamma_R - 3X_C I_D}{\pi} \quad (4.14)$$

$$V_{dI} = \frac{3\sqrt{2}\alpha_I V_{tI} \cos \gamma_I - 3X_C I_D}{\pi} \quad (4.15)$$

where V_{dR} and V_{dI} are the rectifier and inverter direct current voltage, α_R and α_I are the rectifier and inverter firing angle, V_{tR} and V_{tI} are the rectifier and inverter alternating current terminal voltage, γ_R and γ_I are the rectifier and inverter extinction angle, X_C is the commutation reactance, and I_D is the direct current voltage.

Rectifier station one (Rect-1) and rectifier station two (Rect-2) transmit power from Bus_6 and Bus_11 respectively to the inverter station (Bus_9), replacing some transmission lines (L7_8b, L8_9b, L10_11b) in the network. Fault susceptibility of the MTDC system depends solely on its overall converter controller coordination; therefore, each converter controller was pre-set and corrected to suit the study case scenarios. The current controller in Figure 4.4 outputs the firing angle order after calculating the difference among the filtered direct current (I_{dc}) measured and the reference current order (I_{order}), and the current error is fed into a proportional and integral (PI) controller.

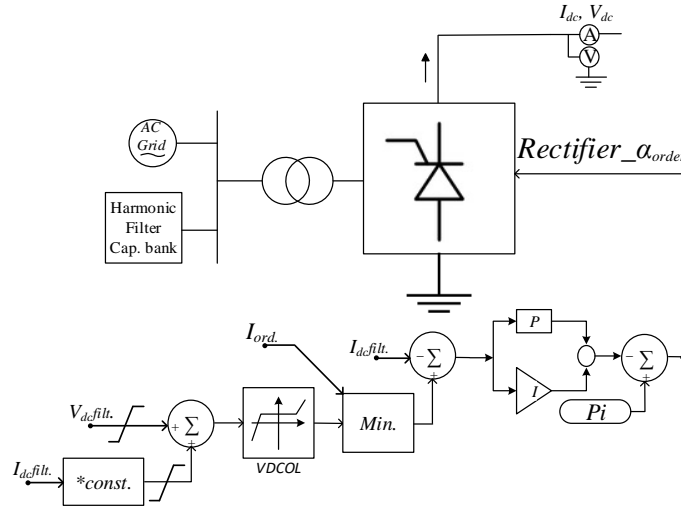


Figure 4.4: Rectifier current controller, where $I_{dc\,filt.}$ = filtered current, $V_{dc\,filt.}$ = filtered voltage, $*const.$ = constant, $VDCOL$ = voltage-dependent current order limiter, Pi = constant (3.142), PI = proportional and integral controller, I_{ord} = current order, I_{dc} and V_{dc} = direct current voltage and current, α_{order} = firing angle order.

The rectifiers operate as a current controller, while the inverter, because of the minimum value selector, uses the gamma controller. The extinction angle (γ) (or voltage) controller in Figure 4.5 sets and regulates the voltage level of the converter. It also maintains the voltage polarity across the inverter link until the next commutation process.

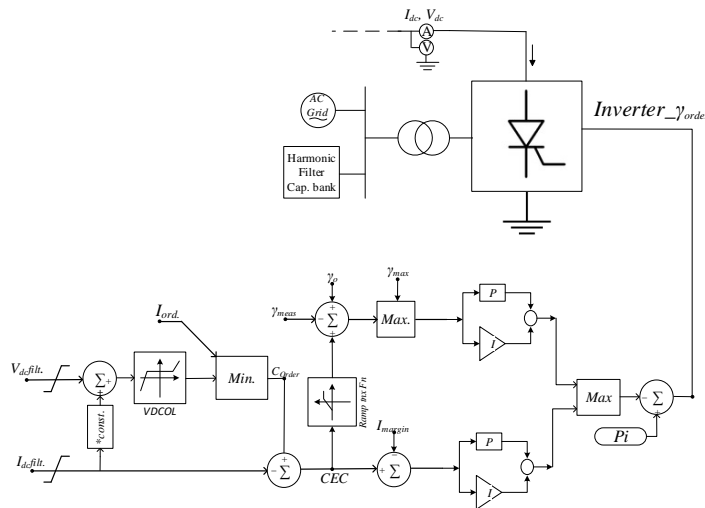


Figure 4.5: Inverter voltage controller, where $I_{dc\,filt.}$ = filtered current, $V_{dc\,filt.}$ = filtered voltage, $*const.$ = constant, $VDCOL$ = voltage-dependent current order limiter, Pi = constant (3.142), PI = proportional and integral controller, I_{ord} = current order, I_{dc} and V_{dc} = direct current voltage and current, γ_{order} = firing angle order, CEC = current error, γ_{meas} , γ_o , and γ_{max} = measured, initial, and maximum extinction angles respectively.

The firing angle (α) order comes from the *PI* regulator that takes the difference between the commutation margin γ (delay between the valve extinction and the voltage of the valve just before turning positive) and the pre-set value of the extinction angle (γ_o). During a situation where the difference ($\gamma - \gamma_o$) is larger than necessary, the *PI* controller stops at the α -max, or the firing angle is reduced until γ equals the set value. However, during a fault, the inverter has the capability of mode shifting from voltage control to current control. The power controller coordinates and oversees the converter actions of the entire DC link. It takes a variable power order, which, when divided with the system voltage gives the current order signals for the inverter. The master controller shown in Figure 4.6 helps to balance the power and current order of the entire converter by ensuring that DC current summation across all converters equals zero ($\sum I_{dc}=0$). This controller uses measured DC voltage at each converter station with a pre-set power order to generate the current order for each of the converter systems.

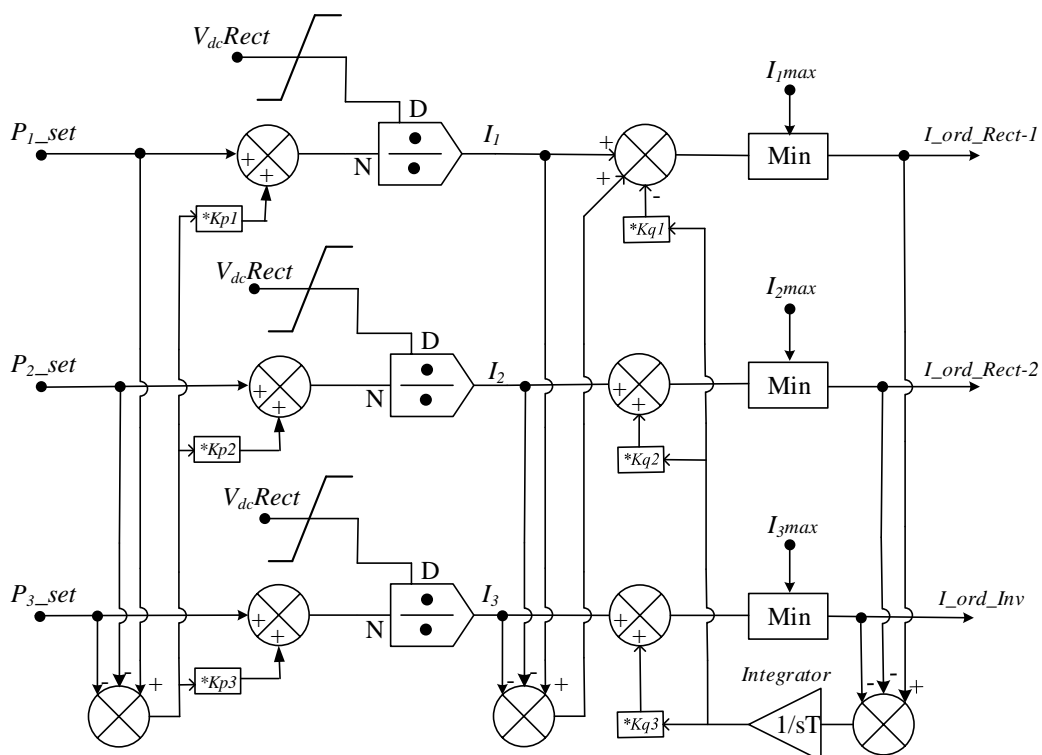


Figure 4.6: Overall current controller for the multiterminal direct current system, where P_1 , P_2 , and P_3 = power setpoint for each converter station, V_{dc_Rect} = rectifier direct voltage, I_1 , I_2 , and I_3 = calculated current from each converter station, I_{1max} , I_{2max} , and I_{3max} = maximum setpoint for each converter station current, and I_{ord_Rect-1} , I_{ord_Rect-2} , and I_{ord_Inv} = rectifier 1, rectifier 2, and inverter current order respectively.

It also compensates for DC line losses and power order compensation by using weighting factors kq and kp respectively. Sharing of excess power order value to avoid overloading any of the substations is done using the kq to fulfil $\sum Kq=1$. Each of the converter stations was also equipped with the voltage-dependent current order limiter (VDCOL) controller, which serves as a corrective measure in aiding the reduction of the current (I_{dc}) that in turn reduces the power (P_{dc}) transfer across the link during the system perturbation. The VDCOL controller reduces the occurrence of commutation failure, especially at the inverter station [24].

4.5 RESULTS AND DISCUSSION

The results following a dynamic analysis on PSCAD/EMTDC simulation software include the generator active power, oscillation speed, and the generator field voltage. Both scenarios maintained a stable operating state after systems disturbance with a positive damping coefficient although with different amplitudes and waveform distortion.

4.5.1 First Scenario

The generators' active power in Figure 4.7 shows the synchronous generator 2's (Gen_2's) lowest dip of 200 MW during a fault, followed by Gen_1 attributable to the close distance to the transmission line fault.

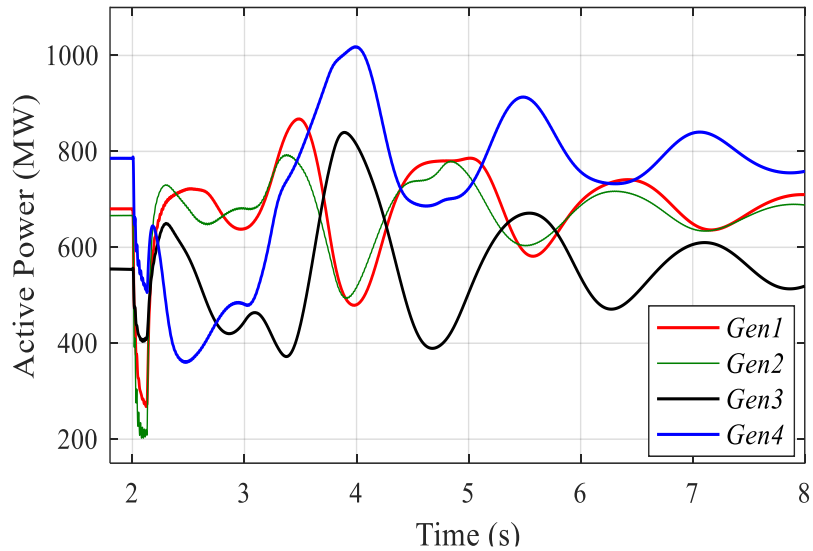


Figure 4.7: Synchronous generator active power during the first scenario, where *Gen1*, *Gen2*, *Gen3*, and *Gen4* = synchronous generators 1 to 4.

The Gen_4 had the worst post-fault condition, with active power output reaching 1073 MW. Nearly 1.53 pu of its steady-state value following a drop in active power generated from Gen_3 because of a prolonged generator disturbance reaching 3s simulation time on Gen_4. The Gen_3 also followed the same pattern as Gen_4, being similar to each other in A2. The two generators swung together against Gen_1 and Gen_2 in A1, as in Figure 4.8.

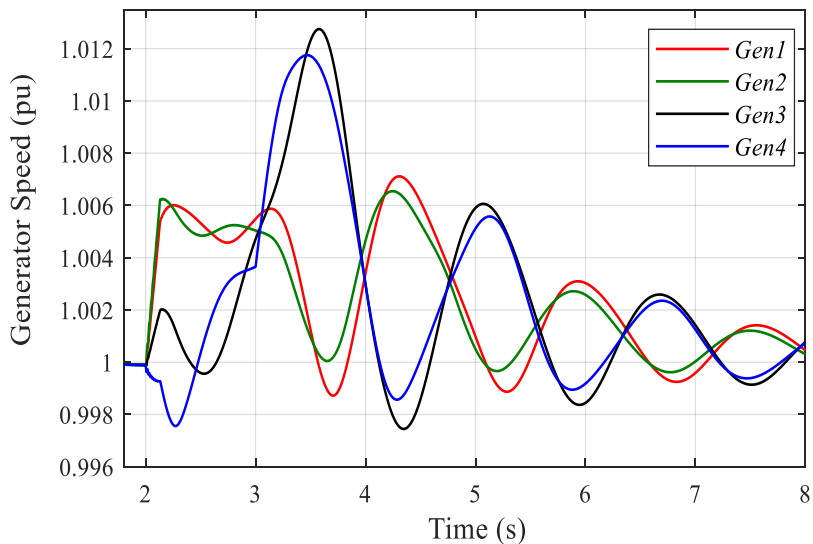


Figure 4.8: Generator speed during the first scenario, where *Gen1*, *Gen2*, *Gen3*, and *Gen4* = synchronous generators 1 to 4.

The highest oscillatory modes were recorded in Gen_3 and Gen_4 subplot, increasing up to 1.013 pu because of the accelerating power of the machine in matching up the expected load demand in A2. The system maintained a stable operating condition, however, with a high oscillation frequency. The machine field voltage of Gen_1, Gen_2, and Gen_4 in Figure 4.9 recorded a continuous swing between the minimum and maximum field voltage of -4.53 pu and 5.64 pu, respectively, until 6.5s simulation time.

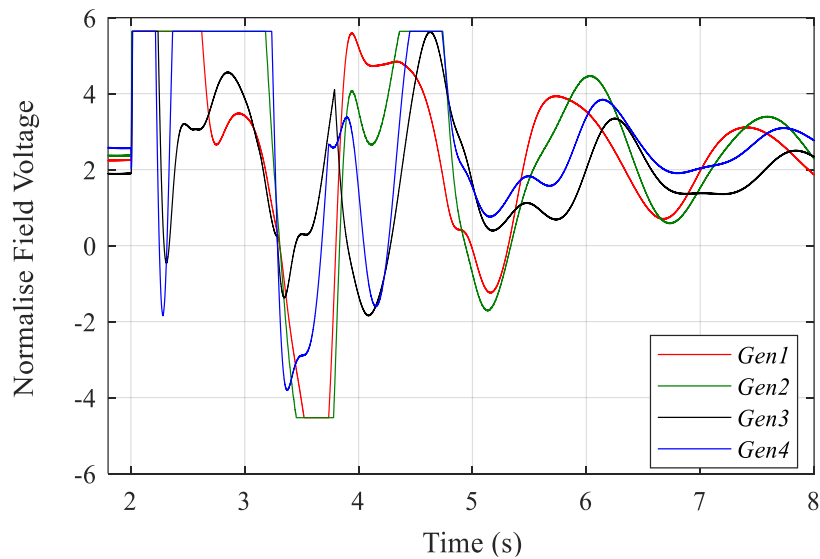


Figure 4.9: Generator field voltage during the first scenario, where *Gen1*, *Gen2*, *Gen3*, and *Gen4* = synchronous generators 1 to 4.

The generators' AVR and PSS controller had already yielded its damping torque in maintaining stable operating points, as seen in the field voltage, thus generating an insufficient damping coefficient to restore the system to its steady-state operating point quickly. A further increase in the fault clearing time ($t_c = 0.19s$) would lead to the incapability of the generator controllers to fully restore the system to its system steady-state stability point.

4.5.2 Second Scenario

The results were compared to those of the first scenario to determine which of the interconnections performed better in reducing the inter-area oscillation. The active generator power in Figure 4.10 showed a reduced power swing during a system disturbance. The Gen_3

recorded the highest power amplitude of 905 MW after the fault because of continuous generator fault on Gen_4, resulting in higher inertia in restoring the steady-state operating point of the entire system. This led to a lower generator swing for the post-fault condition as the MTDC link reduced the transfer of fault current from one generating station to another, unlike the first scenario where the generator fault on Gen_4 caused a large reduction in power generated by Gen_3. After eight cycles of simulation time, sufficiently damped generator oscillations with low magnitudes were all recorded as all the oscillation amplitude were quickly damped from the enhancement gotten from the robust MTDC controller support. Also, the generators' oscillations were fully damped at exactly 12s simulation time. Figure 4.11 shows the generators' frequency swings. Being an incoherent machine system with A1 having different inertia constants to A2, the generators in A1 swing against those in A2. Gen_1 and Gen_2 in A1 recorded the highest oscillation value of 1.0075 pu. The generator field voltage, shown in Figure 4.12, reached the first maximum swing value of 5.64 pu at 2s. With the MTDC link in operation, this value recorded a slight reduction in the minimum and maximum swing compared to the AC lines operating scenario.

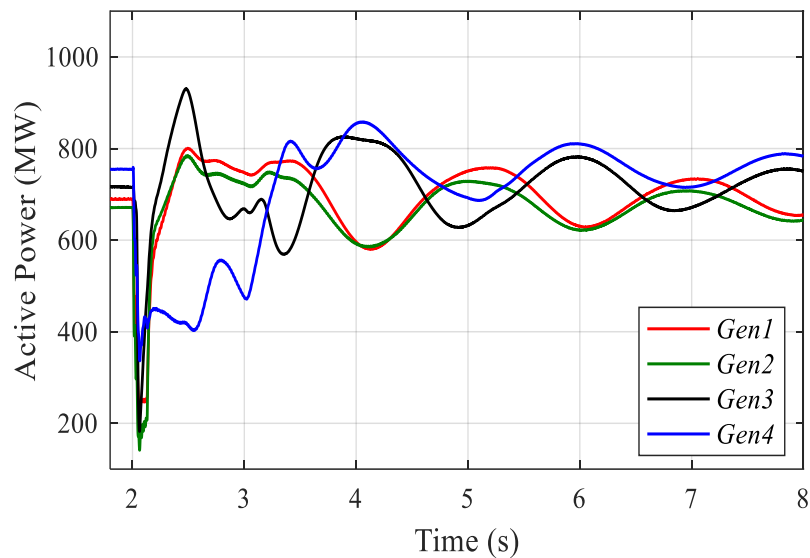


Figure 4.10: Synchronous generator active power during the second scenario, where *Gen1*, *Gen2*, *Gen3*, and *Gen4* = Synchronous generator 1 to 4.

Gen_3. After eight cycles of simulation time, sufficiently damped generator oscillations with low magnitudes were all recorded as all the oscillation amplitude were quickly damped from the enhancement gotten from the robust MTDC controller support.

Also, the generators' oscillations were fully damped at exactly 12s simulation time. Figure 4.11 shows the generators' frequency swings. Being an incoherent machine system with A1 having different inertia constants to A2, the generators in A1 swing against those in A2.

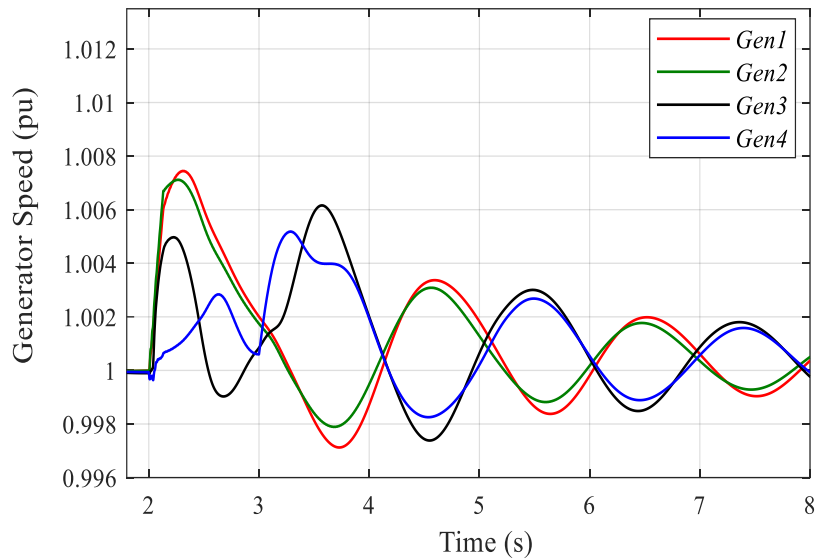


Figure 4.11: Generator speed during the second scenario, where *Gen1*, *Gen2*, *Gen3*, and *Gen4* = Synchronous generator 1 to 4.

The Gen_1 and Gen_2 in A1 recorded the highest oscillation value of 1.0075 pu. The generator field voltage in Figure 4.12 reached the first maximum swing value of 5.64 pu at 2s. With the MTDC link in operation, this value recorded a slight reduction in the minimum and maximum swing compared with the AC lines operating scenario.

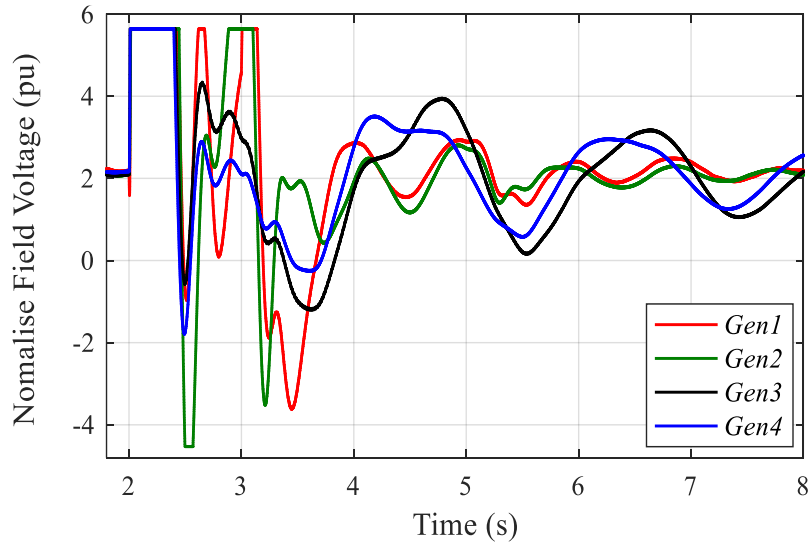


Figure 4.12: Generator field voltage during the second scenario, where *Gen1*, *Gen2*, *Gen3*, and *Gen4* = synchronous generators 1 to 4.

Figure 4.13 shows the active DC power across the three-terminal converters. The Rect-1 station (800 MW converter connected to *Gen_4* in replacement of line L10_11b) showed an increase in power transfer across the link between 2s and 4s simulation time because of the large reduction in power generated by *Gen_3* because of the system's disturbance.

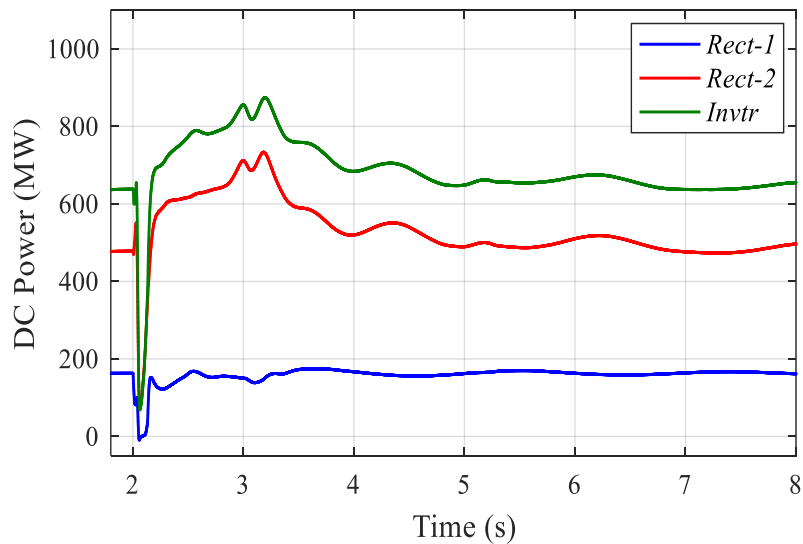


Figure 4.13: Converter power, where *Rect-1*, *Rect-2*, and *Invtr* = rectifier 1, rectifier 2, and inverter station respectively.

While Rect-1 (300 MW converter link connected in replacement of line L7_8b and L8_9b) recorded a zero power dip during the short circuit fault, it was not affected by the generator power swing. Also, a temporary overcurrent can be seen at the inverter's current plot in Figure 4.14. This current overshoot is due to fault current contribution from all parallel converters (minimal in monopole point-to-point connection).

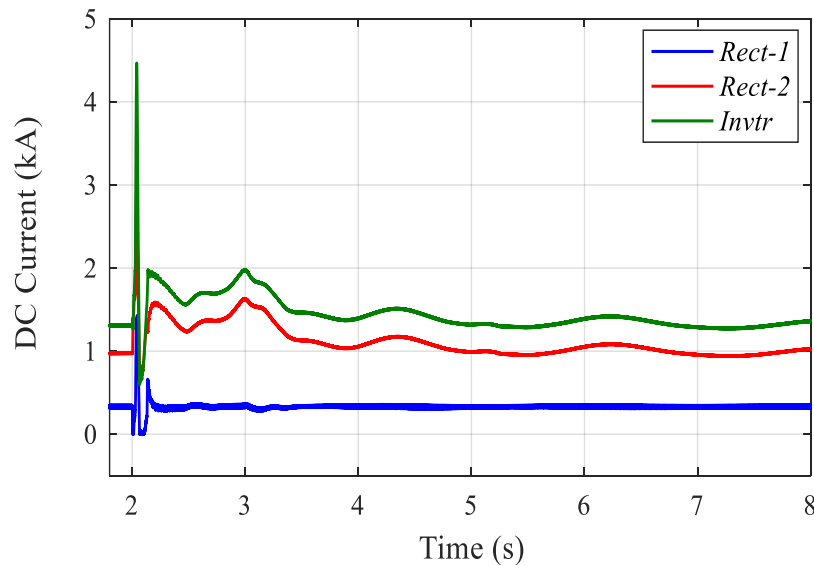


Figure 4.14: Converter current, where *Rect-1*, *Rect-2*, and *Invtr* = rectifier 1, rectifier 2, and inverter station respectively.

However, this temporary spike is within an acceptable limit as the thyristor valve for a multi-terminal system is rated to allow twice the rated valve current to keep it from being damaged. The DC voltage plot in Figure 4.15 shows converter voltage dipping down to 0.2 pu during the fault. This situation could further lead to a reverse in the direction of power flow. However, with the converter current still at positive zero value, this caused a fixed zero power transfer across the link during the two short-circuit faults; thus, the reverse power flow into both rectifiers' stations is thereby avoided with the help of the converter control setup.

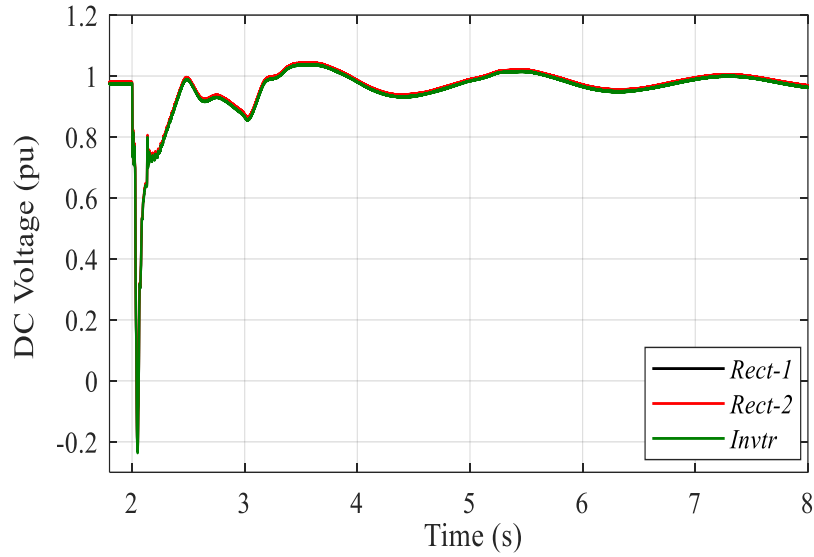


Figure 4.15: Converter voltage, where *Rect-1*, *Rect-2*, and *Invtr* = rectifier 1, rectifier 2, and inverter station respectively .

The three-phase AC voltage plot shown in Figure 4.16 recorded a minimal dip at 2.0s and transient distortion at 2.05s, but recorded no cases of commutation failure at the inverter station during and after the fault.

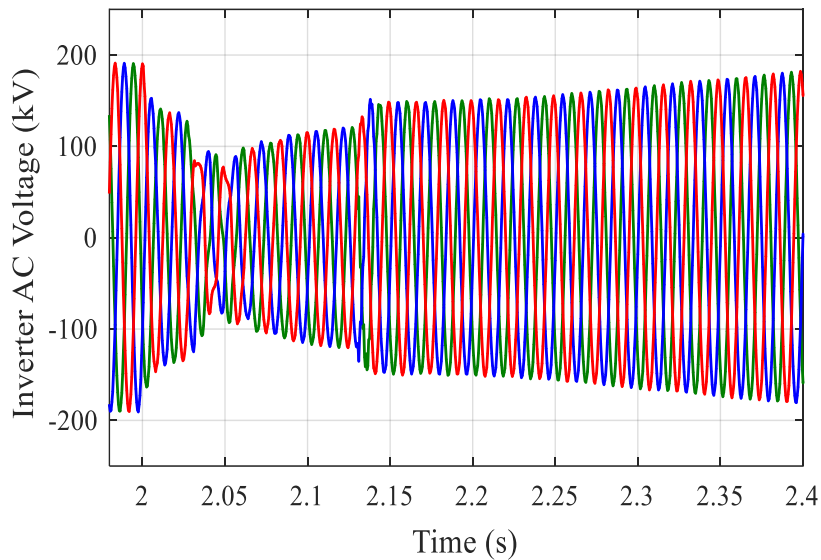


Figure 4.16: Inverter (alternating current) voltage.

The VDCOL plot during the fault condition is shown in Figure 4.17. It reduces the reference current in Rect-2 to allow minimum power flow across the link. Figure 4.18 shows

that the inverter mode shifted from the current control setpoint to the voltage control point during the TFSC fault, thus maintaining a fixed voltage profile across all the converter stations during the fault. The converter-firing angle in Figure 4.19 recorded a sharp decrease at the inverter station because of the TFSC, while a transient increase was noticed across all rectifiers' valves.

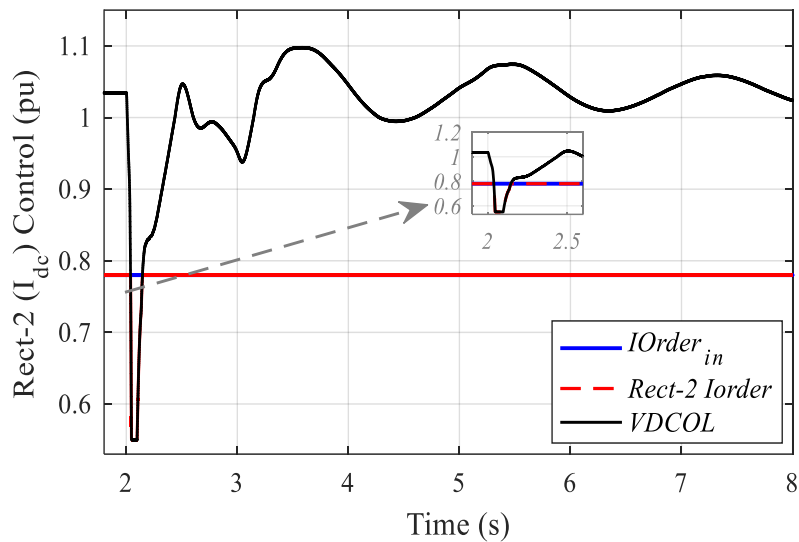


Figure 4.17: Mode shift for rectifier 2 station, where Rect-2Iorder = rectifier 2 current order, VDCOL = voltage dependent current order limiter.

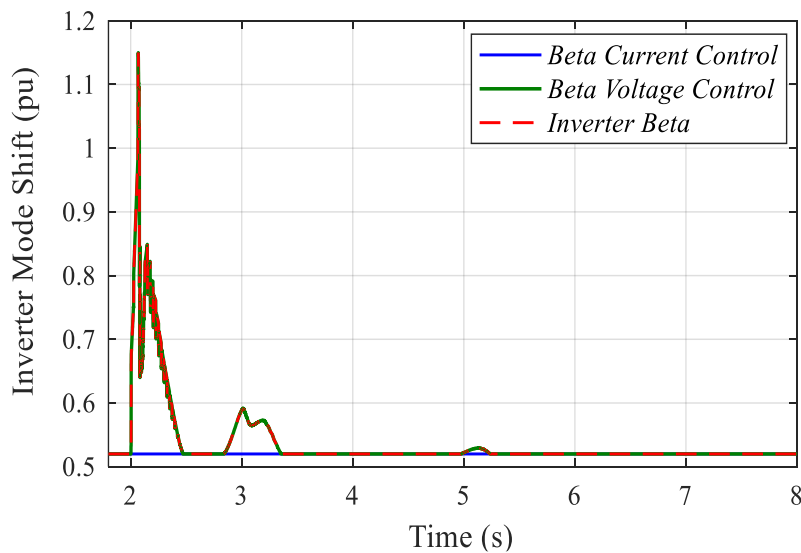


Figure 4.18: Mode shift for the inverter extinction angle.

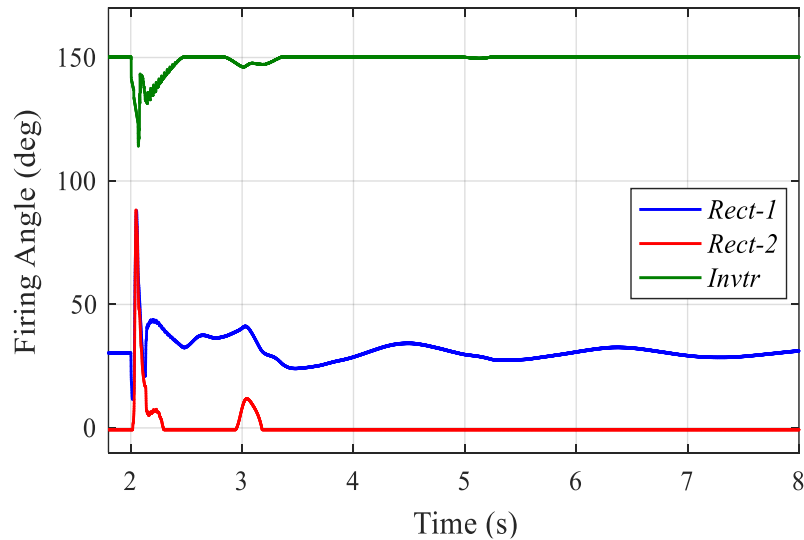


Figure 4.19: Converter firing angle, where *Rect-1*, *Rect-2*, and *Invtr* = rectifier 1, rectifier 2, and inverter station respectively.

Following the fault, Bus_7, 8 and 9 were monitored for the dynamic response of the voltage profile. The bus voltages for both scenarios are presented in Figures 4.20 and 4.21, respectively. During the first scenario of HVAC lines, the dynamic response showed that Bus_8 is the weakest in the network because of its distance from both areas' generating plants, followed by Bus_7. This plot also showed that the increment in the transmission distance between Bus_10 and Bus_11 has no reducing effect on the Bus_9 voltage profile compared with other buses in both scenarios. Figure 4.21 also shows that the second scenario (with MTDC link) generated fewer oscillations, with Bus_8 still having the worst post-fault oscillations. The system-voltage profile was improved during the second scenario as all the system's steady conditions were stabilised after about four cycles.

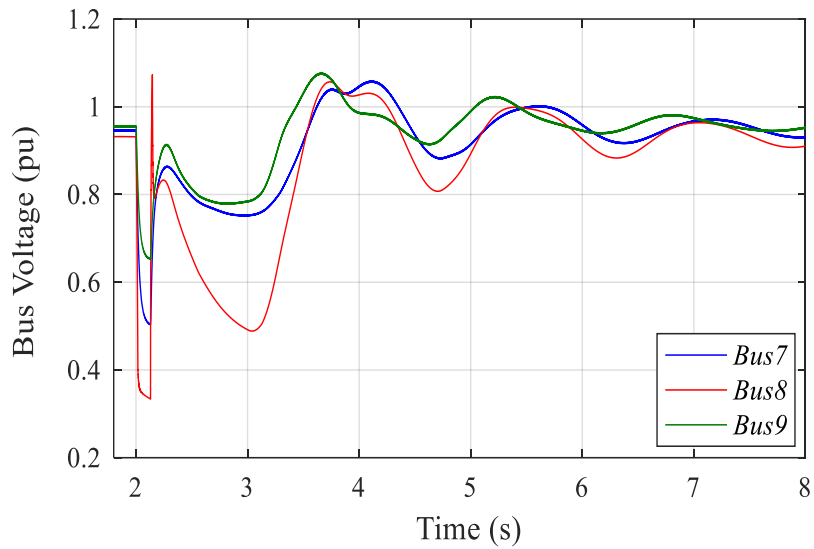


Figure 4.20: Bus voltage during the first scenario of high voltage alternating current lines.

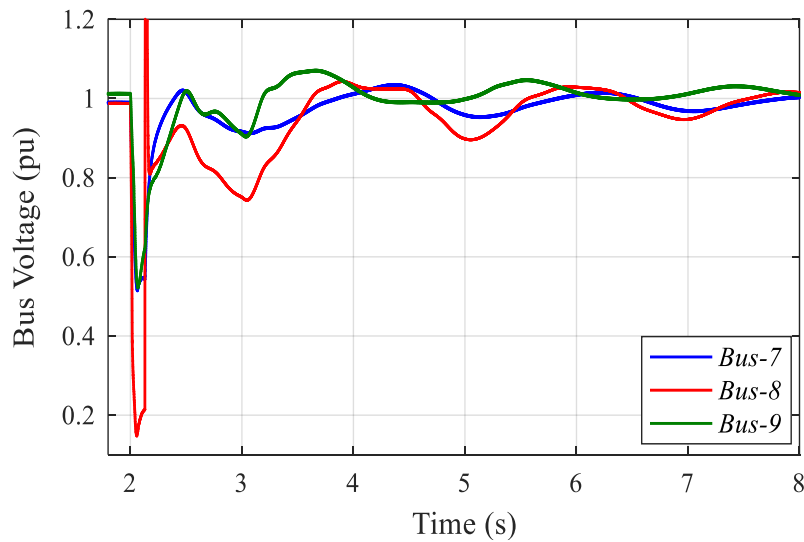


Figure 4.21: Bus voltage during the second scenario of the multi-terminal direct current link.

Inter-area power transfer between Bus_7 and Bus_9 shown in Figure 4.22 confirmed the very slow damping of the inter-area power oscillations for the initial scenario of having only AC transmission lines. The active power during this scenario had undergone a transient post-fault condition, thus contributing more to the oscillations before the steady-state condition could be reached.

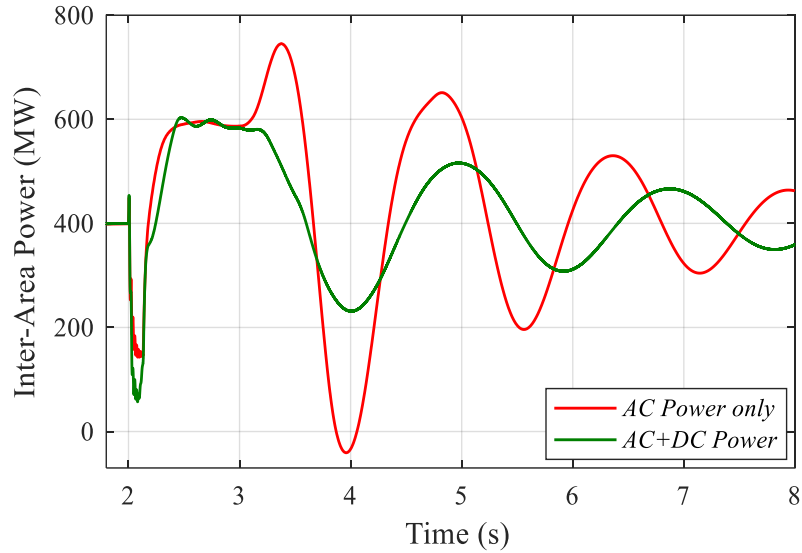


Figure 4.22: Inter-area power transfer during both operating scenarios, where AC and DC are alternating current and direct current respectively.

Figure 4.22 shows that, for the same disturbance with the introduction of the MTDC link, the damping on the inter-area power oscillations increased as the amplitude of the inter-area power transfer across the areas recorded a significant positive damping rate, thereby providing more stable steady-state operating conditions. The active power transfer during this scenario corresponds to the power across the AC lines (L7_8 to L8_9) plus the DC power across Rect-1 station. It shows that the damping ratio generated a 37% reduction of the initial value of the oscillation amplitude in the third oscillation period.

Figure 4.23 shows the damping rate value recorded across the inter-area busbar after the third oscillation for a different P_{dc} setpoint for Rect-2. Points a to b, with the active power of 200–340 MW) showed a linear increase in the damping support from the MTDC link with the first scenario of double AC lines falling in between this operating point, providing approximately 34.7% damping after the third oscillation. Points b to c recorded a small increase, while c to d recorded a significant increase in the damping support given by the MTDC link. Point e witnessed the damping saturation point where a further increase in the P_{dc} for Rect-2 brought about a decrease in the damping support to the system oscillation amplitude due to excess active power in the entire AC/DC system.

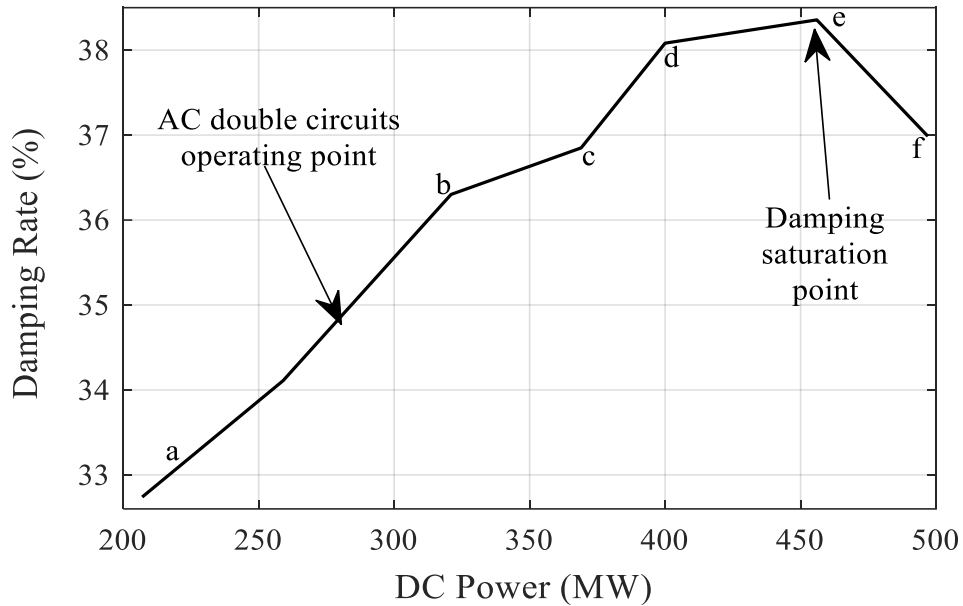


Figure 4.23: Damping rate for different converter power values across Rectifier 2 station, where AC and DC = alternating and direct current.

4.6 CONCLUSION

Two methods of power transmissions were carried out on a modified Kundur two-area four-machine system with regard to the impact of a fault on the AC-DC networks. Following the system fault on the test network, the poorest damped modes of the active power and synchronous speed of the generator in each grid scenario were observed during a time-domain response. These all confirmed that the multi-terminal direct current (MTDC) systems implemented in this study provide better damping of the oscillation with reduced amplitudes compared with the first scenario with high voltage alternating current lines only. The results also showed that excess power transfer across the MTDC link has a detrimental impact on the AC network inter-area oscillation. Therefore, better control of the current order (I_{order}) added more inertia support to the synchronous generators by providing sufficient controllability to the system and finally leading to better damping of the generator inter-area swings.

4.7 ACKNOWLEDGEMENT

The study acknowledges the support by Eskom Power Plant Engineering Institute Specialization Centre for HVDC and FACTS; Eskom Tertiary Education Support Programme, and the DTI.

4.8 REFERENCES

- 1 Abdelsalam, H. A. and Abdelaziz, A. Y. 2013. Wide-area automatic voltage regulators controller for damping oscillations based on inter-area modes. *Electric Power Components and Systems*, 41(9), 912-925.
- 2 Abdlrahem, A., Hadidi, R., Karimi, A., Saraf, P. and Makram, E. 2017. Fixed-order loop shaping robust controller design for parametric models to damp inter-area oscillations. *International Journal of Electrical Power & Energy Systems*, 88, 164-174.
- 3 Abdulrahman, I. and Radman, G. 2018. Wide-area-based adaptive neuro-fuzzy SVC controller for damping interarea oscillations. *Canadian Journal of Electrical and Computer Engineering*, 41(3), 133-144.
- 4 Ademola-Idowu, A. and Zhang, B. 2018. Optimal design of virtual inertia and damping coefficients for virtual synchronous machines. arXiv preprint arXiv:1806.08488.
- 5 Anderson, P. M. and Fouad, A. A. 2008. *Power system control and stability*: John Wiley & Sons.
- 6 Azad, S. P., Iravani, R. and Tate, J. E. 2013. Damping inter-area oscillations based on a model predictive control (MPC) HVDC supplementary controller. *IEEE Transactions on Power Systems*, 28(3), 3174-3183.
- 7 Canizares, C., Fernandes, T., Geraldi, E., Gerin-Lajoie, L., Gibbard, M., Hiskens, I. and DeMarco, F. 2016. Benchmark models for the analysis and control of small-signal oscillatory dynamics in power systems. *IEEE Transactions on Power Systems*, 32(1), 715-722.
- 8 Eftekharnejad, S., Vittal, V., Heydt, G. T., Keel, B. and Loehr, J. 2013. Small signal stability assessment of power systems with increased penetration of photovoltaic generation: A case study. *IEEE Transactions on Sustainable Energy*, 4(4), 960-967.
- 9 Elizondo, M. A., Fan, R., Kirkham, H., Ghosal, M., Wilches-Bernal, F., Schoenwald, D. and Lian, J. (2018). Interarea oscillation damping control using high-voltage DC transmission: A survey. *IEEE Transactions on Power Systems*, 33(6), 6915-6923.
- 10 Grigsby, L. L. 2016. *Power system stability and control*: CRC Press.
- 11 Kundur, P., Balu, N. J. and Lauby, M. G. 1994. *Power system stability and control* (Vol. 7): McGraw-hill, New York.

- 12 Li, Y., Rehtanz, C., Ruberg, S., Luo, L. and Cao, Y. 2012. Wide-area robust coordination approach of HVDC and FACTS controllers for damping multiple interarea oscillations. *IEEE transactions on power delivery*, 27(3), 1096-1105.
- 13 Liu, H., Zhu, L., Pan, Z., Bai, F., Liu, Y., Liu, Y. and Bhatt, N. 2017. ARMAX-based transfer function model identification using wide-area measurement for adaptive and coordinated damping control. *IEEE Transactions on Smart Grid*, 8(3), 1105-1115.
- 14 Milano, F., Dörfler, F., Hug, G., Hill, D. J. and Verbič, G. 2018. Foundations and challenges of low-inertia systems. Paper presented at the 2018 Power Systems Computation Conference (PSCC).
- 15 Mondal, D., Chakrabarti, A. and Sengupta, A. 2020. *Power system small signal stability analysis and control*. Academic Press.
- 16 Oni, O. E., Swanson, A. G. and Carpanen, R. P. 2018. Modelling and control of multiterminal LCC HVDC. Paper presented at the 2018 IEEE PES/IAS PowerAfrica.
- 17 Oni, O. E., Swanson, A. G. and Carpanen, R. P. 2019. Small signal stability analysis of a four machine system with strategic placement of monopolar LCC-HVDC link. Paper presented at the 2019 Southern African Universities Power Engineering Conference/Robotics and Mechatronics/Pattern Recognition Association of South Africa (SAUPEC/RobMech/PRASA).
- 18 Preece, R., Milanović, J. V., Almutairi, A. M. and Marjanovic, O. 2012. Damping of inter-area oscillations in mixed AC/DC networks using WAMS based supplementary controller. *IEEE Transactions on Power Systems*, 28(2), 1160-1169.
- 19 Saghafi, H., Karshenas, H. and Bakhshai, A. 2015. Application of integrated series compensator in damping power oscillations in standalone microgrids. *Canadian Journal of Electrical and Computer Engineering*, 38(1), 2-9.
- 20 Sanchez-Gasca, J., Wang, L. and Kundur, P. S. 2017. Small-signal stability and power system oscillations. Power system stability and control. McGraw-Hill, New York.
- 21 Siemens. Small signal stability analysis module: Network eigenvalue analysis for PSSCE. Retrieved from <https://www.siemens.com/content/dam/webassetpool/mam/tag-siemens-com/smdb/energy-management/services-power-transmission-power-distribution-smart-grid/consulting-and-planning/power-systems-simulation-software/psse-small-signal-stability-analysis-sag.pdf>.
- 22 Wandhare, R. G. and Agarwal, V. 2014. Novel stability enhancing control strategy for centralized PV-grid systems for smart grid applications. *IEEE Transactions on Smart Grid*, 5(3), 1389-1396.

- 23 Witzmann, R. 2001. *Damping of interarea oscillations in large interconnected power systems*. Paper presented at the Proceedings on the International Conference on Power Systems Transients.
- 24 Zou, X. 2018. Frequency and damping characteristics of generators in power systems. MSc in Electrical Engineering dissertation. Virginia Tech.

Table 4.1: Multiterminal high voltage direct current data

Parameter	Rect-1	Rect-2	Invtr
Rated/Actual power (MW)	300/198	1000/460	1200/700
Rated/Actual DC current (kA)	0.3/0.2	1.0/0.5	1.2/0.75
α for rectifier, γ_0 for inverter	14.8	18	15
Transformer per 6 pulse thyristor			
Rating (MVA)	350	1000	1200
Voltage (kV)	230/500	230/500	500/230
Leakage reactance (pu)	0.18	0.18	0.18
PI Controller			
Proportional Gain	1.0989	1.5363	1.5363
Integral time constant (s)	0.01092	0.01524	0.01524
VDCOL			
Threshold input	0.4-1.0	0.4-0.9	0.4-0.9
Threshold output	0.55-1.5	0.55-1.0	0.55-1.0

Table 4.2: Synchronous machine data

Generator Data		AVR and PSS	
r_a	0.0025 pu	<i>Input signal</i>	Speed
x_l or x_p	0.130 pu	T_R	0.01 sec
x_d	1.81 pu	V_{imax}	10 pu
$x'd$	0.3 pu	V_{imin}	-10 pu

$x''d$	0.25 pu	K_A	200 pu
$T'd0$	8.0 sec	$Efmax$	7.0 pu
$T''d0$	0.03 (s)	$Efmin$	-6.4 pu
xq	1.7 pu	K_{STAB}	20
$x'q$	0.55 pu	T_W	10 sec
$x''q0$	0.25 pu	T_1	0.05 sec
$T'q0$	0.4 (s)	T_2	0.02 sec
$T''q0$	0.03 (s)	V_{stmax}	0.2
H	6.5 A1, 6.177 A2	V_{stmin}	-0.2

Table 4.3: Transmission line data

DC Transmission line (T-model) data	
R(Ω /km)	0.01
Reactor (H)	0.5968
DC filter (μ F)	15
AC Transmission line data	
r (pu/km)	1e-4
x_L (pu/km)	1e-3
b_c (pu/km)	1.75e-3

Nomenclature

H	Inertia constant in s
K_D	Machine load damping coefficient
ra	Armature resistance in p.u
xd	Unsaturated d axis synchronous reactance in p.u

xq	Unsaturated q axis synchronous reactance in p.u
$x'd$	Unsaturated d axis transient reactance in p.u
$x'q$	Unsaturated q axis transient reactance in p.u
$x''d$	Unsaturated d axis sub transient reactance in p.u
$x''q$	Unsaturated q axis sub transient reactance in p.u
x_l or x_p	Leakage or Potier reactance in p.u
$T'd0$	d axis transient open-circuit time constant in s
$T''d0$	d axis sub transient open-circuit time constant in s
$T'q0$	q axis transient open-circuit time constant in s
$T''q0$	q axis sub transient open-circuit time constant in s
T_e	Exciter time constant in s
P_{max}	Maximum turbine output in p.u
K_{STAB}	Stabilising gain,
T_1	First lead time constant,
T_2	First lag time constant,
T_W	Washout time constant,
K_A	Regulator integral gain,
T_R	Transducer time constant,
$\Delta\omega_r$	Change in angular speed,
E_{fd}	Exciter output voltage,
V_{stmax}, V_{stmin}	Minimum and maximum regulator outputs,
V_{ref}	Reference voltage regulator,

V_s	Combined power system stabilizer and possibly discontinuous control output after any limits or switching,
E_t	Terminal voltage of transducer and load compensation elements
R	Direct current line resistance in Ω/km
r	Alternating current line resistance in pu/km
x_L	Alternating current line reactance in pu/km
bc	Alternating current line capacitive impedance in pu/km
pu	Per unit
PI	Proportional and integral
Rect-1	Rectifier 2
Rect-2	Rectifier 1
Invtr	Inverter
VDCOL	Voltage dependent current order limiter
PSS	Power system stabiliser
AVR	Automatic voltage regulator
AC	Alternating current
DC	Direct current
α	Firing angle for rectifier
γ_0	Initial extinction angle for inverter
MW	Active power in mega watt
MVA	Apparent power in mega volt ampere
KV	Kilo-volt

KA

Kilo-ampere

s

Second

**CHAPTER 5: IMPLEMENTATION OF A MULTITERMINAL LCC
HVDC WITH AUXILIARY CONTROLLER ON
SOUTH AFRICA'S 765KV CORRIDOR**

PAPER EIGHT

This chapter addresses objective four and is presented in a manuscript format. The paper is submitted to IEEE Canadian of Electrical and Computer Engineering.

Implementation of a Multiterminal LCC HVDC with Auxiliary Controller on South Africa's 765kV Corridor

Abstract— The deployment of a 765kV transmission line on Eskom's South African Grid marks the beginning of a new era in power industries. Furthermore, the integration of renewable energies by independent power producers (IPPs) leads to an infrastructural change in the stability performance of the entire grid. These developments are expected to bring a multiterminal direct current (MTDC) system to practical implementation on this grid. Therefore, this study focuses on the dynamic response of the South African transmission grid during system disturbance. In the carrying out of this study, the South African grid was modelled on PSCAD, and its performance was evaluated. The impact of MTDC link on the grid's interarea power oscillation was also investigated. An additional current order controller for the MTDC link was developed, and its' impact on the MTDC power transfer analysed. The results show better system performance and reduced interarea power swings with the inclusion of MTDC link.

Index Terms—Fault clearing time, interarea oscillation, LCC high voltage direct current, Multiterminal direct current (MTDC), rotor angle, short circuits ratio.

5.1 INTRODUCTION

The South African economy has undergone some sustainable economic growth and increasing prosperity since independence [1, 2]; however, the electric power deficits experienced by the national grid over the last decade are becoming a big challenge [3]. These problems arise from the inadequate planning for load growth and failure to integrate new generating plants to compensate for the ever-increasing load demand. The decommissioning of aged synchronous generators furthermore compounds these problems, which often makes the power utilities to operate the grid as close as possible to the maximum transmission capacity. Another problem faced is the weak tie-lines due to long-distance transmission making the voltage and power control more and more critical with increase transmission losses. This congested transmission grid is very susceptible to voltage collapse; therefore, load shedding is often introduced to avert this risk of total system collapse [3-5].

Due to the abundance of coal reserves, the electricity generated in the country is mainly from fossil fuels. This means of generation is well known to be a significant contributor to greenhouse gases, a significant role in the depletion of the ozone layer. Renewable energy sources present a viable promising solution to a more environmentally friendly across generation, transmission, and even on the consumer side. It offers the benefit of an increase in the economic growth rate in the country. Thus, making South African governments welcome the integration of renewable energy by the independent power producers (IPPs) into the national grid [6-8]. However, renewable energy integration requires better grid code compliance and a stable transmission medium [9]. Therefore, a high voltage direct current (HVDC) system is often used for the interlink between the source and the grid before being distributed using ac lines; an example is the ± 533 kV 1920 MW Cahora Bassa interlinking Mozambique and South Africa [10], ± 800 kV 6000 MW NER-Agra Multiterminal HVDC [11], ± 500 kV 4.5GW Zhangbei VSC-HVDC Power Transmission Project [12], etc.

Both ac and dc transmission come with their capabilities and limitations; ac transmission allows quick and easy voltage transformation from one voltage level to another; however, its' susceptibility to a cascading problem during systems disturbance makes the dc transmission system a more viable option. Other advantages of the dc transmission systems are bidirectional power controllability, enhanced system stability, reduced losses, asynchronous interconnection, and reduced right of way [13, 14].

This dc systems are gaining more publicity and are expected to have rapid growth in both the short and long run. Many researchers have evaluated and compared their mechanism, structure, topologies, along with other control measures [15]. Studies on the levelled cost, expected growth, configurations, and deployment are all mentioned in [15, 16]. On power system interarea oscillations, the convectional solution is by careful coordination of the generator's power system stabiliser and the automatic voltage regulators. Other secondary controllers like the governor are added for better reliability of these generating plants. Elizondo et al., in [17], give comprehensive literature on the problems arising from small signal stability and the future trend. On the South African grid, Minnaar et al. in [18] recorded different types of fault that occurred on the South Africa transmission network. They further conducted a reliability check of the grid based on the probabilistic fault performance parameters with respect to season, time of day, and climate. They found that most of the fault on this grid is due to bird streamers with 38% occurrence, lightning with 26%, and fires with 22%. Also, in [5],

Corsi et al. applied a coordinated automatic real-time secondary voltage regulator (SVR) to South African transmission grid thereby providing an improved power quality as well as controllability and stability to the grid. The study on the impact of HVDC link on the South African grid during a three-phase short circuit was further carried out by Mbangula et al., in [19]. This study investigates the rotor angle stability of the South African transmission grid, focusing only on a two-terminal converter technology. Oni et al. discusses the modelling of multiterminal HVDC (MTDC) system in [20], evaluated the performance analysis using a single machine infinite bus system and 4 area machine networks [21] and [22] respectively. They found out that the MTDC network has a significant improvement during a system disturbance. However, those studies in literature do not focus on the impact of a complementary controller on the MTDC link nor analyse the dynamic study of the MTDC link on the South African network.

Therefore, this study focuses on the performance evaluation of the South African transmission grid when interconnected with a three-terminal LCC HVDC system. In carrying out this study, a comprehensive dynamic system model was developed to facilitate the study of the system and form the basis for postulating an appropriate and optimal operating point. This research was also carried out to identify the potential usage of MTDC network on the South African grid and to investigate the performance analysis of MTDC link and the complementary controller on the entire grid operating performance. Given the complexity of the grid network, five of eight grids were modelled on PSCAD, and the impact of a substantial three-phase short circuits fault was analysed on the grid elements. Synchronous damping of the oscillations, bus voltage, and converter response during the steady-state and post-fault conditions have been presented in this paper.

5.2 CHALLENGES AND POSSIBILITY OF SA GRID

The South African power utility is one of the worlds' largest electrical power utilities in Africa, covering the generation, transmission, and distribution of power all over the South African region and to neighbouring Southern African region [22]. The only DC line on this network is the 1300km, ± 533 kV Cahora Bassa HVDC line that interlinks Sango substation near Zambezi river in Mozambique and Apollo substation in South African Central grid [23, 24]. Other electric power transfer is mainly via long AC lines using either 756kV, 400kV, or 275kV transmission lines. The entire grid is characterized by long weak tie-lines and therefore has a low Short Circuit Ratios (SCR). Thus, becoming a matter of necessity to analyze the

various possible interaction effects between the AC and MTDC networks. It will be noted that at low SCR values, transient DC quantities are possible of exhibiting a commutation failure, especially at the inverter AC station. Among other challenges are the AC/DC interaction during overvoltage, harmonic oscillations during load shedding, converter commutation failures, low mechanical inertias, recovery during system disturbance and voltage stability. Considering these effects therefore requires a careful design and control measures to appropriately fit the operational scenarios of MTDC network incorporated on the South African Grid.

Another finding is the exponential growth rate of the load demands in the Central grid of the country. Figure 5.1 shows the provincial load demands during peak season, with the Central grid standing at 10,231 MW, followed by the Eastern grid with 6,160 MW in 2017 peak load demand. The impact of cold weather during the winter season leaves the entire grid in limbo, causing different transient load demands (see Table 5.1). Besides, the exponential load growth in the Central Grid alone is expected to record an increase of ≈ 5.2 GW in the year 2028, as published by Eskom in their transmission development plan (TDP 2019 – 2028), as shown in Table 5.2 [25]. While these problems may persist, the investigation into the usage of MTDC system on this network cannot be overemphasized, as this will bring more knowledge into the reduction of active and reactive power to losses, improved stability margin, and the ease of renewable energy integration. The South African generation capacity is mainly coal-based due to much coal reserves. Moreover, the plan to integrate an additional power of 17800 MW of renewable energy by 2030 will require an alternative and efficient means of transmission for this renewable source that is expected to represent about 20% of the country's installed capacity.

Table 5.1: Impact of Load Demand During the Winter Season

Day	Min/max peak load	Summer (GW)	Winter (GW)
Monday	Min	22.5	21.5
	Max	34.5	35.3
Tuesday	Min	22.5	22.8
	Max	34.1	35.2
Wednesday	Min	22	22.5
	Max	33.2	35.1
Thursday	Min	22	22.5
	Max	33.5	35
Friday	Min	22.5	22.8
	Max	32.8	33.8
Saturday	Min	22.5	22.8
	Max	32.7	32.7
Sunday	Min	21.1	21.6
	Max	32.5	32.8

Table 5.2: Load Progression in the Central Grid

Year	Zonal Demand				Grid Peak
	West Rand	Johann- esburg	East Rand	Vaal	
2019	3749	3600	3248	1838	11439
2020	3841	3687	3314	1957	11751
2021	3966	3794	3476	1972	12204
2022	4113	3832	3579	2006	12634
2023	4213	3896	3629	2025	12901
2024	4334	3966	3717	2063	13299
2025	4508	4141	3813	2093	13702
2026	4721	4267	3889	2111	14033
2027	4942	4398	3985	2135	14547
2028	5138	4542	4100	2165	15057

5.3 NETWORK MODELLING

The South African grid is divided into seven geographical operating units, each consisting of generation, transmission, and a distribution network. In the carrying out of this study, six out of the eight grids were modelled with transmission voltage levels of 765kV and 400kV, as shown in Figure 5.2. The networks used are that of the Northern, Central, North-West, Southern, and Western Grid. Table 5.3 in the appendix section highlights the generator used and their installed capacity. The synchronous generator control model consists of the IEEE Type AC4A alternator supplied rectifier excitation system and single input power system stabiliser (PSS1A) for the controlling of the generator stator voltage. Three network configurations were considered. The first configuration explores the steady-state analysis of the network without the inclusion of the MTDC network; the second scenario analyses the impact of the MTDC on the network. The third network implemented an auxiliary complementary controller to generate a new dc current order (I_{dcnew}) for the MTDC link. Details and diagrams of the excitation systems and the PSS used are well explained in [21]. Performance analysis was carried out on PSCAD/EMTDC. This simulation tool was used for its' best electromagnetic transient studies and also because its main application is in the implementation of AC/DC network.

5.3.1 MTDC Link with Complementary Controller

The MTDC system used in this study is a three-terminal LCC HVDC link with two rectifiers and one inverter, as shown in Figure 5.3. LCC HVDC system was utilised due to its advantage over VSC HVDC for long-distance and bulk power transfer. It also has excellent overcurrent capability with well-established technology and robust devices as well as a proven circuit. Furthermore, from the research carried out by Minnaar *et al.* in [18], the South African transmission grid has long-distance transmission lines and is prone to overhead line faults, therefore LCC HVDC system is preferred in these applications because of its resilience to DC-side short circuit faults. The LCC HVDC system can also operate very well during a low DC voltage and DC fault [25].

The first rectifier used in this study is connected at the *Mat_PS* substation with a distance of 1540km from the inverter station at Hera Substation, while the second rectifier is connected at the *Koe_PS* substation with 540km distance interval from the inverter station. Both rectifiers export power to the Hera substation in the Central grid.

stations are in current control mode as shown in Figure 5.4, thus commute by varying the firing angle α or by controlling ac voltage using the on-load tap changers (OLTC). The inverter station defines the voltage level of the entire MTDC link. The defining of the voltage level is done with the extinction angle of $\gamma = \gamma_o$ control. The maximum value (γ_{max}) is pre-selected from the constant extinction angle (γ_o) and the measured (γ_{meas}), which when subtracted from pi gives the firing angle (α_i) for the inverter station (also in Figure 5.4, Data in Appendix Table 5.4).

The overall power controller shown in Figure 5.5 helps to generate the current order for the three converters. It also helps to balance the power and current order of the entire converter by ensuring that dc current summation across the converters equals zero ($\sum I_{dc} = 0$). The data for this controller has been provided in Appendix Table 5.5.

An additional supplementary controller is added for a better dc power control during systems disturbance. This auxiliary controller, as shown in Figure 5.6, uses the measured differential changes in the ac power to generate the additional dc current for the three converters. The dc current (I_{dc}) is then added to I_{ord} from the overall current controller.

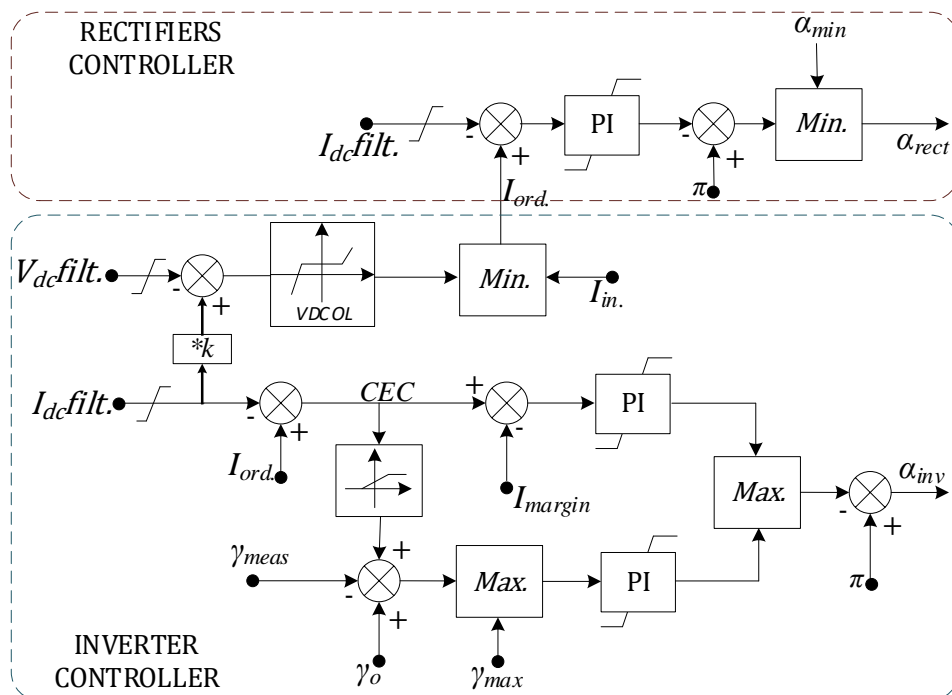


Figure 5.4: Current and voltage controller

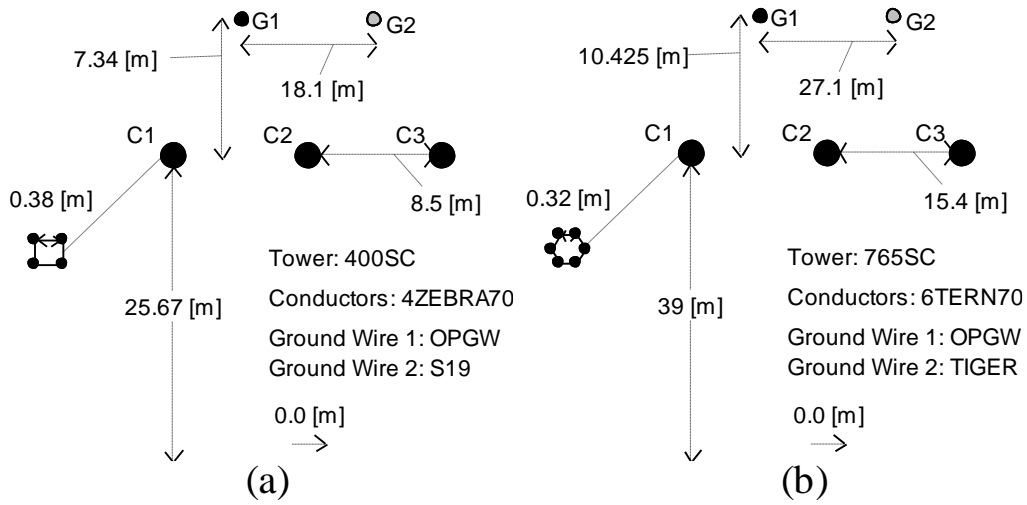


Figure 5.7: Tower geometry for the overhead lines (a) 400kV geometry, and (b) 765kV geometry.

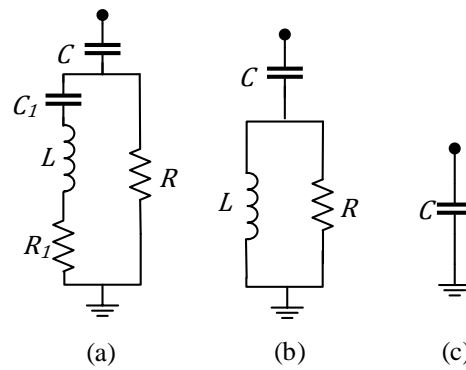


Figure 5.8: (a) C-type filter, (b) high pass filter, and (d) capacitor bank

$$C = \frac{Q_c}{2\pi fV^2} \quad (1)$$

$$L = \frac{V^2}{2\pi fQ_c(h_o^2 - 1)} \quad (2)$$

$$C_1 = \frac{Q_c}{2\pi fhV^2}(h^2 - 1) \quad (3)$$

$$R_1 = \frac{qV^2}{hQ_c} \quad (4)$$

$$Z = \left(\frac{1}{R} + \frac{1}{j\omega L} \right)^{-1} \quad (5)$$

$$q = \frac{R}{2\pi fL} \quad (6)$$

Where h is the harmonic order; Q_c is the filter reactive power; V is the system voltage; ω is the natural frequency, and q is the quality factor. C and C_1 are the series and common capacitance respectively; f is the fundamental frequency; L is the inductance; Z is the total impedance; R and R_1 are the series and parallel resistance respectively.

5.4 SIMULATION RESULT

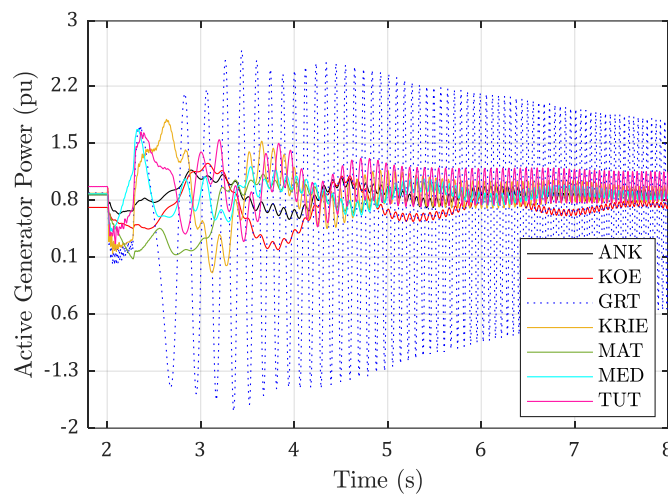
The grid was modelled on PSCAD/EMTDC, the response of the system was evaluated following a 270ms three-phase fault on the transmission lines between Hera and Grootvlie (He_Gr) substation. The fault was applied 10% into the transmission line from Grootvlie bus. The type of fault was carried out following different scenarios of fault analysis on the system, and it was found out that this fault location produced the most critical clearing time for the entire network. Therefore, the system's response during this particular system disturbance was used as the base case.

During the dynamic analysis, the generator power output, rotor angle, generator speed, and the bus voltage were presented graphically on a subplot. Following this severe disturbance at the *He_Gr* transmission line at $t=2s$ simulation time, $20\mu s$ solution time steps and $100\mu s$ channel plot step were used in computing the results. The parameter depicted on a subplot was for better illustration of the system performance before, during, and after the disturbance. The dc power, voltage and the firing angle for the converters were illustrated on a plot. For the synchronous generator plot, *Med_PS*, and *Mat_PS* were chosen to represent the Northern grid generating plant, *Grt_PS*, *Krie_PS*, and *Tut_PS* were selected to represent the North-East grid, while *Koe_PS* and *Ank_PS* represent the generators from the Western grid. Furthermore, for the bus voltage plotted, strategic busbar was chosen from the main generating substation for the evaluation of the voltage profile.

The dynamic stability response of the network with and without MTDC network is given in Figures 5.9 to 5.15. Figures 5.9a and 5.9b depict the generator active power plots without and with MTDC link respectively. On these plots, each generator power supply is represented on a per unit (pu) scale. The combination of both scenarios is shown in Figure 5.9c. On this plot, the *GRT_PS* is already out of step with its active power swinging between $\approx \pm 2$ pu value.

The results in Figure 5.11a with *Grt_PS*, a generating plant at the North-East grid, has proximity to the short circuit's fault. Thus, the generator loses synchronism at first swing. Since disturbance applied to the network has the critical clearing time of the system, the results thus show that following the disturbance, the first swing in the rated active power in the line has a larger amplitude of 2 pu. Others generating plant was able to maintain stability, however, with a very poor damping factor causing a torsional oscillation, especially at the western grid. This impact can be observed in the oscillations shown in Figure 5.9a. However, following the same disturbance with the MTDC system, the results in Figure 5.9b show that positive damping has been added to the generators' oscillations on the network. Therefore, the implementation of the MTDC model on the grid provided a better performance compared to the first case study. The *Mat_PS* and *Grt_PS* with the worst post-fault condition were able to maintain a stable operating point after the third cycle.

Figures 5.10a and 5.10b show the generator rotor angle (δ) dynamics in radian. In this Figure 5.10a, the *Grt_PS* synchronous generator went out of step from the rest of the synchronous machine. It recorded a rapid increase in the rotor angle while other generators witnessed a steady increase with the continuous oscillation.



(a)

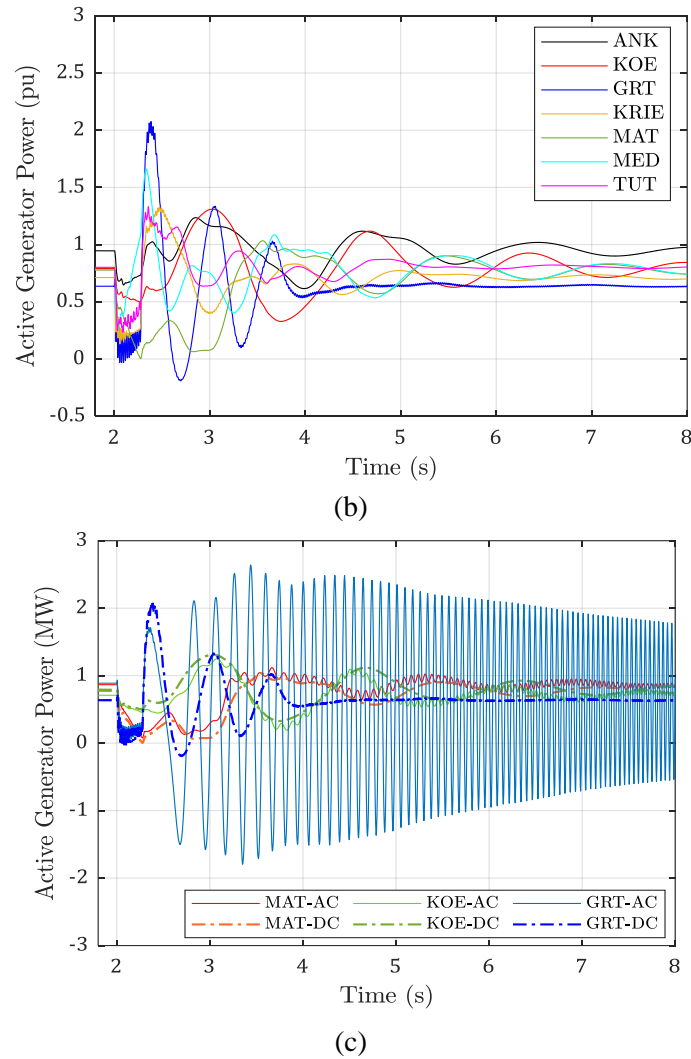
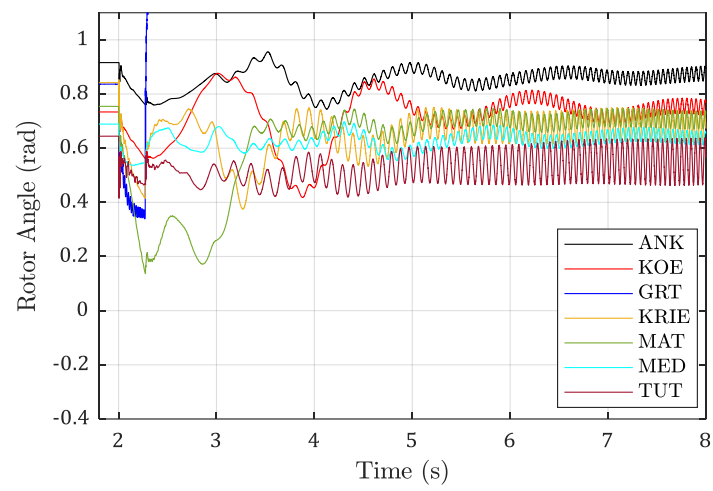


Figure 5.9: Active power for the synchronous generator (a) without the MTDC link, (b) with MTDC link, (c) Comparative plot of the active power of three generators in each grid.

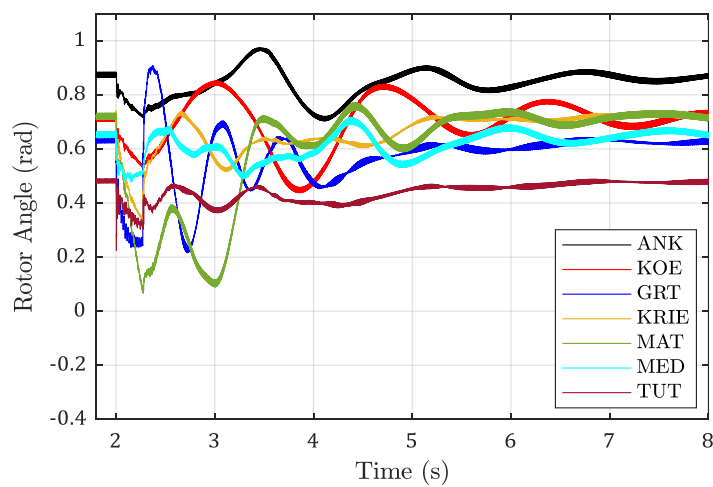
These generators, having yielded their excitation and AVR controls, remained unstable even after clearing the fault due to insufficient decelerating torque to reduce the rotor speed, i.e., the generators exhibited positive damping (T_D) torque but with a negative synchronising torque (T_S), causing a non-oscillatory instability. The unstable state involving the rotor angle speed is usually referred to as electromechanical oscillations. The control systems are intended to restore the power system to stable conditions and to align the mechanical torque with the electromagnetic torque of each generator, thereby ensuring the stability of the rotor speeds and that of the rotor angles. The inclusion of MTDC link on the network enhanced the stability condition, as seen in Figure 5.7b. The generators experienced few rotor angle oscillations but were able to maintain a stable post fault condition when the fault was cleared. The turbine governor adjusts the mechanical torque, and the voltage regulator is trying to restore the voltage. The first oscillation of the rotor angle is of interest, which may indicate whether or not

the generator would remain synchronised. The second observation on these plots is the interarea oscillations between the Northern grid generators (*Med_PS* and *Mat_PS*) and the Western Grid generator (*Ank_PS* and *Koe_PS*). These interarea swings are due to the long and weak transmission lines between the two grids.

The generators' angular speed response is shown in Figures 5.11a and 5.11b. In the first plot (without the MTDC link), *Grt_PS* recorded a sharp angular acceleration up to 1.033pu at time $t=2.34$. The generator's post fault condition experienced unexpanded kinetic energy, which resulted in a continuous increase of the rotor speed and thus led to a loss of synchronism. Other generators were in stable condition but with insufficient damping torque. Figure 5.11b shows a better generator speed with quickly damped oscillations. The rotor angle eventually settled to a normalised new reference value. However, *Mat_PS* and *Med_PS* have the worst post fault condition.

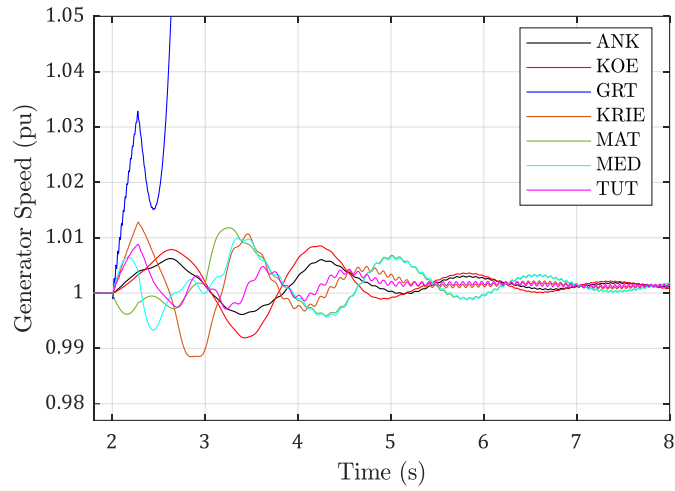


(a)

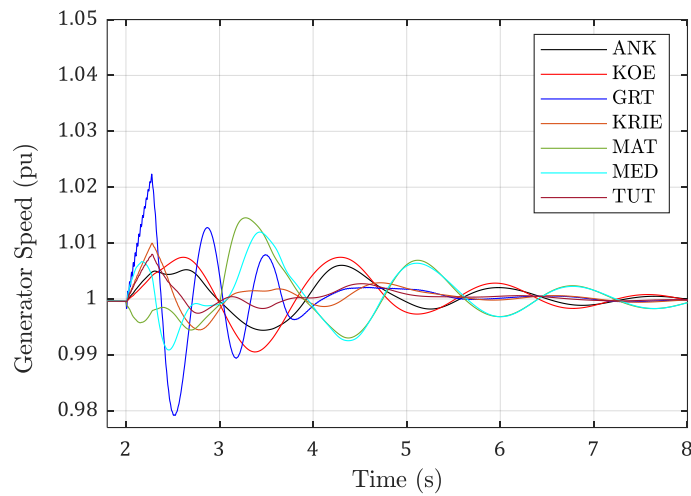


(b)

Figure 5.10: Rotor angle for the synchronous generator (a) without the MTDC link, (b) with MTDC link



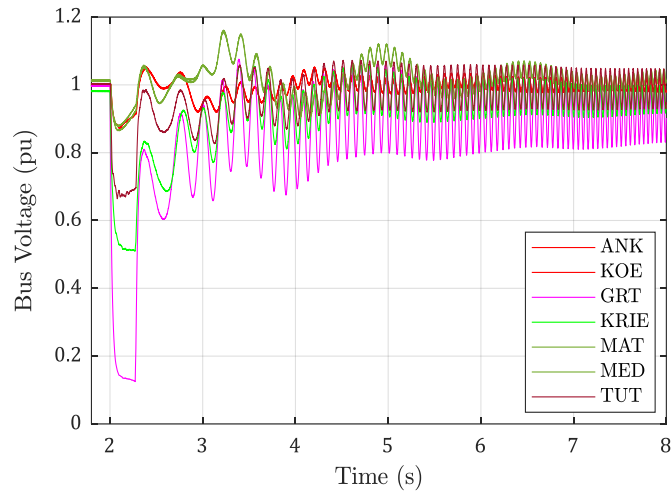
(a)



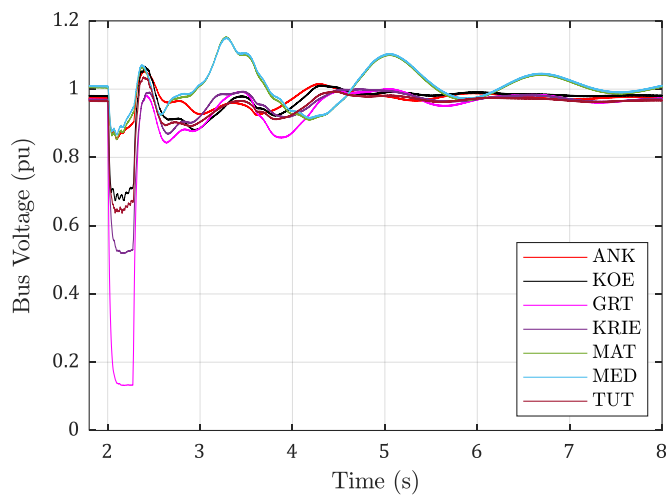
(b)

Figure 5.11: Angular Speed for the synchronous generator (a) without the MTDC link, (b) with MTDC link

As earlier stated, specific busbar was selected and monitored for voltage profile variation. The plot in Figures 5.12a and 5.12b show this voltage profile without and with MTDC link respectively. *Grt* bus has the lowest dip of 0.16pu in Figures 5.12a and 5.12b. These dips occurred due to the high fault impedance generated from the fault proximity. It is followed by *Krie* bus, and *Tut* bus accordingly. Also, the system without the inclusion of MTDC in Figure 5.12a experienced high voltage oscillations between the range of 0.7 - 1.1pu. The dynamic voltage response in Figure 5.12b with the implementation of the MTDC link shown a steady and stable post fault condition. However, the *Med* busbar recorded the worst post voltage profile due to due to the high impedance of the line from the generator to the load.



(a)



(b)

Figure 5.12: Bus voltage profile (a) without the MTDC link, (b) with MTDC link

The dc power is shown in Figure 5.13 following a three-phase short circuits fault on the *Gr_He* transmission line. The plot shows the converters' dc power with and without a supplementary controller. This analysis is to evaluate the contributive impact of the supplementary controller on the active power transfer across the multiterminal converters. At simulation time $t=2s$, the power transfer dips to $-8MW$, meaning a reverse transfer into rectifier link. However, with the VDCOL, the corresponding lower voltage of $0.1pu$ is selected, thereby reducing the transfer of excessive fault current into the inverter station.

Subsequent power oscillation is limited by the action of the VDCOL and the inverter extinction angle controller, which mode shifts between the voltage or the current controller during the fault. The supplementary controller produces better damping of the power oscillation for the MTDC link. The rectifier 1, 2, and inverter power with auxiliary (*ARP1*, *ARP2*, and *AIP*) show significant damping than the rectifier 1, 2 and inverter (*RP1*, *RP2* and *IP*) without

the additional controller. Finally, the firing angle for the converters is shown in Figure 5.14. The pre-fault value being 29.75° , 21.97° , and 150.21° for the rectifier 1, rectifier 2, and the inverter station respectively.

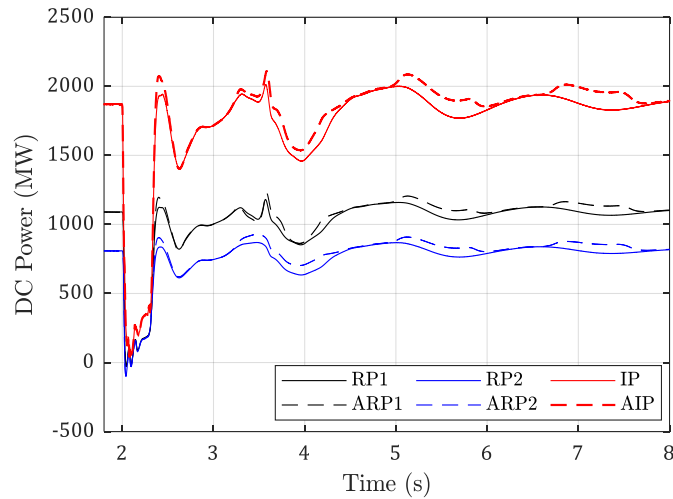


Figure 5.13: MTDC power (where RP1 is rectifier 1 Power, and ARP1 is Rectifier 1 Power with Auxiliary control)

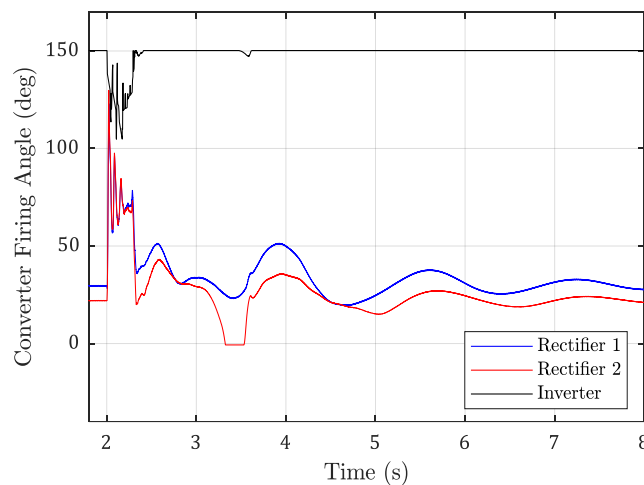


Figure 5.14: Firing angle in (deg)

Figure 5.15 shows the inter-area power transfer between the transmission line linking North-East and the Central grid. The transmission lines considered for the first scenario are the *Merc_Herm*, *Merc_Mid*, and *Grt_Hera*, while the interarea power transfer during the scenario corresponds to the power across the ac lines (*Merc_Herm*, *Merc_Mid*, and *Grt_Hera*) plus the dc power across Rectifier 1 station. From this plot, the impact of the negatively damped torque (T_d) is evident during the first scenario. With very poor damping, the active power has undergone a post-fault harmonic and thus unable to meet the steady operating condition. The implementation of the MTDC link provided an enhancement into the damping of the inter-area

power oscillations as the network recorded a significant positive damping torque. Thus, providing a more stable post-fault condition. The impact of the supplementary controller on the damping of interarea power during the disturbance is also shown in this plot.

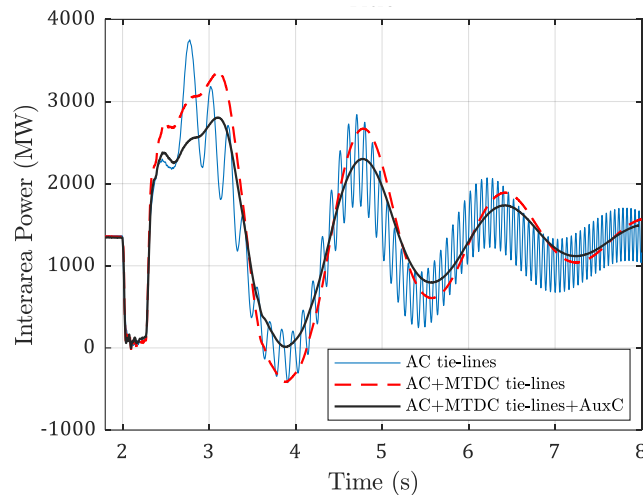


Figure 5.15: Interarea Power transfer across the Northern and north-east border

5.5 CONCLUSION

The detailed response of South Africa's transmission grid during a dynamic RMS simulation is presented in the paper. Also, the benefits of implementing a +600kV three-terminal line commutated converter link has been compared on the network's voltage, interarea oscillation as well as rotor angle stability. Initial response during a system disturbance shows a loss of synchronising effect from both the AVR and PSS, which causes the generator to lose synchronism with subsequent oscillations. A negative damping torque for the rotor angle and negative synchronising torque for the interarea oscillations was observed during the first scenario. While *Grt_PS* was already out of step, the other generators experience a harmonic power oscillation amplitude at a continuous increase in the rotor angle degree. Also, the additional impedance was added to the system, which resulted in a more weakened grid strength. As a result of these, more harmonics are generated in the voltage profile. The modelling of the MTDC link on the grid provided a better system performance because the MTDC controller provided a robust and enhance improvement for the AC network. This improvement can be observed as the results in this paper showed that positive damping had been added on inertial swing mode of all the generators as well as on the interarea oscillations. They were thus showing the benefits of incorporating an MTDC link into a weak ac grid.

The voltage profile was significantly improved, and so is the minimisation of the generator oscillations. Among all the benefits, the power carrying capacity at a reduced loss stood out. Therefore, the study gives a better understanding of the implementation of the MTDC link on the South African network. Adopting this research into the South Africa grid will help reduce transmission losses with enhanced system stability margin. Finally, the auxiliary controller should be considered as it showed a good potential for the mitigation of excessive active power dip of the MTDC link during the system disturbance.

5.6 REFERENCES

- [1] S. Du Plessis and B. Smit, "Economic growth in South Africa since 1994," *University of*, 2006.
- [2] M. Lundahl, *Growth Or Stagnation?: South Africa Heading for the Year 2000*. Routledge, 2019.
- [3] J. G. Wright and J. R. Calitz, "Setting up for the 2020s: Addressing South Africa's electricity crises and getting ready for the next decade. Version 1.1," 2020.
- [4] J. Molepo, "Blackout: The Eskom Crisis, James-Brent Styan: book review," *Journal of Public Administration*, vol. 53, no. 3, pp. 795-798, 2018.
- [5] S. Corsi, F. De Villiers, and R. Vajeth, "Secondary voltage regulation applied to the South Africa transmission grid," in *IEEE PES General Meeting*, 2010: IEEE, pp. 1-8.
- [6] O. M. Longe, L. Myeni, and K. Ouahada, "Renewable Energy Solution for Electricity Access in Rural South Africa," in *2019 IEEE International Smart Cities Conference (ISC2)*, 2019: IEEE, pp. 772-776.
- [7] J. R. Calitz and J. G. Wright, "Statistics of utility-scale solar PV, wind and CSP in South Africa in 2018," 2019.
- [8] J. Larmuth and A. Cuellar, "An updated review of South African CSP projects under the renewable energy independent power producer procurement programme (REIPPPP)," in *AIP Conference Proceedings*, 2019, vol. 2126, no. 1: AIP Publishing LLC, p. 040001.
- [9] A. Q. Al-Shetwi, M. Hannan, K. P. Jern, M. Mansur, and T. Mahlia, "Grid-connected renewable energy sources: Review of the recent integration requirements and control methods," *Journal of Cleaner Production*, vol. 253, p. 119831, 2020.

- [10] P. Goosen, C. Reddy, B. Jonsson, T. Holmgren, O. Saksvik, and H. Bjorklund, "Upgrade of the Apollo HVDC converter station," in *Proc. CIGRÉ 6th Southern Africa Regional Conf.*, 2009: Citeseer, pp. 1-6.
- [11] S. Barman, A. R. Paul, and H. J. Bahirat, "Control strategy for ± 800 kV 6000 MW NER-Agra Multi-Terminal HVDC Project," in *2018 20th National Power Systems Conference (NPSC)*, 2018: IEEE, pp. 1-6.
- [12] H. Pang and X. Wei, "Research on key technology and equipment for Zhangbei 500kV DC grid," in *2018 International Power Electronics Conference (IPEC-Niigata 2018-ECCE Asia)*, 2018: IEEE, pp. 2343-2351.
- [13] O. E. Oni, I. E. Davidson, and K. N. Mbangula, "A review of LCC-HVDC and VSC-HVDC technologies and applications," in *2016 IEEE 16th International Conference on Environment and Electrical Engineering (EEEIC)*, 2016: IEEE, pp. 1-7.
- [14] L. Reed, M. G. Morgan, P. Vaishnav, and D. E. Armanios, "Converting existing transmission corridors to HVDC is an overlooked option for increasing transmission capacity," *Proceedings of the National Academy of Sciences*, vol. 116, no. 28, pp. 13879-13884, 2019.
- [15] A. Alassi, S. Bañales, O. Ellabban, G. Adam, and C. MacIver, "HVDC transmission: technology review, market trends and future outlook," *Renewable and Sustainable Energy Reviews*, vol. 112, pp. 530-554, 2019.
- [16] O. E. Oni and I. E. Davidson, "Technical performance and cost analysis of a 600kV HVDC link on South Africa's EHV network," in *2017 IEEE PES PowerAfrica*, 2017: IEEE, pp. 88-94.
- [17] M. A. Elizondo *et al.*, "Interarea oscillation damping control using high-voltage dc transmission: A survey," *IEEE Transactions on Power Systems*, vol. 33, no. 6, pp. 6915-6923, 2018.
- [18] U. Minnaar, C. Gaunt, and F. Nicolls, "Characterisation of power system events on South African transmission power lines," *Electric power systems research*, vol. 88, pp. 25-32, 2012.
- [19] K. Mbangula, I. Davidson, and R. Tiako, "Improving Power System Stability of South Africa's HVAC Network Using Strategic Placement of HVDC Links," *CIGRE Science & Engineering Journal (CSE)*, vol. 5, pp. 71-78, 2016.
- [20] O. E. Oni, A. G. Swanson, and R. P. Carpanen, "Modelling and control of multiterminal LCC HVDC," in *2018 IEEE PES/IAS PowerAfrica*, 2018: IEEE, pp. 274-279.

- [21] O. E. Oni, A. G. Swanson, and R. P. Carpanen, "Impact of LCC–HVDC multiterminal on generator rotor angle stability," *International Journal of Electrical and Computer Engineering*, vol. 10, no. 1, p. 22, 2020.
- [22] O. E. Oni, A. G. Swanson, and R. P. Carpanen, "Small signal stability analysis of a four-machine system with placement of multiterminal high voltage direct current link," *Journal of Energy in Southern Africa*, vol. 31, no. 1, pp. 73-87, 2020.
- [23] O. E. Oni and I. E. Davidson, "Harmonic distortion of LCC-HVDC and VSC-HVDC link in Eskom's cahora bassa HVDC scheme," in *2016 IEEE International Conference on Renewable Energy Research and Applications (ICRERA)*, 2016: IEEE, pp. 484-489.
- [24] Eskom, "The Eskom Transmission Development Plan (2019 -2028)," 25 October 2018. [Online]. Available:
http://www.eskom.co.za/Whatweredoing/TransmissionDevelopmentPlan/Pages/Transmission_Development_Plans.aspx
- [25] D. Jovcic, "VSC HVDC Applications and Topologies, Performance and Cost Comparison with LCC HVDC," in *High Voltage Direct Current Transmission*, 2019, ch. 12, pp. 137-163.
- [26] PSCAD, "Passive Filter Design." [Online]. Available: https://www.pscad.com/webhelp/ol-help.htm#Opening_Screen.htm.

5.7 APPENDIX

Table 5.3: Synchronous generator

Generator	Installed capacity (MW)
<i>Med_PS</i>	2000
<i>Mat_PS</i>	3000
<i>Krie_PS</i>	1770
<i>Tut_PS</i>	700
<i>Koe_PS</i>	2300
<i>Ank_PS</i>	2000
<i>Grt_PS</i>	600

Table 5.4: AC Transmission Line Data

	400kV line	765kV line
<i>No of sub conductor</i>	4	6
<i>Bundle spacing</i>	0.38	0.32m
<i>DC-resistance Ohm/m</i>	0.0674	0.0718
<i>GMR (Equivalent radius)</i>	11.56	9.04mm
<i>Outer diameter</i>	28.62	27mm

Table 5.5: Multiterminal High Voltage Direct Current Data

Parameter	Rectifier 1	Rectifier 2	Inverter
<i>Rated power (MW)</i>	2000	2000	4000
<i>DC current (kA)</i>	0.89	0.677	1.57
<i>α for rectifier,</i> <i>γ_0 for inverter</i>	14.8	18	15
Transformer per 6 pulse thyristor			
<i>Rating (MVA)</i>	1000	1000	2000
<i>Voltage ac/dc (kV)</i>	400/600	400/600	400/600
<i>Leakage reactance (pu)</i>	0.18	0.18	0.18

PI Controller			
<i>Proportional Gain</i>	1.0989	1.5363	1.5363
<i>Integral time constant (s)</i>	0.01092	0.01524	0.01524
VDCOL			
<i>Threshold input</i>	0.4-1.0	0.4-0.9	0.4-0.9
<i>Threshold output</i>	0.55-1.5	0.55-1.0	0.55-1.0

Table 5.6: Auxiliary Controller

	Gain	Time Constant				
		T1	T2	T3	T4	T5
<i>G1</i>	1	10s				
<i>G2</i>	0.25		0.6s	0.22s		
<i>G3</i>	1				0.012s	
<i>G4</i>	1					0.12s

Table 5.7: MTDC Transmission line (T-model) data

	R (Ω)	L (H)	C (μ F)
<i>Rectifier 1 to Inverter</i>	14.50	0.61	26
<i>Rectifier 2 to Inverter</i>	5.40	0.58	26

Table 5.8: Filter Design

AC filter	Rectifier 1	Rectifier 2	Inverter
C-type Filter			
<i>C</i>	4.00	1.98	5.50
<i>C1</i>	42.02	21.80	58.00
<i>L</i>	0.242	0.46	0.173
<i>R</i>	51.5	100.7	36.79
<i>Rp</i>	100	100	100

	High Pass Filter		
<i>R</i>	80 Ω	73	80
<i>C</i>	3.9 μf	1.5	4
<i>L</i>	0.0232	0.058	0.023
	H		

CHAPTER 6: CONCLUSION AND RECOMMENDATION

6.1 CONCLUSIONS

The main objective of this thesis was to investigate the performance of MTDC system in an AC network. The study discusses multiple problems relating to small signal stability and rotor angle stability of interconnecting AC networks. In achieving the objectives of this study, a multiterminal LCC HVDC, as well as different test networks, were modelled using PSCAD/EMTDC software, and different fault scenarios were carried out the AC/DC network. The outcome of the study has tremendously increased more knowledge on power systems performance and operation and enhancing of AC network using MTDC network. This research will thus contribute to the improvement in the operational performance of AC transmission networks. The following are the conclusions based on each part of the thesis.

6.1.1 Modelling and Control of the MTDC Network

Chapter 2 of the thesis presented the first objective of the study. It investigates the modelling and control of the MTDC model used. The modelling of the MTDC system requires a robust controller design for quick recovering during a severe fault. In this section, we analysed the effective short circuit ratio (ESCR) of the AC network and thereby carried out the study on the worst-case scenario of the ESCR value. From the results, it was observed that the converter (Rectifier 1) experienced an overcurrent of 5.5kA (≈ 1.8 pu) value of the rated current while the other converters (inverter 1 and Inverter 2) were in the range of 1.3 and 0.1pu at the instant of the three-phase short circuits fault. Also, the inverter 1 station experienced a non-severe commutation failure. Therefore, a quick fault clearing time is needed to prevent the system from subsequent commutation failure due to adverse transient mode shift of the inverter controller. The overall conclusion from this section is that the modelled MTDC system is well equipped enough with a robust controller to prevent any first transient overcurrent and also reduce the occurrence of commutation fault at the inverter side of the AC network.

6.1.2 Impact of LCC–HVDC Multiterminal on Generator Rotor Angle Stability

The second part of the thesis, in chapter 3, addresses the transient stability issues related to MTDC system. The network considered for this chapter is the single machine infinite bus (SMIB) network. To fully understand the initial rotor angle of the network, the active power-angle of the network was first analysed during three scenarios of constant field supply, AVR without PSS, and AVR with PSS. The system recorded slow damping of rotor angle during the

first scenario. The second scenario recorded a second swing rotor angle instability, while the third scenario gives a positive and quick damping capability to the SMIB network. Further adaptation was carried out on this network to accommodate a three-terminal LCC HVDC network, and the results were compared. The generator power–angle (P_e - δ) diagram for both scenarios was also plotted. The result shows that the MTDC system provided a positive damping torque to the AC system during a three-phase short circuits fault, thereby providing a quick recovery of the system after an AC fault.

6.1.3 Small Signal Stability Analysis of a Four-Machine System with Placement of Multi-Terminal High Voltage Direct Current Link

In Chapter 4, the third part of the study was presented. It discusses the inter-area oscillations of the Kundur two-area four-machine network. The optimal location for the placement of the MTDC system was first analysed based on the modification made to the test network. Two scenarios were observed during a time-domain response. The operating point of the MTDC converters was also adjusted by means of varying the I_{order} from the overall controller, and the result was plotted against the damping rate of the system oscillations. The results show that the test network experience better damping of the inter-area oscillation with reduced amplitudes when the modelled MTDC network was used in replacement of the AC lines on the network. Also, during the variation of the MTDC setpoint, the result shows steady quick damping of the inter-area oscillations until a certain point called the damping saturation point. Above this point is an excess power transfer across the MTDC link, which has a detrimental impact on the AC network inter-area oscillation.

6.1.4 Implementation OF A Multiterminal LCC HVDC with Auxiliary Controller on South Africa's 765kV Corridor

In addressing the final objective of this study, the knowledge gained from the test network in chapter 3 and 4 was implemented on the south African grid in chapter 5. In carrying out this study, the South African grid was modelled, and detailed dynamic responses to different stability studies were carried out. The modelling of the transmission line was discussed, converter filter designs were also discussed. A proposed auxiliary controller for the MTDC system capable of reducing the active power oscillation by generating a new current order (I_{dnew}) was also discussed. Initial response during a system disturbance shows a loss of synchronizing effect from both the AVR and PSS, which causes the generator to lose synchronism with subsequent oscillations. A negative damping torque for the rotor angle and

negative synchronizing torque for the interarea oscillations was observed during the first scenario. The conclusion of this chapter is that the implementation of the MTDC link on the South African grid provided a better system performance. The results are seen in the quick damping of the interarea oscillations with a significant improvement to the voltage profile. Among all the benefits, the power carrying capacity at a reduced loss stood out. Therefore, the adoption of this research into the South African transmission network will surely help enhance the stability margin of the grid. Finally, an auxiliary controller proposed provided potential mitigation of excessive active power dip of the MTDC link during the system disturbance.

6.2 RECOMMENDATION FOR FUTURE WORK

This study has provided deep insight into the modelling and control of MTDC network and also in the area of performance evaluation of MTDC system. It fully highlights the several potentials, advantages, and application areas of a line commutated MTDC converter systems. However, there are still a few limitations that could be addressed in the areas of future work. Therefore, suggested future works in the area of MTDC are discussed below.

- The converter utilized could be modified to accommodate the voltage source converter to form a hybrid MTDC network.
- The MTDC controller could be modified to allow reverser of power transfer with the usage of a double controller in each converter station.
- The synchronous generators used could be replaced with a renewable energy source; such as wind farms and PV farms.
- The MTDC network topology could be modified to consider other meshed network topologies.
- The investigation recorded in this thesis was solely the work of dynamic simulation using PSCAD software. This is to help gain insight into the phenomena of power system stability and control. The reasons are due to the availability and cost of various pieces of power equipment needed to carry out the experimental analysis of the study. Therefore, future works arising from this study need to embrace practical and experimental analysis. One main suggestion is to use a real-time simulation such as SPEEDGOAT, RTDS, or OPAL-RT. Hardware-in-the-Loop (HIL) could further be used to validate the quality of the testing.